Real-Time Simulation and Control of Spatio-Temporal Cardiac Excitation using an Analog-Digital Hybrid Circuit Model

Farhanahani Binti Mahmud

March 2011

Real-Time Simulation and Control of Spatio-Temporal Cardiac Excitation using an Analog-Digital Hybrid Circuit Model

A dissertation submitted to

THE GRADUATE SCHOOL OF ENGINEERING SCIENCE

OSAKA UNIVERSITY

in partial fulfillment of the requirements for the degree of

DOCTOR OF PHILOSOPHY IN ENGINEERING

By

Farhanahani Binti Mahmud

March 2011

Preface

This work was conducted under the supervision of Prof. Taishin Nomura and was developed at Division of Bioengineering, Graduate School of Engineering Science, Osaka University, from 2008 to 2011. Part of the work was supported by the Global COE program in “ in silico medicine ” at Osaka University.

This thesis proposes a hardware-implemented technique to simulate electrical states of cardiac tissues for investigating dynamics of the heart. This approach is taken in order to obtain real-time simulations of the cardiac action potential propagation in numerical cardiac cell model. Its main case of study is the development of the analog-digital hybrid circuit model, which is able to represent real-time performance for large scale simulations of cardiac tissue dynamics. The study shows that the hybrid model is expected to be a useful option to modeling and computational techniques toward further understanding of the reentrant mechanisms.

Farhanahani Binti Mahmud
Division of Bioengineering
Graduate School of Engineering Science
Osaka University
Toyonaka, Osaka 560-8531, JAPAN

Contents

Summary

Action potential of a cardiac cell membrane and its conduction in the cardiac tissue provide a basis of the electrophysiological function of the heart through the cardiac excitation-contraction coupling mechanism. Towards a better and a quantitative understanding of electrophysiological mechanisms of the reentrant cardiac arrhythmias at cellular, tissue, and organ levels, mathematical models of cardiac cells, tissues, and the heart have been developed and analyzed by simulating conduction of action potentials in a variety of conditions. However it is inevitable for those models to become large scale in the number of dynamical variables, requiring immense amount of computational time for their dynamic simulations. In this study, an analog-digital hybrid circuit model of electrical excitation of a cardiac cell based on Luo-Rudy phase I (LR-I) model, a typical mathematical model of a cardiac cell was developed. Through its hardware implementation, real-time simulations of the cellular excitations as well as their propagation in a cardiac tissue model have been performed with the hybrid circuit model.

This thesis is organized as follows. It is started with a general introduction in Chapter 1. The research background is discussed in Chapter 2, where physiology of the heart and the mechanism of electrical system which controls the cardiac contraction are elaborated. These are then followed by explaining the basis of knowledge on electrical potentials that exist across cell membranes and describing how they are modeled. Computational techniques of mathematical modeling and hardware-implemented circuits that have been developed over past few decades in understanding the dynamics of cells and excitation-conduction are also reviewed especially in cardiac cell modeling.

Chapter 3 is focusing on the work presented in a single cell model, where a design method of the analog-digital hybrid circuit cell is overviewed, followed by details of the analog-digital hybrid active circuit. The design method of current-voltage (I-V) relationships between ion currents and the membrane potential reproduced by analog and digital circuits is also explained. Furthermore, action potential of the hybrid circuit model is initiated by an external stimulus and the result is compared to the result of the LR-I model. Action potential generation of the hybrid circuit model in response to periodic current impulse trains with different interval (period) T are carried out and comparisons to the result from the LR-I model are presented. Classification of excitation response patterns on the parameter plane spanned by the period T and the intensity A of the impulse trains

in the hybrid model and LR-I model are analyzed, and the results between the two models are also compared. According to the simulations results, the action potential characteristics of the hybrid cell model and the LR-I cell model are comparable as the hybrid cell model generally well reproduces the I-V relationships of ion currents described in the LR-I model, as well as the action potential waveform, and the excitation dynamics in response to periodic current impulse trains with various intervals and intensity levels.

In Chapter 4, the work on investigating the spatio-temporal dynamics and control of reentrant action potential conduction in active cable models is being reviewed. Manner and underlying mechanisms in the initiation of the reentrant action potential conduction in a one dimensional ring-topology-network of the hybrid active circuit cable model are constructed as a model of anatomical reentrant tachycardia. Dynamics of the hybrid active circuit cable model are then compared with those in the numerical simulation of the LR-I cable model. Resetting and annihilation of the reentrant wave under the influence of single and sequence of stimulations are investigated by using the hybrid cable model and comparisons to the result from the LR-I cable model are carried out. Resetting and annihilation of the reentrant wave are of crucial importance in clinical situations where the reentrant cardiac arrhythmias are often controlled and terminated by delivering electrical stimulations to the heart through catheters. Phase resetting curves (PRCs) of both models are presented to show the relationship between the phase reset of the reentry and the phase of single stimulation. According to the PRCs, sequential phase resetting by periodic stimulation that leads to annihilations of the reentry are predicted and illustrated with one-dimensional discrete Poincare mappings. As the results in the simulations of the reentrant action potential conduction, quantitative correspondence between the hybrid cable model and the LR-I cable model was demonstrated using a one dimensional active cable as a model of the anatomical reentry in a cardiac tissue with various conditions. Those include (1) unidirectional block to initiate reentry, (2) phase resetting by single impulsive stimulations, (3) annihilations of the reentry by appropriately timed single stimulations, (4) phase resetting curves (PRCs) that can characterize the reentry dynamics in response to single stimulations at various timings, and (5) sequential phase resetting that leads to annihilation of the reentry as predicted by the one dimensional discrete Poincare mappings.

Finally, general discussion and conclusions are being reviewed in Chapter 5. The overall results of the hybrid circuit model are satisfied with those of the LR-I model, corresponding to the subjects examined in the study. Therefore, by taking into account the satisfactory results and the real-time simulation capability of the hybrid model, these can be concluded that the hybrid model might be a useful tool for large scale simulations of cardiac tissue dynamics, as an alternative to numerical simulations, toward further understanding of the reentrant mechanisms. As a matter of fact, minimizing power consumption and physical size of the circuits need to put into consideration regarding to large-scale development of the hybrid model.

Chapter 1

Introduction

Electrical excitations of cardiac cell membranes and their propagation in the heart tissue control the mechanical contractions of the cells through the cardiac excitation-contraction coupling mechanism, leading to coordinated contractions of the heart to pump blood. The excitation event is finely controlled by influx and efflux of transmembrane currents through various types of ion channels permeable to specific kinds of ions[1].

The cardiac excitation can be characterized by an action potential, where the action potential is generally has 5 phases. Figure 1.1 shown here represents the ventricular cardiac action potential waveform with the phase classification. The cardiac action potential is often generated in response to a supra-threshold current stimulation applied to a cell, in which fast inward Na^+ current causes a rapid increase in the membrane potential (phase 0), followed first by transient outward K^+ current causing the small downward deflection of the action potential (phase 1), and then by slow inward Ca^{2+} current that almost counterbalances slow delayed rectifier K^+ current for producing the action potential plateau (phase 2). A rapid repolarization then takes place, where the slow inward current is terminated, while the slow delayed rectifier K^+ outward current as well as other types of outward and inward K^+ currents are maintained (phase 3). Finally, the membrane potential resettles at the resting potential (phase 4).

The resting membrane potential of normal cardiac cell is approximately-80 to 85 mV and it rises from its normally negative value to a positive value up to 60 mV to 80mV during the excitation. The action potential lasts for about 200 ms. The excitability of the cell is determined by how much the Na^+ and Ca^{2+} channels regain their capability to inflow the currents after prior excitations, causing the refractoriness of the cell. Refractoriness here means the condition during which time the cells cannot fully respond to the stimulus. Thus if another stimulation is applied before the cell regains its excitability enough, it

cannot induce the action potential fully or even partially, leading to complex phase-locked, sometimes chaotic, responses when the membrane is stimulated by a periodic sequence of current injections[2, 3].

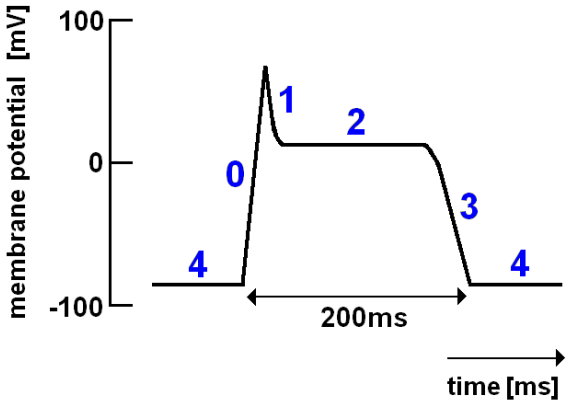

Figure 1.1: Phases of the cardiac action potential

The excitability and refractoriness of cardiac cells are features commonly shared by a class of nonlinear dynamical systems called excitable systems[4]. The heart consists of a huge number of such excitable cells connected locally via electrical synapses, referred to as the gap junctions, that allow spatial conductions of the action potentials through the heart tissue, leading to the coordinated contraction of the heart for every single beat. In a normal heart, the action potential wave dies when it reaches a complete activation of myocardium because of a refractoriness effect of the cardiac tissue that has excited before. Under uncommon conditions, the propagating wave does not die out completely but re-excite the myocardium that has recovered from the refractoriness. In this case, excitation would rotate around an area of conduction block. Most evident is reentry of cardiac excitation, which occurs when previously activated tissue is repeatedly activated by the propagating excitation wave as it reenters the same region and reactivates it at a high frequency.

Apropos of the heart is a typical dynamical system of excitable media, among other systems in physics, chemistry, and biology, in which all of them share phenomenologically common behaviors associated with the excitability and refractoriness of the media, such as reentry excitations including spiral and scroll waves of excitations[5, 6, 7, 8]. The most common type of reentry is circus movement reentry. As for the heart dynamics, some cardiac arrhythmias are perpetuated by reentrant mechanisms, in which a local excitation

conducts through a part of the heart to recirculate back to the original site, causing a rapid heart beat referred to as the reentrant tachycardia[9].

Methodologies that have been employed so far to theoretically understand the nonlinear dynamics of excitable media include mathematical modelings and their computer simulations as well as electronic experiments that utilize hardware-implemented nonlinear circuits, by which experimentally observed dynamics of real-world chemical, physical, and physiological excitable media could be reproduced and analyzed qualitatively and/or quantitatively. The use of mathematical models with their computer simulations is favorable because of their large capability of describing physical and/or physiological mechanisms in detail, allowing practically one-to-one correspondence between parameters in the models and physical quantities.

The mathematical modelling in excitable media is pioneered by Hodgkin and Huxley, who formulated a mathematical description of action potential generation in the giant squid axon in 1952[10]. Indeed, mathematical models of the cardiac action potential in single cells continue their remarkable development and improvement after the Hodgkin-Huxley model. As for, much of the mathematics of cardiac cell modeling is drawn from the Hodgkin-Huxley formulation. Progress in mathematical modeling and computational techniques has facilitated using simulations as a tool for investigating cardiac dynamics. In which, models of cardiac cells are defined by mathematical descriptions of electrical events at the cellular level that give rise to cardiac action potentials. Starting from the simplified cardiac model, the FitzHugh-Nagumo model[11] that described a generic excitable media of the cardiac cells, the Noble Purkinje model[12], the Beeler and Reuter[13], the Luo-Rudy ventricular model[3, 14, 15] have been developed to represent different regions of the heart. Until today, the models become more advance but complicated from year to year as variables parameters in the mathematical descriptions are increased in order to represent the cellular processes in more detail. Thus, tissue models consisting of a large number of single cell models cause a new problem in the amount of computations required to obtain meaningful results from their simulations[16]. Due to this drawback, most research articles dealing with cardiac tissue models give their excuses for not to use the latest detailed single cell models as their compartmental nodes, but use rather simple models instead.

Meantime, hardware-implemented excitable media have their own long history of in-

vestigation, comparable to that for the mathematical models, as traced back to circuits of excitable systems proposed in 1960's[17, 18, 19]. To this day, the hardware models provide valuable tools for real-time simulations whose computational speeds are independent of the number of cells connected if one tries to perform action potential conduction on a multiple coupled analog circuits as a model of a cardiac tissue. However, they are less suited in modeling biophysically-detailed and complicated mechanisms of the ion currents. Only a few studies have succeeded to design analog circuits that are biophysically detailed and have quantitative correspondence to a real cell[20].

One of main issues for studying excitation conductions in the field of cardiac physiology and pathology is to understand how the action potential conduction and reentry dynamics at the tissue level are influenced by a cellular level dysfunction of specific ion channels[21, 22] that cause abnormal cellular excitation such as in the long QT syndrome[23]. In order to provide comprehensive answers to this sort of question using a mathematical or hardware circuit model of cardiac tissue, it is required for every cellular model (compartmental node) used in the tissue model to include physiologically and quantitatively plausible models of ion channel currents rather than simple and qualitative models.

Thus, throughout the study, an analog-digital hybrid circuit model of an excitable cell that can quantitatively reproduce the action potential generation and phase-locked and chaotic responses to periodic current pulse stimulations observed in Luo-Rudy phase I (LR-I) model[3] for a mammalian cardiac ventricular cell is proposed. Firstly here, the circuit model is reported briefly. Then a model of spatially distributed extension of a one-dimensional cardiac tissue with its hardware implementation is proposed. The circuit model allows us to perform real-time simulations of spatially conducting cardiac action potentials. In particular, simulation results show that the circuit tissue model can exhibit real-time dynamics for initiation of the reentry induced by unidirectional block and for phase resetting that leads to annihilation of the reentry in response to impulsive current stimulations at appropriate locations and timings. The dynamics of the hybrid model are compared to those obtained numerically in LR-I model in order to demonstrate that the circuit model can be utilized for simulating large scale cellular network in real-time as an alternative to numerical simulations.

Chapter 2

Background

2.1 Electrical System of the Heart

The heart is composed of two atria and two ventricles with four chambers to operates as a pump in supplying blood through the circulatory system. It is composed of three major types of cardiac muscle: atrial muscle, ventricular muscle, and specialized excitatory and conductive muscle fiber. As shown in Figure 2.1, the specialized excitatory and conductive fibers are mainly consist of sinoatrial (SA) node in which the normal rhythmic self-excitatory impulse is generated, atrioventricular (AV) node in which the impulse from the atria is delayed before passing into the ventricles, AV bundle, which conducts the impulse from the atria into the ventricles, and left and right bundles of Purkinje fibers, which conduct the cardiac impulse to all parts of the ventricles. They provide an excitatory system for the heart and a transmission system for rapid conduction of electrical signal, called action potential, through the heart. This mechanism will be explained later in this section.

Figure 2.2 illustrates a typical anatomy section of cardiac muscle showing arrangement of the cardiac muscle fibers in a latticework. Cardiac muscle has myofibrils that contain actin and myosin filaments interdigitate and slide along each other during the process of contraction. The angulated dark areas crossing the cardiac mucsle fibers in Figure 2.2 are called intercalated discs, referred to as gap junctions. They are cell membranes that separate individual cardiac cells from each other. Electrical resistance through the in-

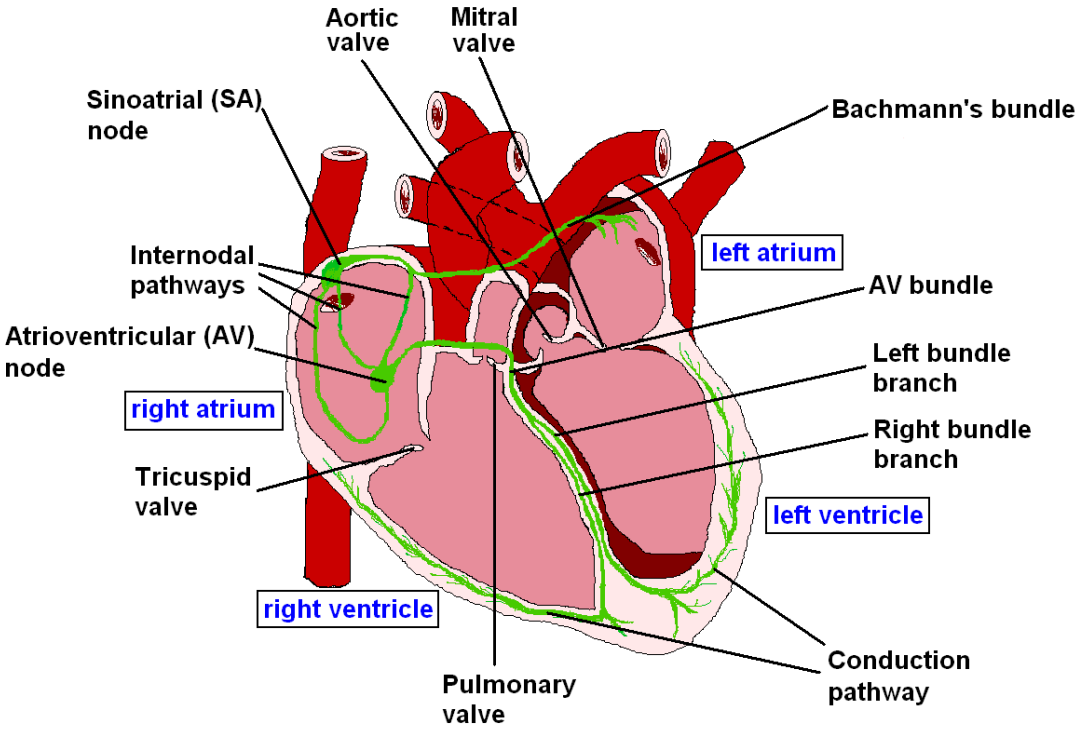

Figure 2.1: The heart

tercalated disc is only 1/400 the resistance through the outside membrane of the cardiac muscle fibers[24]. Therefore, ions flow with relative ease along the axes of the cardiac muscle fibers so that the action potential travel from one cardiac muscle cell to another, past the intercalated discs, without significant obstruction. In other words, the cardiac muscle cells are so tightly bound that when one of these cells becomes excited, the action potential spreads to the entire of heart from cell to cell throughout the latticework interconnection.

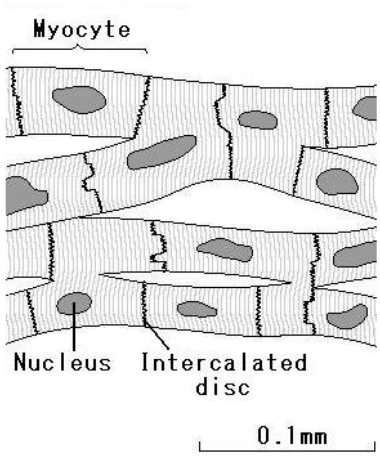

Figure 2.2: The cardiac muscle

The period from the end of one heart contraction to the end of the next is called the cardiac cycle. The cardiac cycle consists of a period of relaxation called diastole followed by a period of contraction called systole. The electrical activity events during the cardiac cycle can be recorded by an electrocardiogram, known as an ECG. Figure 2.3 illustrates the ECG wave during the cardiac cycle. The relationship of the ECG wave to the cardiac cycle may be explained as follows. Each cycle is initiated by spotaneous generation of the action potential in the SA node. The SA node is located in the right atrium. When the right atrium is full with blood, the electrical signal spreads across the cells of the right

and left atria through atrial muscle fibers, such as Bachmann's bundle. This signal causes the atria to contract. This pumps blood through the open valves (tricuspid valve and mitral valve at the right and left side of the heart, respectively) from the atria into both ventricles. The P wave on the ECG in Figure 2.3(a), marks the contraction of the atria as shown in 1 of (b) in the Figure 2.3. Here, in the Figure 2.3(b), the dark green dots correspond to the conduction of the action potential signal, and the disc-shaped symbols in red and blue are respectively subjected to oxygen-rich blood and oxygen-poor blood.

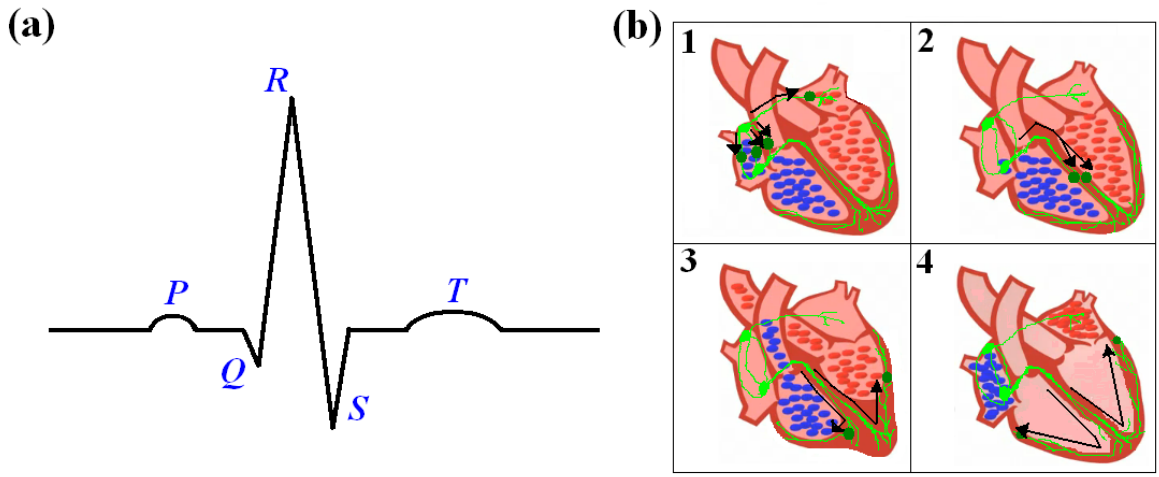

Figure 2.3: The electrocardiogram wave and the cardiac cycle

Then, the signal arrives at the AV node near the ventricles and it is slowed for an instant to allow the right and left ventricles to fill with blood. On the ECG wave, this interval is presented by the start of the line segment between the P and Q wave. The signal is released and moves next to AV bundle located in the ventricles. From the AV bundle, the signal fibers divide into left and right bundle branches through the Purkinje fibers that connect directly to the cells in the walls of the ventricles, which run through the septum as shown in 2 of (b) in Figure 2.3. On the ECG, this represented by the Q wave. The signal spreads quickly across the ventricles (3 of (b) in Figure 2.3). As the signal spreads across the cells of the ventricle walls, both ventricles contract, but not at exactly the same moment. The left contracts an instant before the right ventricle. As for,

the contraction of the left ventricle pushes blood through the aortic valve to the rest of the body and the contraction of the right ventricle pushes blood through the pulmonary valve to the lungs. On the ECG, the R wave marks the contraction of the left ventricle and the S wave marks the contraction of the right ventricle. As the signal passes, the walls of the ventricles relax and await the next signal, where according to the ECG, the T wave marks the point at which the ventricles are relaxing, that is, the T wave occurs slightly prior to the end of ventricular contraction (4 of (b) in Figure 2.3).

This contraction process continues over and over in a normal rhythmic rate of approximately 70 beats per minute. The rhythmical contraction of the heart works continuously, much like a pump, in order to provide a major source of power for moving blood through the vascular system. It is said that the SA node is the normal pacemaker of the heart as it controls the heart's rhythmicity. This is because of its rate of rhythmic discharge is greater than either the AV node or the Purkinje fibers, and that of any other part of the heart.

However, under abnormal conditions, where some other part of the heart develops a rhythmic discharge rate that is more rapid than that of the SA node, the pacemaker of the heart shifts from the SA node to the other part of the heart. A pacemaker elsewhere than the SA node is called ectopic pacemaker and this will cause abnormal impulse generation of the heart which that might induce abnormal sequence of contraction. Moreover, it is known that the relationship of a refractory period to the rapidity of transmission of the cardiac impulse throughout the ventricles plays an important role in causing synchronous contraction of the heart. Here, the refractory period, also known as the duration of the muscle contraction is generally about 150 ms in atrial muscle and 200 ms in ventricular muscle. That is any serious delay in transmission of the impulse through the ventricle can make it possible for the impulse from the last excited ventricular muscle to reenter the first muscle. This, in turn, sets up a reentrant circuit which causes abnormal impulse conduction in the heart. These phenomena of abnormal impulse generation and conduction

are thought to be able to create conditions that cause serious cardiac arrhythmias, the abnormal rhythmicity of the heart. Therefore, to prevent or to treat this problem, better understanding of underlying mechanisms to these phenomena will be necessary.

2.2 The Membrane Potential

Electrical potentials exist across the membranes of all cells of the body and some cells, such as nerve, skeletal muscle and cardiac cells, are excitable, that is capable of producing and transmitting action potentials along their membrane in response to electrochemical impulses. Generally, an excess of negative ions (anions) accumulates immediately inside the cell membrane along its inner surface, and an equal number of positive ions (cations) accumulates immediately outside the membrane. The effect of this is the development of a membrane potential during a polarized state at a resting membrane potential with the cell more negatively charged inside than outside the membrane. As illustrated in Figure 2.4, basically, the cell membrane is endowed with a sodium and potassium pump, where sodium being pumped to the exterior and potassium to the interior, however, because about three sodium ions are pumped out of the cell for about two potassium ion that is pumped in, more positive ions are pumped out of the cell than into it. Moreover, the resting membrane is normally more permeable to potassium as to sodium and since most of the anions inside the cell are nondiffusible, the negative charges remain inside of the cell so that the cell becomes electronegative, while the outside becomes electropositive. This causes the membrane potential inside the cell falls to approximately -85 mV, that is the resting membrane potential of the membrane.

A sequence of changes in the membrane permeability mainly for sodium ions and potassium ions could cause changes in the membrane potential. Where the first stage, which is called a depolarization, is a sudden increase in the permeability of the membrane to sodium ions causes the cell positively charged on the inside and the rapid raise of the membrane potential and the second stage, which is called a repolarization, is an increase

in potassium ions permeability causes the membrane potential to reestablish and back to normal. This short-lasting event in which the electrical membrane potential of a cell rapidly rises and falls is called an action potential.

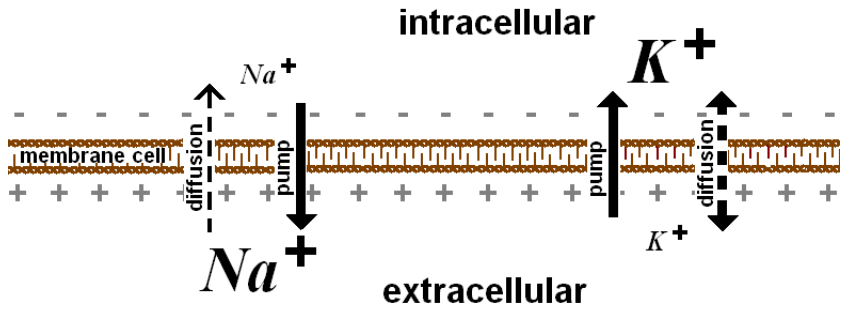

Figure 2.4: Establishment of a membrane potential in the resting membrane

History in the research of the membrane potential began with the idea that cardiac cells could produce action potentials in response to an electrical stimulus, which proposed by Henry Bowditch in 1871, based on his studies on contraction of heart muscle by stating that tissues respond to stimuli in an all-or-none manner[25]. He established the two properties that define excitable tissues which are related to the concept of threshold for stimulation and the response of excitable tissues to stimuli above threshold that is not depend on the intensity of the stimuli. The threshold is the starting point of the excitability in the cell according to a refractory state, the condition of the cell which it cannot supporting the passing of the action potential wave at a certain amount of time. However, the first action potentials were not measured in cardiac cells but in a nerve cell of the the giant axon of the squid, because of its large size. Hodgkin and Huxley[26, 27] and Curtis and Cole[28, 29] were the first to measure an action potential in the squid axon using the intracellular micropipette for measuring voltage and current across the membrane of a cell by inserting the micropipette inside the cell. Then, with advances in microelectrode to measure in much smaller cells, Ling and Gerard[30], and Nastuk and Hodgkin[31] were able to record the resting and the action potential in skeletal muscle cells. Caroboeuf and Weidman[32] and Draper and Weidmann[33] were the first to measure the resting membrane potential

and the action potential in mammalian cardiac muscle. Woodbury et al.[34] were the first to measure it in frog heart. The characteristics of the cardiac action potential, such as resting membrane potential and rapid upstroke, are similar to that in nerve and skeletal muscle cells. Nevertheless, the cardiac action potential has a duration of 100-500 ms, different to nerve and skeletal cell potentials that have duration of less than 5 ms.

The membrane potential can be developed by specialized membrane-spanning protein that control the movement of ions either by passive electrodiffusion through transmembrane pores (channels) or translocation across the membrane by carrier proteins (pumps, exchangers and transporters). When a concentration difference of ions across a membrane causes diffusion of ions through the membrane, thus creating a membrane potential, the magnitude of the potential is determined by the ratio of tendency for the ions to diffuse in one direction. If a permeable membrane separates two solutions, A and B, and if ion X is present on either side of the membrane, the relative probability of finding a particle in either solution A or solution B is given by the Boltzmann equation:

$$\frac{P_B}{P_A} = \exp\left(-\frac{u_B - u_A}{kT}\right) \tag{2.1}$$

where,

u_A : *the energy of the particle in solution A*

u_B : *the energy of the particle in solution B*

P_A : *the probability of a particle being in state A*

P_B : *the probability of a particle being in state B*

k : *Boltzmann's constant*

T : *absolute temperature*

Equation (2.1) can be constructed in terms of molar energies and concentrations, to

take account of the properties of the bulk solutions rather than individual components:

$$\frac{[X]_B}{[X]_A} = \exp\left(-\frac{U_B - U_A}{RT}\right) \tag{2.2}$$

where,

$[X]_A$: *concentration of ion X in state A*

$[X]_B$: *concentration of ion X in state B*

U_A : *molar energy of state A*

U_B : *molar energyvof state B*

R : *gas constant*

Rearranging Eq. (2.2) and taking logs gives the following equation:

$$U_B - U_A = -RT \ln\left(\frac{[X]_B}{[X]_A}\right) \tag{2.3}$$

This shows the molar energy difference in state A and B due to the concentration gradient. If the ion is charged, there will be not only a chemical force, but also an electromotive force. The electrical potential acting on anion of valence z in a potential field of Ψ is $zF\Psi$. In the steady state, there will be no net flux of ions across the membrane. The potential across the membrane at which there is no net movement of ions is termed the equilibrium potential of that ion, and is calculated as follows:

$$0 = -RT \ln\left(\frac{[X]_B}{[X]_A}\right) + zFE_{eqm} \tag{2.4}$$

$$E_{eqm} = \left(\frac{RT}{zF}\right) \ln\left(\frac{[X]_B}{[X]_A}\right) \tag{2.5}$$

where,

E_{eqm} : *the equilibrium potential*

F : *the Faraday constant*

This is the Nernst equation. The equilibrium potential, E_{eqm}, also called the Nernst potential can be interpreted as the potential at which an ion is in equilibrium with its diffusional force. The uncoupled movement of a charged species through an open channel

can be described by the equation:

$$I_X = g_X(V_m - E_{eqm,X}) \tag{2.6}$$

where,

I_X : *net current due to movement of ion X through the channel*

g_X : *conductance of the channel to ion*

V_m : *transmembrane voltage*

$E_{eqm,X}$: *equilibrium or Nernst potential for ion*

This equation describes an ohmic conductor, as there is a linear relationship between current and voltage. Even though the Nernst equation can be used to calculate the correct reversal potential for an ion and the net driving force for an ion, the net flux is not always linearly related to the voltage difference, as implied by this equation.

As described before, in resting membrane potential, sodium ions are concentrated outside the cell and potassium ions are concentrated inside the cell, and cells are permeable to potassium ions because inward rectifier potassium channels are open at the resting membrane potential. This results in the diffusion of potassium ions from inside the cell to outside due to the gradient in potassium concentration and causes the accumulation of positive charge outside the cell, and negative charge inside the cell. Meanwhile, an electric field, which increases in magnitude as more potassium ions leave the cell, forces oppose diffusion forces and tend to move potassium ions from outside to inside the cell. The growing electric field will eventually prevent the efflux of more pottasium ions until a situation of equilibrium will be reached. Therefore, if the cell membrane at rest were permeable only to potassium ions, the ion current flowing through the membrane at rest would be zero, and the resting membrane potential would be exactly the potassium equilibrium potential or Nernst potential. According to the Eq. (2.5), the potassium equilibrium potential can

be written as follows:

$$E_{eqm,K^+} = \left(\frac{RT}{F}\right)\ln\left(\frac{[K]_o}{[K]_i}\right) \tag{2.7}$$

where,

$[K]_o$: *the potassium concentration outside the cell*

$[K]_i$: *the potassium concentration inside the cell*

However, measured resting membrane potentials are not always identical to the potassium equilibrium potential. This indicates that the membrane is also permeable to ions other than potassium at negative membrane potentials. Thus, a more accurate estimation of the resting membrane potential can be obtained with the following formula, called the Goldman's equation, that takes into account other ions such as sodium, chloride.

$$E_{eqm} = \left(\frac{RT}{F}\right)\ln\left(\frac{P_K[K]_o + P_{Na}[Na]_o + P_{Cl}[Cl]_o}{P_K[K]_i + P_{Na}[Na]_i + P_{Cl}[Cl]_i}\right) \tag{2.8}$$

where,

P_K : *the permeability of the cell membrane to potassium*

P_{Na} : *the permeability of the cell membrane to sodium*

P_{Cl} : *the permeability of the cell membrane to chloride*

$[K]_o$: *thevpotassium concentration outside the cell*

$[Na]_o$: *the sodium concentration outside the cell*

$[Cl]_o$: *the chloride concentration outside the cell*

$[K]_i$: *the potassium concentration inside the cell*

$[Na]_i$: *the sodium concentration inside the cell*

$[Cl]_i$: *the chloride concentration inside the cell*

If a membrane at rest is permeable to several ions, the resting membrane potential represents a dynamic equilibrium in which the total ion current is zero but the individual ion currents through the different ion channels are not zero. But still, the Nernst potential

for potassium is a good approximation of the resting membrane potential of cardiac cells since the permeability of the membrane to potassium channels at rest is many orders of magnitude larger than the permeability to other ions.

According to experimental measurements of the transmembrane potentials, Hermann suggested that the cell membrane could be represented under subthreshold conditions by a resistance in parallel with a capacitance[35]. Curtis and Cole[36] measured cell membrane resistance and capacitance in nerve cells and showed that the electrical properties of the membrane are well represented by an RC circuit (Figure 2.5). Their experiments showed that cells have a high-conductance cytoplasm that is surrounded by a high-resistance membrane with an electrical capacitance of about 1 μF/cm^2. The capacitor, C represents the capacitance of the lipid bilayer that forms the cell membrane, and the resistor, R represents the conductance of the ion channels that are open at the resting membrane potential.

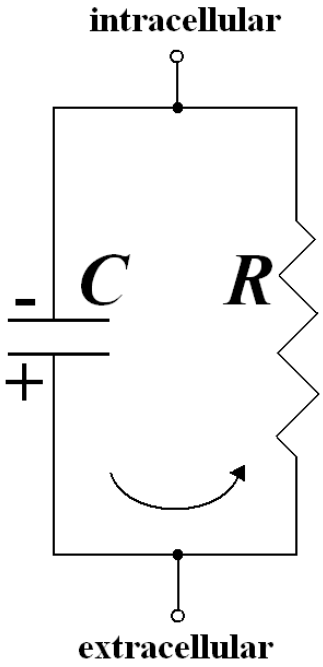

Figure 2.5: The Cole-Curtis model of passive membrane

As long as the membrane of the excitable cell in nerve, skeletal muscle or cardiac muscle remains completely undisturbed, the membrane potential remains at the resting

membrane potential, generally at -85 mV. However, any factor that suddenly increases the permeability of the membrane to sodium is likely to elicit a sequence of rapid changes in membrane potential lasting for several miliseconds, followed immediately thereafter by return of the membrane potential to its resting value. This sequence of potential changes is called the action potential. The action potential occurs mainly in two stage called depolarization and repolarization, and the action potential wave shows its various phases as it passes on a cell membrane. As describe in the introduction, the cardiac action potential consists of five different phases, which is more complex than that of skeletal or nerve cells. Depolarization is the earliest events in excitation, developing a positive state inside of the cell. This positive state inside the cell is called the reversal potential. Almost immediately after the depolarization phase of an action potential that has just previously changed the membrane potential to a positive value, the normal resting membrane potential returns. This is called repolarization.

Some of the factors that can evoke an action potential are electrical stimulation of the membrane, application of chemicals to the membrane to cause increased permeability to sodium, mechanical damage to the membrane, heat, cold or almost any other factor that momentarily disturbs the normal resting state of the membrane. Action potential generation is the result of ion current flowing through many ion channels that are embedded in the cell membrane. Those channels are permeable to different ions (sodium, potassium, calcium) and open and close at different voltage levels with different time constants. The ion current flowing through a channel is determined not only by the biophysical characteristics of the channel but also by the intracellular and extracellular environment that surrounds the cell membrane. For ion channels to perform their physiological function, there has to be a gradient in ion concentrations on both sides of the membrane. Sodium and calcium concentrations are higher outside that inside the cell; potassium concentration is higher on the inside. In maintaining those gradients, ion pumps transform metabolic energy into potential electrochemical energy that is used by the ion channels. Briefly,

ion channels can be thought of as mediating the dynamic portions of the action potential and in contrast, pumps and exchangers contribute to the overall behavior of the action potential, but they have slower effects than the rapidly opening and closing channels.

In having a quantitative understanding of action potential generation and propagation, the characterization of the individual currents which flow across the cell membrane, either by ion channels or pumps and exchangers, that contribute to the action potential has been required. Still, after all currents have been characterized, a quantitative understanding of the cell action potential is possible only when all ion currents are intergrated to reproduce the action potential. To intergrate the different ion currents to reconstruct the action potential, a parallel conductance model describe by an equivalent electrical circuit was proposed as shown in Figure 2.6, which was pioneered by Hodgkin and Huxley[10]. Since then, the research in area action potential generation and propagation has been active. The capacitor, C_m represents the membrane capacitance. The branches of the circuit represent the different ways in which ions move between the intracellular and extracellular spaces through the membrane and originate an ion current. Ions can move as a result of concentration gradients through channels whose conductance is time and voltage dependent, or through channels with constant conductance (background or leak). Ions can also be transported across cell membranes by pumps and exchangers that are necessary to restore concentration gradients, which also results in ion currents that contribute to the action potential. The battery on a particular branch represents the equilibrium (or Nernst) potential (E_i) for that ion, and the variable resistance represents that the resistance (R_i) (or conductance (G_i)) of the channel changes as a function of membrane voltage and time.

Furthermore, the total transmembrane current in the parallel conductance model can be expressed by the sum of membrane capacitive and ion currents as Eq. (2.9). Note that, the above equation is for computations of an action potential in a single cell where there are no spatial changes in transmembrane potential. The number of branches and the formulation of the currents depend on the type of tissue to model and they have

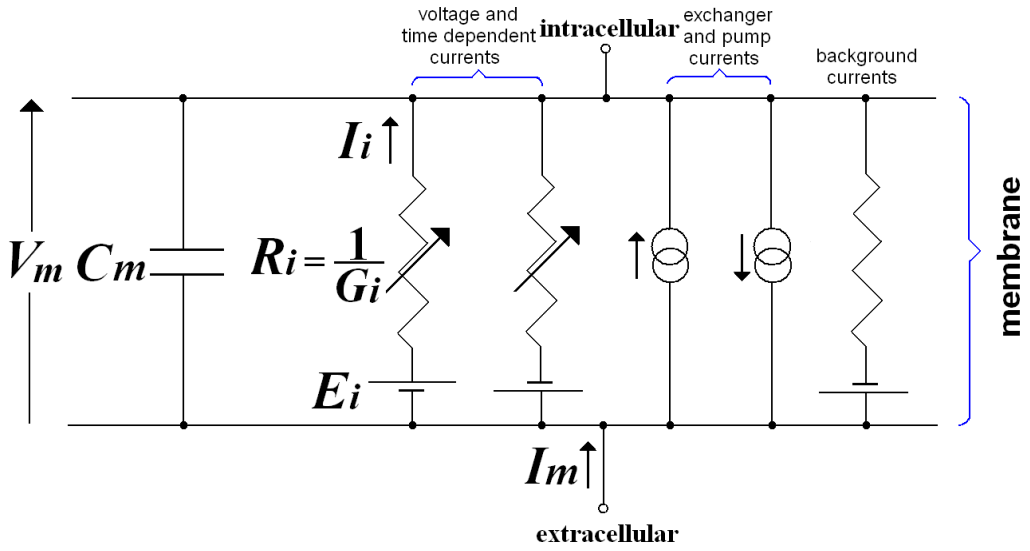

Figure 2.6: The parallel conductance model of active membrane

changed over time as the discovery of new currents or the reformulation of old currents. These action potential models and the mathematical description of the action potential, specifically in cardiac cell, will be described further in the next section.

$$I_m = C_m \frac{dV_m}{dt} + I_{ion} = C_m \frac{dV_m}{dt} + \sum I_i \tag{2.9}$$

where,

I_m : *the total membrane current*

C_m : *the specific membrane capacitance to ion*

V_m : *the transmembrane voltage*

I_{ion} : *the total ion current*

I_i : *the ion current*

2.3 Mathematical Models of Excitable Membrane

Since early twentieth century, experimental researches on the membrane potential and the action potential have made it possible to reveal the underlying mechanisms in the electrical state of the heart. Although the experimental studies are generally preferable, investigating the cardiac electrical behavior experimentally poses a number of challenges, such as a limitation on quantity of variables for monitoring or deprivation of high-resolution data in investigating larger preparations. On the other hand, modelling techniques for a computer simulation of cardiac electrical behavior are not associated with such complications. At the same time, it became clear that, a mathematical description use to simulate the cardiac action potential would be useful to interpret experimental data and also to generate hypothese that could later be tested experimentally. Action potential models have been very useful in investigating different features of cardiac electrophysiology, from action potential generation in a single cell to action potential conduction in multidimesional structure of cardiac tissues.

It is known that the action potential is the result of the interaction of cellular components, including the dynamics of the different ion channels embedded in the cell membrane, changes in concentrations of ions inside and outside the cell, and how cells are connected. Hodgkin and Huxley[10] who are the first group that intend to formulate mathematically the cellular prosesses to lead the generation of the action potential. They proposed an ion model that is specified by 3 types ion channel currents that are involved in the generation of the action potential to represent the flow of sodium, potassium and chloride (leakage or background) through the membrane of squid axon. It is known that the formulation in ion models have always changed over time because of the revelation of new or more accurate currents. And, it is also depends on a specific tissue or a cell that is needed to be modeled. Basically, in formulating an ion model of the action potential, the kinds of currents that should be part of the model have to be determined to model the individual ion channels. As for, the ion channels dominate depolarization and repolarization, and the process of

the repolarization is largely understood as the dynamic interaction of the membrane ion channels. Consequently, in many situations the action potential can be approximated well using a model containing only channels. Nonetheless, for the ion channels to perform their function, modelling the right changes in ion concentrations should be also put into consideration.

Once all ion currents and changes in ion concentrations have been formulated, the need to be intergrated in the equivalent electrical circuit of the parallel conductance model to produce an action potential. To compute the action potential, the intergration of the governing differential equation is as follows:

$$I_m = C_m \frac{dV_m}{dt} + I_{ion} \tag{2.10}$$

$$C_m \frac{dV_m}{dt} = I_m - I_{ion} \tag{2.11}$$

where,

I_m : *the total membrane current* [μA/cm^2]

C_m : *the specific capacitance* [μF/cm^2]

V_m : *the transmembrane voltage* [mV]

I_{ion} : *the summation of all ion current* [μA/cm^2]

The simplest way to intergrate the equation is to use the forward Euler method:

$$\frac{V_m^{t+\Delta t} - V_m^t}{\Delta t} = \frac{-I_{ion}^t}{C_m} + \frac{I_m^t}{C_m} \tag{2.12}$$

$$V_m^{t+\Delta t} = V_m^t - \Delta t \left(\frac{-I_{ion}^t + I_m^t}{C_m} \right) \tag{2.13}$$

From equation (2.13), the transmembrane potential at a later time ($V_m^{t+\Delta t}$) can be calculated from the transmembrane potential (V_m^t), the total ion current (I_{ion}^t) and the total membrane current (I_m^t) at a given time (t). In simulating the action potential, the total membrane current (I_m^t) stated here is the axial current, corresponding to such as external current stimulations. Δt is the time discretization step and the value of the time discretization step has to be small enough to calculate V_m accurately during rapid changes

in the transmembrane potential. Typically, a value of Δt=1 μs is used.

Most of the modern electrophysiological concepts and methods were developed by the computational technique of the action potential models in nerve cells. Nevertheless, mathematical modeling in single cell that contributes to the action potential in cardiac cells also has been used extensively to increase the understanding of cardiac electrophysiology and has proven its usefulness. The typical parameters of the cardiac cell for reference in the cardiac cell modeling are shown in Table 2.1 [37]. Initiated in the first modeling attempt by

Table 2.1: The typical parameters of the cardiac cell

Symbol	Value	Definition
d_c	15 μm	Cell radius
I_c	15 μm	Cell length
σ_i	4 mS/cm	Intracellular conductivity
σ_e	20 mS/cm	Extracellular conductivity
C_m	1 μF/cm^2	Specific membrane capacitance
R_m	6 kΩcm^2	Specific membrane resistance
V_{rest}	-84 mV	Resting potential

FitzHugh[11] and Noble[12], continued by Beeler and Reuter[13], Luo and Rudy[3, 14, 15], and many others, until today[38] where a large number of detailed physical state variables has been introduced in the models, taking new experimental observations at cellular and sub-cellular levels into account[39, 40, 41]. Recent studies have started to use those detailed biophysical models to investigate excitation conductions in heart tissues[42, 43, 22, 44].

It is known that, the atria function principally as entry ways to the ventricles and the major function is in the ventricles, where the ventricles supply the main force that propels blood through the circulatory system of the body. Furthermore, the development of stray impulses in the heart or reentrants can cause ventricular fibrillation and the rapidity of transmission of the cardiac impulse throughout the ventricles plays an important role in preventing serious cardiac arrhythmias. As regards, in this study, we applied an ion channels-based model of the ventricular action potential, which is called the Luo-Rudy phase I (LR-I) model in developing the analog-digital circuit model. The detailed

description and formulation of the LR-I model will be described in the next subsection.

2.3.1 The Luo-Rudy Phase I Model

The Luo-Rudy phase I (LR-I) is the ion channel-based model for the action potential generation in a mammalian cardiac ventricular cell. The LR-I model is based on the Hodgkin-Huxley formulation, described by a set of nonlinear ordinary differential equations that includes eight dynamic state variables (see equation (2.16) to (2.23)) for describing six types of ion channel currents that are responsible for generating the five phases, from phase 0 to 4, during cardiac action potential. As shown in Figure 2.7, LR-I model can be represented by its equivalent electrical circuit containing a capacitive component C_m [1 μF/cm^2] representing the capacitance of the cell membrane per unit area and six resistive components representing the six types of ion channels allowing influx and efflux of ion currents across the cell membrane. V_m [mV] is the membrane potential. The voltage source in each channel represents the electro-chemical potential referred to as the Nernst potential of the corresponding ion. The six ion channel currents are summed to give the total channel current I_{ion} [μA/cm^2] as in equation (2.14) Placing I_{ion} in parallel to the current through the capacitive component of the membrane circuit C_m yields the expression of equation (2.15) for the total current flow I_m [μA/cm^2] through the membrane. Therefore, the rate of change of membrane potential V_m is given as equation (2.16).

$$I_{ion} = I_{Na} + I_{si} + I_K + I_{K1} + I_{Kp} + I_b \tag{2.14}$$

$$I_m = C_m \frac{dV_m(t)}{dt} + I_{ion} \tag{2.15}$$

$$\frac{dV_m(t)}{dt} = \frac{1}{C_m}(I_m - I_{ion}) \tag{2.16}$$

The ion channel currents are the time-dependent fast inward sodium current I_{Na}, the time-dependent slow inward current I_{si} carried mainly by calcium ions, the time-dependent potassium current I_K, the time-independent potassium current I_{K1}, the time-independent

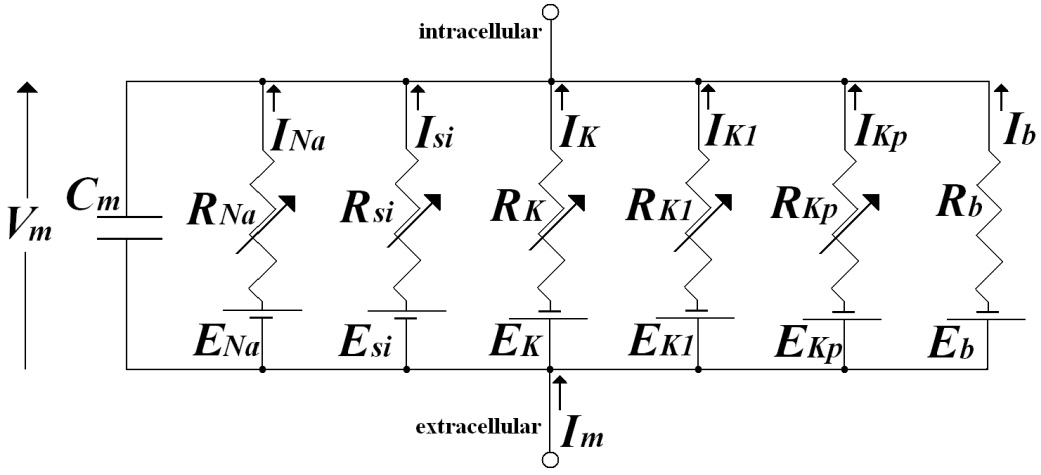

Figure 2.7: An equivalent circuit representing membrane based on Luo-Rudy Phase I (LR-I) model

plateau potassium current I_{Kp}, and the time-independent background current I_b carried by sodium, potassium and calcium ions. They are described as;

$$\begin{array}{lcllcl} I_{Na} & = & g_{Na}(V_m - E_{Na}), & I_{si} & = & g_{si}(V_m - E_{si}), \\ I_K & = & g_K(V_m - E_K), & I_{K1} & = & g_{K1}(V_m - E_{K1}), \\ I_{Kp} & = & g_{Kp}(V_m - E_{Kp}), & I_b & = & g_b(V_m - E_b), \end{array}$$

g_x [mS/cm^2], with $x = Na$, si, K, $K1$, Kp, or b, represents the channel conductance, which is equal to the inverse of the channel resistance, $1/R_x$. Note that the term time-independent current here does not actually mean that the corresponding channel conductance is constant over time, but it means that the current-voltage (I-V) relationship of the channel does not change over time. Although the conductance g_x of the voltage-dependent channel changes depending on V_m, the I-V relationship does not change over time if g_x is simply a static function of V_m, defining the time-independent current. The I-V relationship of the time-dependent current changes over time, but is asymptotic to the steady-state I-V relationship. The I-V relationship of the time-dependent current during its transient is often referred to as the transient or instantaneous I-V relationship. In LR-I model, the conductances g_{K1} and g_{Kp} are expressed by steady-state (static) functions of V_m, and g_b is constant. Thus, these three channel currents do not exhibit transient I-V relationships, but only their steady-state I-V relationships.

The channel conductances are presented as:

$$\begin{array}{lcllcl} g_{Na} & = & G_{Na}m^3hj, & g_{si} & = & G_{si}df, \\ g_K & = & G_K X X_i, & g_{K1} & = & G_{K1}K1_\infty, \\ g_{Kp} & = & G_{Kp}K_p, & g_b & = & 0.03921, \end{array}$$

$$\begin{array}{lcllcl} here, & & & & & \\ G_{Na} & = & 23, & G_{si} & = & 0.09, \\ G_K & = & 0.282\sqrt{[K]_o/5.4}, & G_{K1} & = & 0.6047\sqrt{[K]_o/5.4}, \\ G_{Kp} & = & 0.0183, & & & \end{array}$$

According to the Hodgkin-Huxley formulation, the concept of gating properties is used to determine the rate of change of open state in ion current channels. Gating is treated as a stochastic process, where channels can be only in either the closed or open state. Therefore, if the fraction of channels in open state in n, the fraction of closed channels must be (1-n) and the dynamic responses of the currents are controlled by the rate constants α and β, which are time- and voltage-dependent :

$$1 - n(closed) \underset{\beta}{\overset{\alpha}{\rightleftharpoons}} n(open)$$

In the LR-I model, channels of ion currents in the LR-I model could have several independent gating properties, each of which would have to be in the correct state to allow current flow, as for a single gating property would give a current with a simple exponential activation and deactivation rates. The I_{Na} channel is best fitted with activation being represented by three gating properties (m^3), and inactivation by two gating properties (h and j), where all are time-dependent. The I_K channel is controlled by a time-dependent activation gate (X) and a time-independent inactivation gate (X_i). The I_{si} channel is best fitted with a time-dependent activation gate (d) and a time-dependent inactivation gate (f), the I_{K1} channel with one time-independent inactivation gate ($K_{1\infty}$), and I_{Kp} channel with one time-independent inactivation gate (K_p). The time dependent gating properties

m, h, j, X, d and f are described by the ordinary differential equation, as follows:

$$\frac{dm(t)}{dt} = \alpha_m(V_m)(1 - m(t)) - \beta_m(V_m)m(t) \tag{2.17}$$
$$\frac{dh(t)}{dt} = \alpha_h(V_m)(1 - h(t)) - \beta_h(V_m)h(t) \tag{2.18}$$
$$\frac{dj(t)}{dt} = \alpha_j(V_m)(1 - j(t)) - \beta_j(V_m)j(t) \tag{2.19}$$
$$\frac{dX(t)}{dt} = \alpha_X(V_m)(1 - X(t)) - \beta_X(V_m)X(t) \tag{2.20}$$
$$\frac{dd(t)}{dt} = \alpha_d(V_m)(1 - d(t)) - \beta_d(V_m)d(t) \tag{2.21}$$
$$\frac{df(t)}{dt} = \alpha_f(V_m)(1 - f(t)) - \beta_f(V_m)f(t) \tag{2.22}$$

Equations for the time independent gating properties for X_i, $K1_\infty$ and K_p are shown as follows:

$$\begin{aligned} for\, V_m &> -100\,[\mathrm{mV}] \\ X_i &= 2.837\frac{\exp(0.04(V_m + 77)) - 1}{\exp(0.04(V_m + 35))(V_m + 77)} \\ for\, V_m &\leq -100\,[\mathrm{mV}] \\ X_i &= 1 \end{aligned}$$

$$\begin{aligned} K1_\infty &= \frac{\alpha_{K1}}{\alpha_{K1} + \beta_{K1}} \\ Kp &= \frac{1}{1 + \exp\left(\frac{7.488 - V_m}{5.98}\right)} \end{aligned}$$

Here, the rate constants α and β for the gating properties described priorly are defined in the following equations.

$$\begin{aligned} \alpha_m &= \frac{0.32(V_m + 47.13)}{1 - \exp(-0.1(V_m + 47.13))} \\ \beta_m &= 0.08\exp\left(\frac{-V_m}{11}\right) \end{aligned}$$

$$
\begin{aligned}
for\ V_m &\geq -40\ [\mathrm{mV}] \\
\alpha_h &= \alpha_j = 0 \\
\beta_h &= \frac{1}{0.13\Big(1+\exp\big(\frac{V_m+10.66}{-11.1}\big)\Big)} \\
\beta_j &= \frac{0.3\exp(-2.535\cdot 10^{-7}V_m)}{1+\exp(-0.1(V_m+32))} \\
for\ V_m &< -40\ [\mathrm{mV}] \\
\alpha_h &= 0.135\exp\big(\frac{80+V_m}{-6.8}\big) \\
\beta_h &= 3.56\exp(0.079V_m)+3.1\cdot 10^5\exp(0.35V_m) \\
\alpha_j &= \frac{(-1.2714\cdot 10^5\exp(0.2444V_m)-3.474\cdot 10^{-5}\exp(-0.04391V_m))(V_m+37.78)}{1+\exp(0.311(V_m+79.23))} \\
\beta_j &= \frac{0.1212\exp(-0.01052V_m)}{1+\exp(-0.1378(V_m+40.14))}
\end{aligned}
$$

$$
\begin{aligned}
\alpha_d &= \frac{0.095\exp(-0.01(V_m-5))}{1+\exp(-0.072(V_m-5))} \\
\beta_d &= \frac{0.07\exp(-0.017(V_m+44))}{1+\exp(0.05(V_m+44))} \\
\alpha_f &= \frac{0.012\exp(-0.008(V_m+28))}{1+\exp(0.15(V_m+28))} \\
\beta_f &= \frac{0.0065\exp(-0.02(V_m+30))}{1+\exp(-0.2(V_m+30))}
\end{aligned}
$$

$$
\begin{aligned}
\alpha_X &= 0.0005\exp(0.083(V_m+50))(1+\exp(0.057(V_m+50))) \\
\beta_X &= 0.0013\exp(-0.06(V_m+20))(1+\exp(-0.04(V_m+20)))
\end{aligned}
$$

$$
\begin{aligned}
\alpha_{K1} &= \frac{1}{1+\exp(0.2385(V_m-E_{K1}+59.215))} \\
\beta_{K1} &= \frac{(0.49124\exp(0.08032(V_m-E_{K1}+5.476))+\exp(0.06175(V_m-E_{K1}-594.31)))}{1+\exp(-0.5143(V_m-E_{K1}+4.753))}
\end{aligned}
$$

Furthermore, E_x [mV] , with $x = Na$, si, K, $K1$, Kp, or b, represents the Nernst potential of the corresponding ion current channel, described as follows:

$$
\begin{aligned}
E_{Na} &= (RT/F)\ln([Na]_o/[Na]_i), & E_{si} &= 7.7-13.0287\ln([Ca]_i), \\
E_K &= (RT/F)\ln\Big(\tfrac{[K]_o+PR_{NaK}[Na]_o}{[K]_i+PR_{NaK}[Na]_i}\Big), & E_{K1} &= (RT/F)\ln([K]_o/[K]_i), \\
E_{Kp} &= E_{K1}, & E_b &= 59.87,
\end{aligned}
$$

where,

$[Ca]_i$: *the calcium concentration inside the cell* [mM]

R : *gas constant* 8.314 [J/kmol]

T : *absolute temperature* [K]

F : *the Faraday constant* 96485 [C/mol]

PR_{NaK} : *the* Na/K *permeability ratio* 0.01833

$[K]_o$: *the potassium concentration outside the cell*, 5.4 [mM]

$[K]_i$: *the potassium concentration inside the cell*, 145 [mM]

$[Na]_o$: *the sodium concentration outside the cell*, 140[mM]

$[Na]_i$: *the sodium concentration inside the cell*, 18 [mM]

Here, the changes in calcium concentration inside the cell are described by the ordinary differential equation, as follows:

$$\frac{(d[Ca]_i)}{dt} = -10^{-4} I_{si} + 0.07(10^{-4} - [Ca]_i) \tag{2.23}$$

2.4 Hardware-Implemented Excitable Membrane Models

Another approach that has been used to simulate the action potential is by using hardware implementation of specialised electronic circuit models for membrane excitation. Circuit models can provide solutions to problems in which conventional programmed systems find very hard to deal with. Implementing a hardware-realisable technique in dedicated the excitable membrane modelling has a number of important advantages, providing valuable tools for real-time simulations whose computational speeds are independent of the size of the systems, i.e., the number of excitable nodal compartments used in the systems. Also, with the growing technologies of LSI, it provides self-contained, physically robust solutions for application areas where it might not be feasible to install a PC/workstation running neural or cardiac excitatory network software, that gives a contribution for autonomous robots in industrial and exploration uses or for medical engineering applications.

Since the 1960s, various developments and studies have been conducted for modeling and implementing membrane excitation on analog circuits[17, 18, 19]. In particular, Nagumo et al[18] demonstrated that their active transmission line involving nine active nodal compartments could simulate propagating action potentials along a nerve axon, in which each active node was implemented by a tunnel diode with an N-shaped current-voltage (I-V) relationship mimicking the one in Bonhoeffer-van der Pol model[45].

Although less attempt[46] has been made for hardware implementations of spatially distributed excitable media after Nagumo et al, developments of circuit models mimicking neuronal and cardiac cellular dynamics have continued. Hoshimiya et al[47] proposed an electronic circuit model of excitable membrane realized by a single time-dependent (transient) I-V relationship determining a total membrane current through different types of ion channels. Yagi[48], Maeda et al[49, 50] and Sekine et al[51, 52] constructed analog circuit models with two or three ion channel currents with their I-V relationships activated at different time scales for their transient change in order to simulate bursting or pacemaker type neuronal excitations.

These circuit models are beneficial for studying nonlinear dynamics of excitable media qualitatively. Commonly, the goal in hardware-oriented membrane excitation models is not to simulate the cellular process that lead to the generation of action potential, but just the dynamics of the action potential. In those models, the action potential is the result of predefined rules or mathematical functions that do not correlate precisely with membrane or intracellular processes, due to qualitative designs of their I-V relationships of ion channel currents. The reason is that unlike the mathematical models, it is usually difficult to establish explicit correspondence between currents in a hardware circuit model and ion channel currents of an excitable cell. Only a few studies have succeeded to design analog circuits that are biophysically detailed and have quantitative correspondence to a real cell[20].

As for this reason, in this study, an attempt has been made to develop a specialized electronic circuit for real-time simulation in membrane excitation model and at the same time intend to complement the disadvantage in implementing analog circuits of membrane excitations, by developing hardware-oriented of an analog-digital hybrid model reproducing quantitatively action potential generation in a cardiac cell membrane. This was achieved by reproducing the I-V relationships of ion currents using both analog and digital circuits based on the standard ion model of membrane excitation in ventricular cardiac cell, LR-I model. The design element will be elaborated further in the following chapter.

Chapter 3

Cardiac Action Potential in Analog-Digital Hybrid Circuit Model

3.1 Introduction

Generally, changes in membrane potential of cardiac cells are a result of the flow of ions through ion channel with conductivity that is voltage and/or time dependent and changes in ion concentrations. Figure 3.1 is a diagram of a cardiac cell representing the main ion channels embedded in the cell membrane. Cardiac cell respond characteristically to applied electrical impulsive currents. If an electrical stimulus has an intensity that is above certain threshold, ion channels are activated and the cell generates an active response called an action potential, and the cell is excited. Computational modeling approach has been used extensively to compute the cardiac action potential for a better understanding of cardiac electrophysiology. In general, ion channel-based models of cardiac cell are formulated with nonlinear mathematical equations that describe the cellular processes by relying on experimental and clinical measurement, leading to the generation of the action potential. This study are focusing on using a standard ion channel-based model, the Luo-Rudy phase I model of the ventricle action potential.

It is known that, the ion channel-based models have been useful to analyze many of phenomena in the dynamical cardiac electrophysiology as they contribute to several approaches that differ in amount of biophysical detail according to differenr regions and

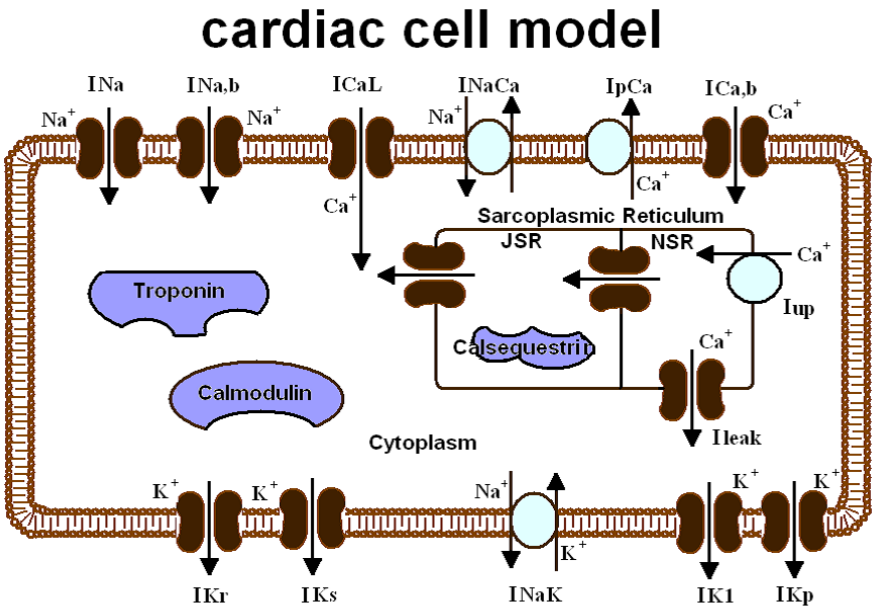

Figure 3.1: A cardiac cell model. The arrow indicate the flow direction of the ion currents, in inward or outward

function of the heart. However, in many situations the ion channel-based model of the action potential will be used to study propagation of cardiac action potential waves and interaction among them. These single cell models need to be coupled together to perform a large scale of simulation of the excitation propagation that would require an immense amount of computational time to run. Therefore, an analog-digital hybrid circuit model that is capable of generating the action potential of ventricle cell quantitatively is developed to perform real-time simulations of the electrical excitation propagation waves. This was achieved by reproducing current-voltage (I-V) characteristics of ion currents based on Luo Rudy phase I (LR-I) model using both analog and digital circuits.

In this chapter, a general construction of the analog-digital hybrid circuit cell is overviewed and the design method of reproducing the current-voltage (I-V) relationships of ion currents based on the LR-I model by analog and digital circuits are also explained. To review the validity of the hybrid circuit model in a context of action potential generation and its response corresponding to the periodic current impulse trains, the simulations by the LR-I model are also performed for the comparison.

3.2 Design Method

The analog-digital hybrid active circuit for a single cardiac cell model, referred to here as the hybrid cell model, includes analog circuits and a digital circuit of dsPIC microcontroller. Figure 3.2 illustrates the analog-digital hybrid circuit model proposed in this study. The model is presented as the parallel combination of a capacitance C_m and the branches of analog and digital part representing the ion channels in Figure 2.7. Four out of the six branches, corresponding to the ion channels I_{K1}, I_{Kp}, I_b and I_{Na}, were designed by using analog circuits, and the remaining two branches, corresponding to the ion channels I_K and I_{si}, were lumped together by using the single dsPIC. Action potentials of the hybrid cell model were produced by injecting external current stimulations, I_{ext}, which should be equal to I_m in equation (2.15). Figure 3.3 shows the picture of the hybrid cell model.

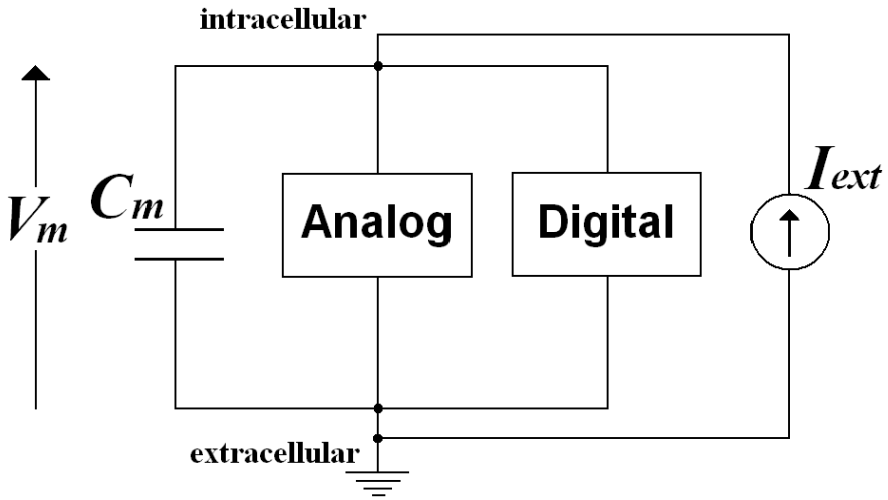

Figure 3.2: An equivalent circuit of the analog-digital hybrid cell model. Ion channel currents are implemented by analog and digital circuits that are placed in parallel with C_m representing the membrane capacitance.

In the LR-I model, the amount of each ion current depends on V_m. Some are time-independent (i.e., they are constant if V_m is constant), and some are time-dependent (i.e., dynamic). For both cases, it may be possible to characterize each ion current by a rela-

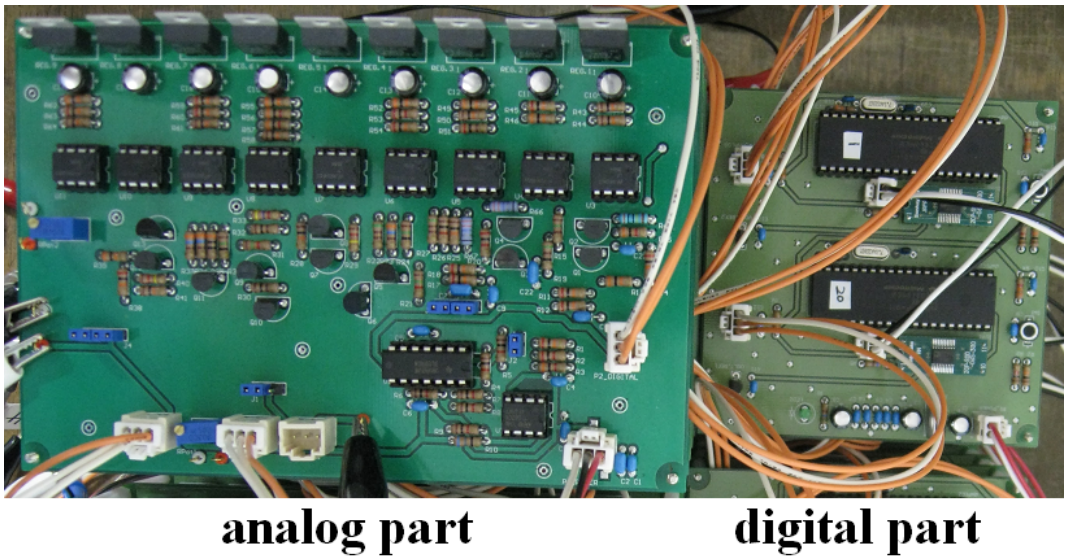

Figure 3.3: Photograph of the analog-digital hybrid circuit for a single cardiac cell model.

tionship between voltage V_m and resulting channel current, known as the current-voltage (I-V) relationship. The time-independent current has a steady-state I-V relationship and the time-dependent current is often referred to as a transient I-V relationship but is asymptotic to the steady-state I-V relationship. A validation criterion for each of the six branches in the hybrid cell model to be quantitatively close to the corresponding ion channel in LR-I model was set if the transient and/or steady-state nonlinear I-V relationships of the ion channel in LR-I could be reproduced quantitatively by the circuit branch in the hybrid cell model. The established electronic circuits should reproduce the relationships. In this study, analog circuits were used to implement the time-independent ion currents of I_{K1}, I_{Kp}, and I_b, and the time-dependent fast sodium current I_{Na} which has a relatively short time constant. Each of these analog circuits was designed by exploiting the intrinsic (I-V) relationships of bipolar transistors (Tr), resistors (R), capacitors (C) and voltage sources (V) to reproduce the steady-state I-V relationships for I_{K1}, I_{Kp}, and I_b, and the transient as well as the steady-state I-V relationships for I_{Na}. The variables in the LR1 model such as gating variables, conductances, ion currents, and membrane voltage were identified to electrical variables in the circuits (conductances, currents, and voltages). An electronic circuit simulation tool (Altium Designer version 6, Australia) was utilized to

design these analog circuits.

The time-dependent ion currents with long time constants, I_K and I_{si} were reproduced by the digital part of the hybrid cell model using a 16-bit high-performance dsPIC30f4011 microcontroller (Microchip Technology, USA) with a processing frequency of 120 MHz. This processing speed was thought to be considerable as initiatives have been taken to speed up the calculation process held by the dsPIC. To increase the speed of calculation, Certain datas were accessed from constructed tables stored in the memory (ROM) rather than calculating the functions in equations which represent the ion channel currents.

The time scale of the hybrid model was set to the same as the LR-I model. The current and voltage scales of the hybrid model (milli-ampere and volt) are not the same as those of the LR-I model (micro-ampere and milli-volt). The scale conversions of the voltage and the current were made because values of the ion currents and the membrane potential in the LR-I model are too small and difficult to handle in the scale of the analog circuits. In particular, the scales were converted as follows: 8 μA of LR-I to 3 mA of the hybrid cell model, -100 mV of LR-I to 0 V of the hybrid and 120 mV of LR-I to 5 V of the hybrid cell model. In formulae, the scale conversions of the voltage and the current are expressed as follows:

$$\begin{array}{lcl} \dfrac{V_{LR-I}\ [\mathrm{mV}] + 100}{220} \times 5 & \rightarrow & V_{hybrid}\ [\mathrm{V}] \\ I_{LR-I}\ [\mu\mathrm{A}] \times \left(\dfrac{3}{8}\right) & \rightarrow & I_{hybrid}\ [\mathrm{mA}] \end{array} \tag{3.1}$$

3.3 Circuit Diagrams of The Hybrid Cell Model

Figure 3.4 illustrates the overall circuit of the hybrid cell model with its marginal circuits, where the core part is just depicted as two boxes denoted by the digital and analog parts. Detailed circuit diagrams of the analog and digital parts of the core circuit are shown separately in Figure 3.5 and Figure 3.6, respectively. The circuit branches of (a), (b), (c), and (d) in Figure 3.5 represent I_{K1}, I_{Kp}, I_b, and I_{Na}, respectively. The overall hybrid cell model is powered by the direct current (DC) power supplies of 9 (V+) and

-9 V (V-) as shown in Figure 3.4. Circuit diagrams necessary for providing the voltage sources (V_1 to V_9) in the analog part of Figure 3.5 and a power circuit for generating V_{CC} (5 V) in the digital part of Figure 3.6 are shown in the appendix A. Details of all electronic components used to construct the analog-digital cell model and the source program executed by the dsPIC are provided in the appendix B and C, respectively.

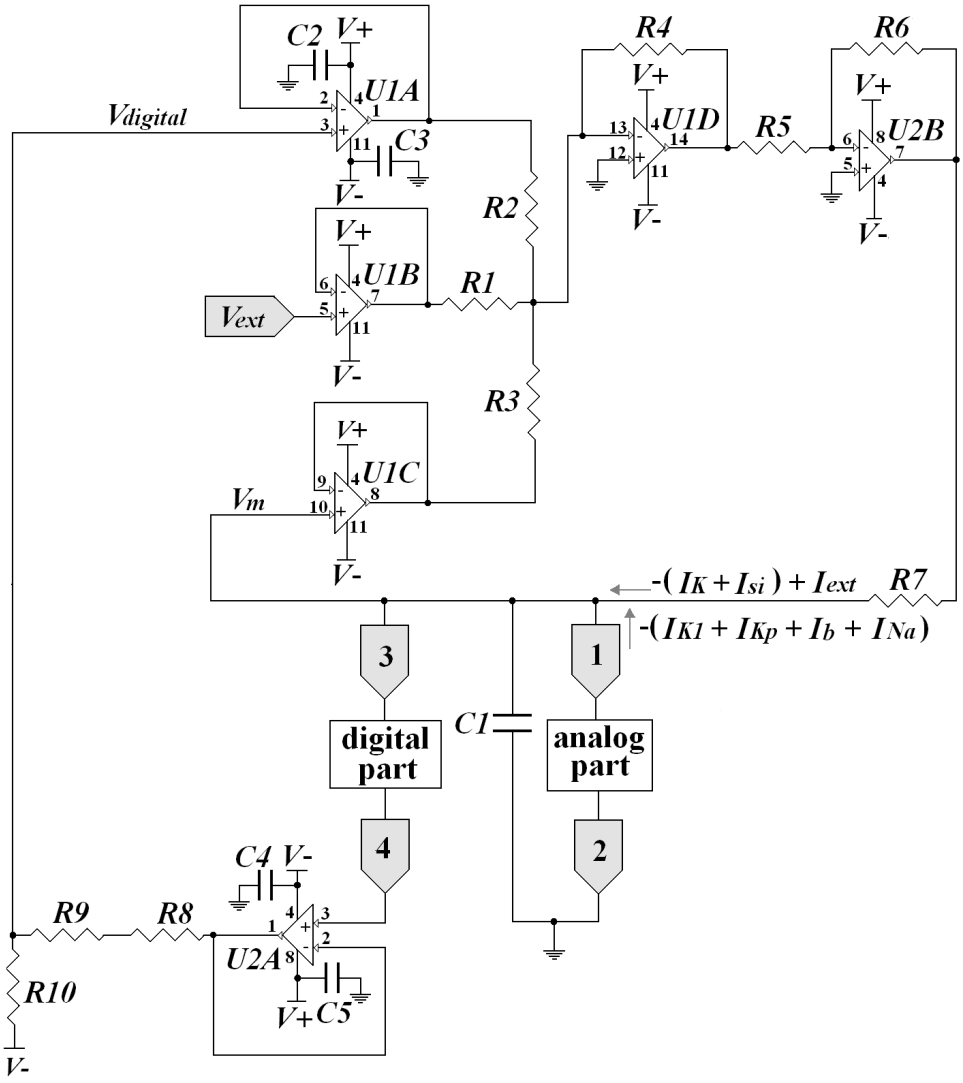

Figure 3.4: The overall circuit diagram of the analog-digital hybrid cell model.

The hybrid cell model behaves in a way that is described as follows: By referring to Figure 3.4, the operation of the hybrid cell model starts with an input voltage signal at the terminal 1 of Figure 3.4 and Figure 3.5, corresponding to the cardiac cell membrane

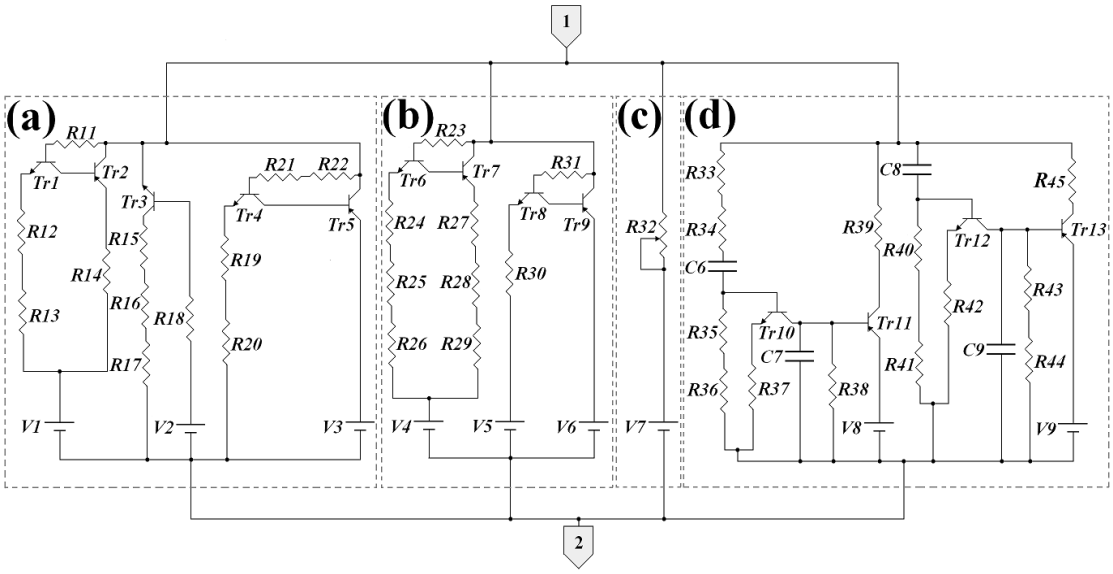

Figure 3.5: The circuit diagram of the analog part in the analog-digital hybrid cell model.

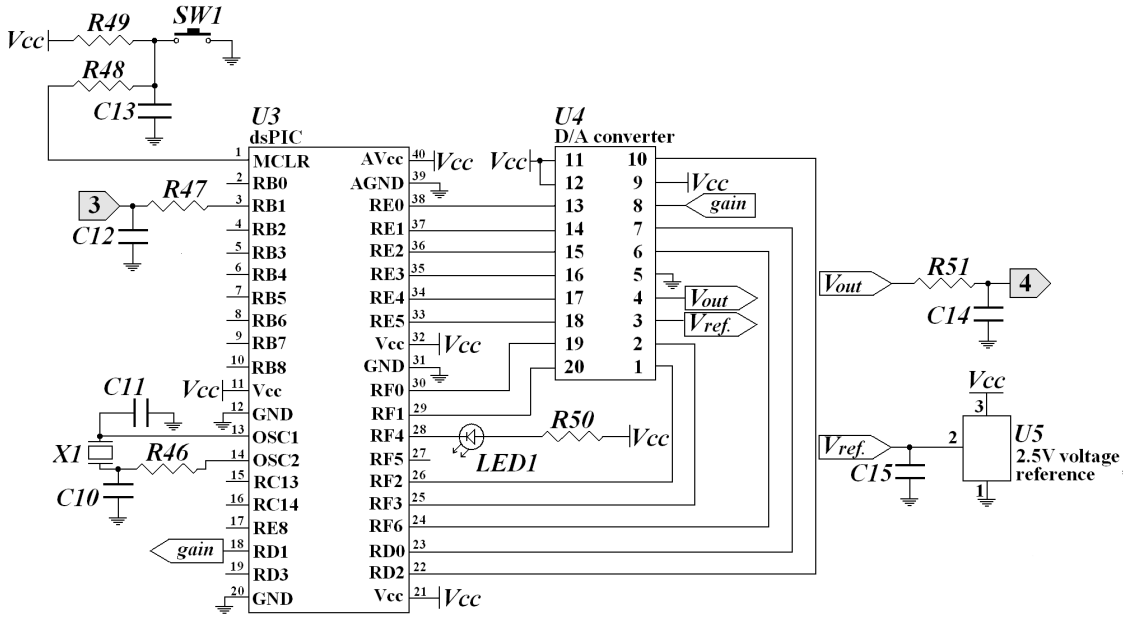

Figure 3.6: The circuit diagram of the digital part in the analog-digital hybrid cell model.

potential V_m. This V_m is fed into a port of a 10-bit analog to digital converter of the dsPIC at the terminal 3 of Figure 3.4, sampled with a frequency of 2.5 kHz. I_K and I_{si} are then computed in the dsPIC at each instant of time for a given V_m to generate the output voltage from the digital part at the terminal 4 of Figure 3.4 through a 10-bit digital to analog converter. This output voltage is proportional to the sum of I_K and I_{si}, determining the value of $V_{digital}$ that is fed-back into the analog circuit. The amount of externally injected pulsatile stimulus current I_{ext} is given by a command voltage pulse V_{ext}. The voltages $V_{digital}$, V_{ext}, and the membrane potential V_m are summed up to generate the potential difference between $V_{digital}+V_{ext}+V_m$ and V_m as $V_{digital}+V_{ext}$ which induces the current $-I_K - I_{si} + I_{ext}$ by using the resistor R_7. Kirchhoff's laws applied at the T-shaped branch at the upper part of the capacitance C_1 of Figure 3.4 ensures that the sum of $-I_K - I_{si} + I_{ext}$, $-I_{Na} - I_{K1} - I_{Kp} - I_b$, and $-C_1 dV_m/dt$ is equal to zero. That is, equally to

$$-C_1 \frac{dV_m}{dt} - I_{ion} + I_{ext} = 0, \tag{3.2}$$

holds as in equation (2.15).

3.4 The Current-Voltage (I-V) Relationships

Basically, the I-V relationship of I_b was realized by using a simple analog circuit which consists of a resistor and a voltage source. For the I_{K1}, I_{Kp} and I_{Na}, three elementary patterns of circuits were used to reproduce these I-V relationships and they were connected in parallel. Meantime, the I-V relationships of I_K and I_{si} were reproduced with the dsPIC by calculating amount of the currents that flow for each time instant according to the changes of the membrane potential V_m.

An example of the first type of these three elementary analog circuit patterns is shown in Figure 3.7(a). Basically, the flow of current I was controlled by Tr_1 which acted as a switch. When the input value of V_1 was smaller than V_2, the current I flowed inversely and was almost terminated as V_1 became larger. The amount of I could be controlled by

changing the value or modifying the location of the resistors. The shape of generated I-V relationship is shown as in Figure 3.7(b).

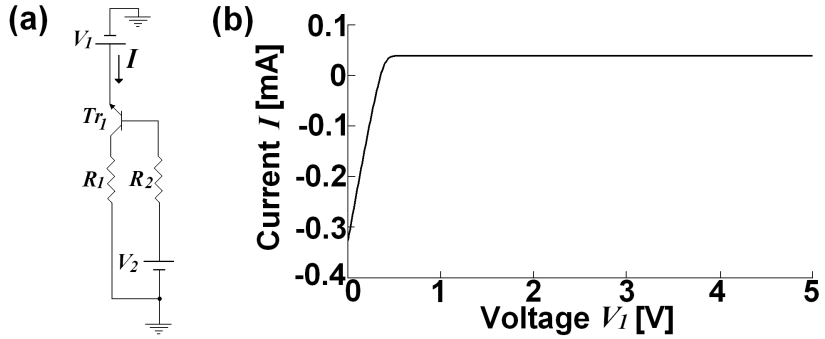

Figure 3.7: An example of the elementary circuit used to reproduce ion current (1st type). (a) and (b) are the circuit pattern and its I-V relationship, respectively: V_1= 0-5 V, V_2=1 V, R_1=10 k Ω, R_2=1 k Ω, Tr_1: npn-2SC1815.

An example of the second type of the elementary circuit patterns is shown in Figure 3.8(a). By referring the I-V relationship produced by this type of circuit as in Figure 3.8(b), there was no flow as the input value of V_1 was smaller than V_2, which caused Tr_1 and Tr_2 to terminate. However, when the input value of V_1 became larger, Tr_1 and Tr_2 turned on, and allowed the current I to flow backward gradually as the value of V_3 was larger than V_1. The amount of I could also be controlled by changing the value or modifying the location of the resistors.

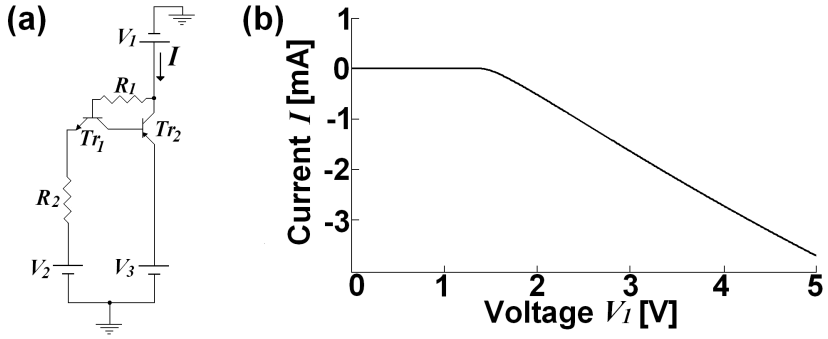

Figure 3.8: An example of the elementary circuit used to reproduce ion current (2nd type). (a) and (b) illustrate the circuit pattern and its I-V relationship, respectively: V_1= 0-5 V, V_2=1 V, V_3=6 V, R_1=1 k Ω, R_2=100 k Ω, Tr_1: npn-2SC1815, Tr_2: pnp-2SA1015.

Figure 3.9(a) and Figure 3.9(b) show the third type of the elementary circuit patterns and its I-V realtionship, respectively. The operational mechanism of this circuit was quite

similar to the second type, but when the input value of V_1 was larger than V_2, the current I flowed forward due to the absence of V_3 included in the 2nd type circuit (Figure 3.8(a)).

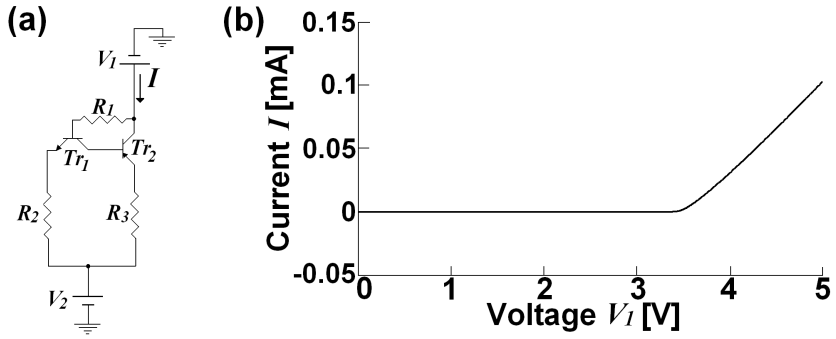

Figure 3.9: An example of the elementary circuit used to reproduce ion current (3rd type). (a) and (b) are the circuit pattern and its I-V relationship, respectively: V_1= 0-5 V, V_2=3 V, R_1=10 k Ω, R_2=100 k Ω, R_3=100 Ω, Tr_1: npn-2SC1815, Tr_2: pnp-2SA1015.

3.4.1 I-V Relationship of I_{K1}

The LR-I time-independent potassium current, I_{K1}, plays a role to maintain the resting potential as it flows at negative potential. The analog circuit used to implement the I-V relationship of I_{K1} is shown in the Figure 3.5(a). Referring to the Figure 3.10 for results of the I-V relationships of I_{K1}, the hybrid model (dashed line) was roughly comparable to the LR-I model (solid line). The appropriate relationship could be obtained by adjusting the parameters of the circuit.

3.4.2 I-V Relationship of I_{Kp}

The LR-I time-independent plateau potassium current I_{Kp} is activated during the plateau phase of the action potential along with the other potassium currents to restore the cell to its resting state. This current does not flow at low but at high membrane potential. The analog circuit shown in Figure 3.5(b) was constructed to reproduce the I-V relationship of I_{Kp}. A comparative graph of the I-V relationships in the I_{Kp} for the LR-I model (solid line) and the hybrid model (dashed line) is shown in the Figure 3.11. Both models were found comparable.

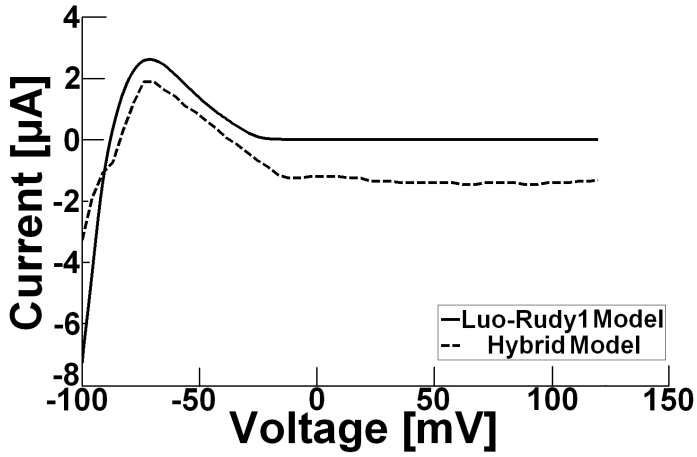

Figure 3.10: The I-V relationship of I_{K1} from the Luo-Rudy phase I model and the hybrid model.

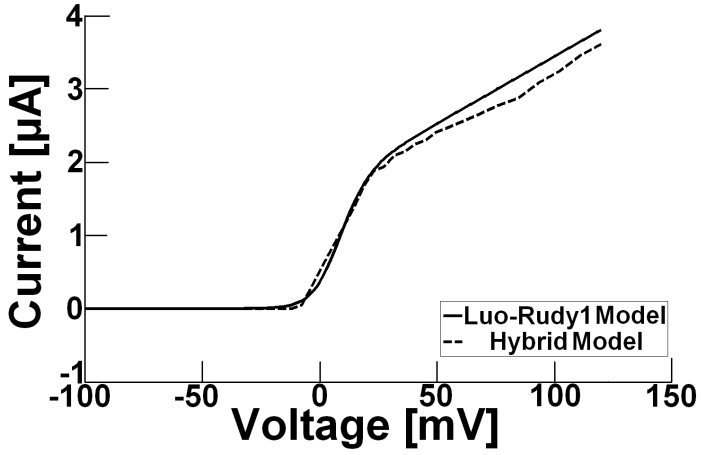

Figure 3.11: The I-V relationship of I_{Kp} from the Luo-Rudy phase I model and the hybrid model.

3.4.3 I-V Relationship of I_b

The background current I_b in LR-I, is a composite current representing the hodgepodge of other currents left in the cell. The I-V relationship of this current is a linear function of membrane potential, and it can be realized by using a simple analog circuit which consists of a resistor and a voltage source as shown in Figure 3.5(c). Plots of I-V relationships of I_b is shown in Figure 3.12. From the Figure 3.12, the I-V relationship of I_b from the hybrid model (dashed line) was generally comparable to the feature of LR-I model (solid line).

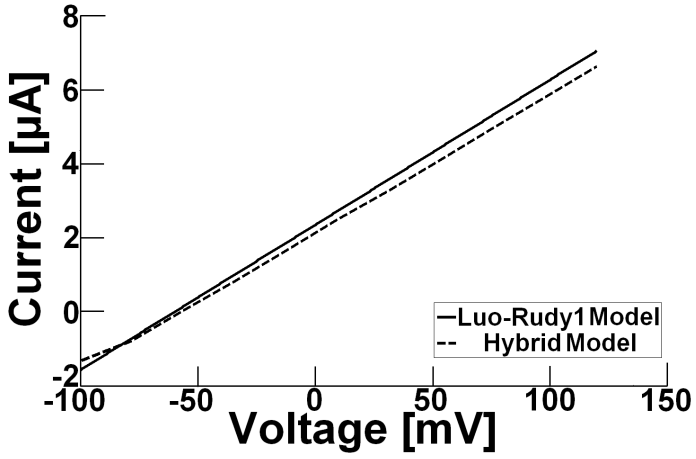

Figure 3.12: The I-V relationship of I_b from the Luo-Rudy phase I model and the hybrid model.

3.4.4 I-V Relationship of I_{Na}

The fast inward sodium current I_{Na} in the LR-I causes the rapid upstroke of the action potential. A short time-constant behavior of I_{Na} was reproduced by adopting the analog circuit as shown in the Figure 3.5(d). RC-differentiation circuits were also applied to produce surge-type transient signal. Dynamics of I_{Na} were analyzed by plotting the ion current over time in response to the voltage step inputs (the voltage clamp experiment) with various clamp voltage from -60 mV to 80 mV as shown in Figure 3.13. In Figure 3.13, the panel (a) is for I_{Na} of the hybrid model, and (b) is for that of the LR-I model.

By comparing the features from both models, it has been found that, I_{Na} in the hybrid model was not quantitatively comparable with those in the LR-I model. However, the time-dependent changes in the current for different voltage step in both models were considerably similar. In Figure 3.14, the panels (a) and (b) show the I-V relationships obtained from the maximum values of I_{Na} along the time-dependent responses against the intensity of the voltage in the hybrid model and that in the LR-I model, respectively. They also showed qualitatively similar dependency on V_m, but they were not quantitatively comparable.

Despite the quantitative difference in I_{Na} between the LR-I and the hybrid models, the reproduced I_{Na} of the hybrid model was considered to be acceptable. It was considered that, although I_{Na} values produced by the voltage steps in the LR-I model were generally larger than those in the hybrid model, total amount of I_{Na} that flowed in a time period of action potential onset in both models were almost the same, as the time constant of I_{Na} was longer in the hybrid model than in the LR-I model.

3.4.5 I-V Relationship of I_K

The LR-I time-dependent potassium current I_K, is activated by the increase of the membrane potential and it is not activated until the cell returns to its resting state. A long time-constant behavior of I_K was reproduced with the use of dsPIC implementation. The dynamic response of the current to the voltage step shown in Figure 3.15(a) and 3.15(b), respectively, are for the hybrid model and for the LR-I model. Both responses were noted to be generally comparable. The graphs shown in Figure 3.16(a) and 3.16(b), depicts the maximum values of I_K against voltage step (I-V relationship) in the hybrid model and in the LR-I model, respectively, and they were also comparable.

3.4.6 I-V Relationship of I_{si}

The slow inward current I_{si} flows due to the entry of Na^+ during the plateau phase. I_{si} changes slowly over time and therefore it was also emulated by the dsPIC. The slow

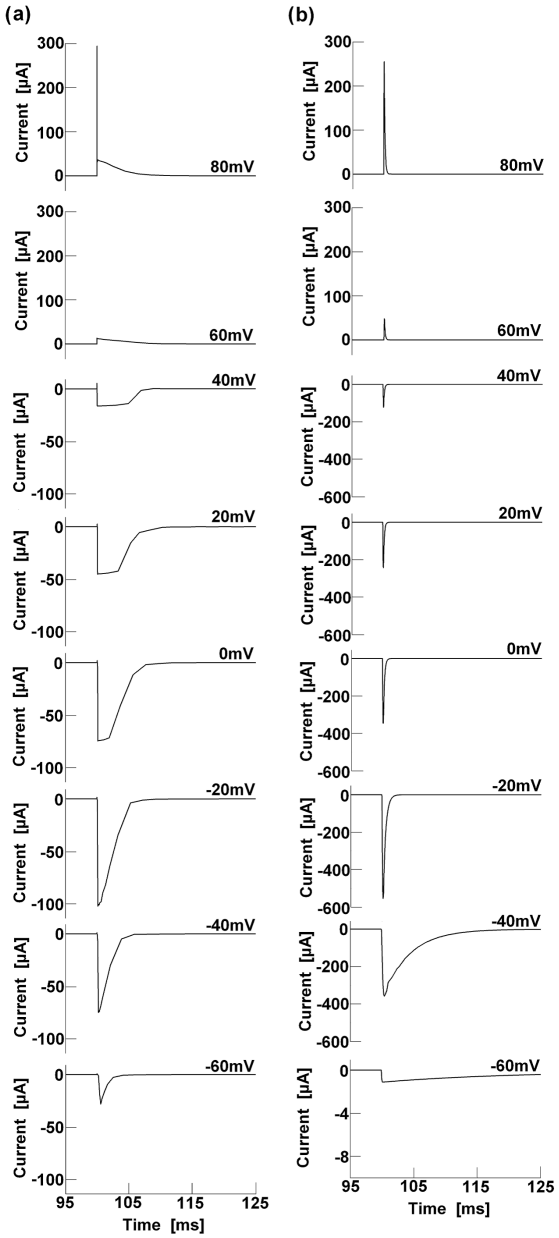

Figure 3.13: Comparison in the I_{Na} as the function of time between the hybrid model and the Luo-Rudy phase I model in response to various intensity of the voltage step (from -60mV to 80mV) for an initial holding voltage of -100 mV.

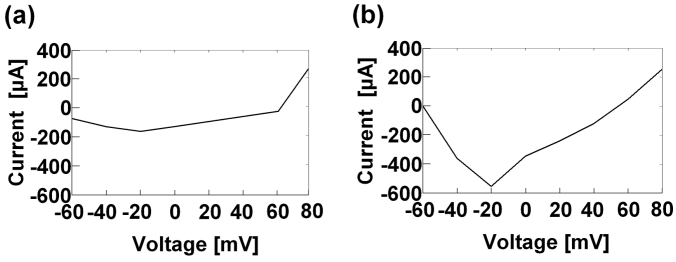

Figure 3.14: Comparison of the maximum values of the I_{Na} against the intensity of the voltage step between the hybrid model and the Luo-Rudy phase I model.

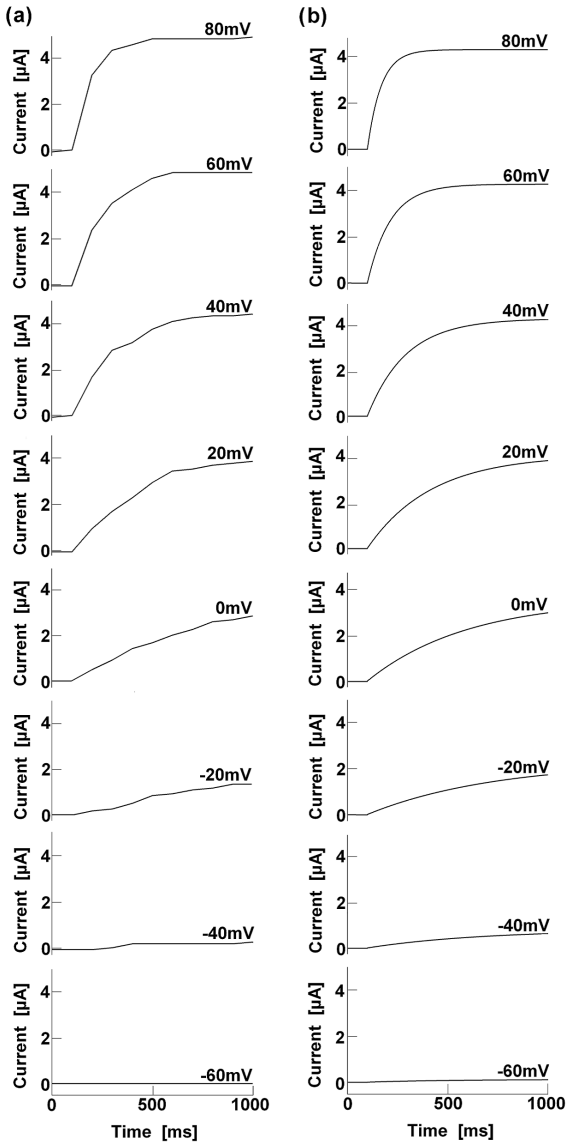

Figure 3.15: Comparison in the I_K as the function of time between the hybrid model and the Luo-Rudy phase I model in response to various intensity of the voltage step (from -60mV to 80mV) for an initial holding voltage of -100 mV.

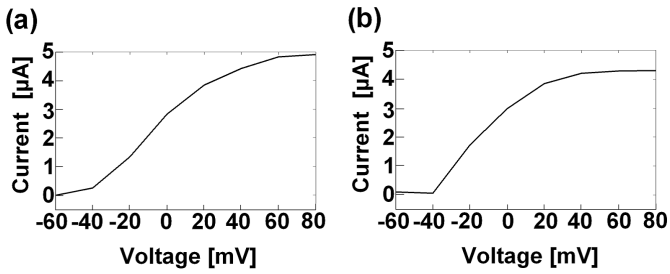

Figure 3.16: Comparison of the maximum values of the I_K against the intensity of the voltage step between the hybrid model and the Luo-Rudy phase I model.

dynamics of I_{si} are shown in Figure 3.17(a) and 3.17(b), where the panel (a) indicates the result in the hybrid model and the panel (b) is for the LR-I model. From this figure, it can be considered that the I-V relationship of I_{si} in the hybrid model was generally comparable to the feature of the LR-I model. The maximum values of I_{si} against voltage step in the hybrid model (Figure 3.18(a)) were also compared with those in the LR-I model (Figure 3.18(b)), and the hybrid model showed performance comparable with the LR-I model.

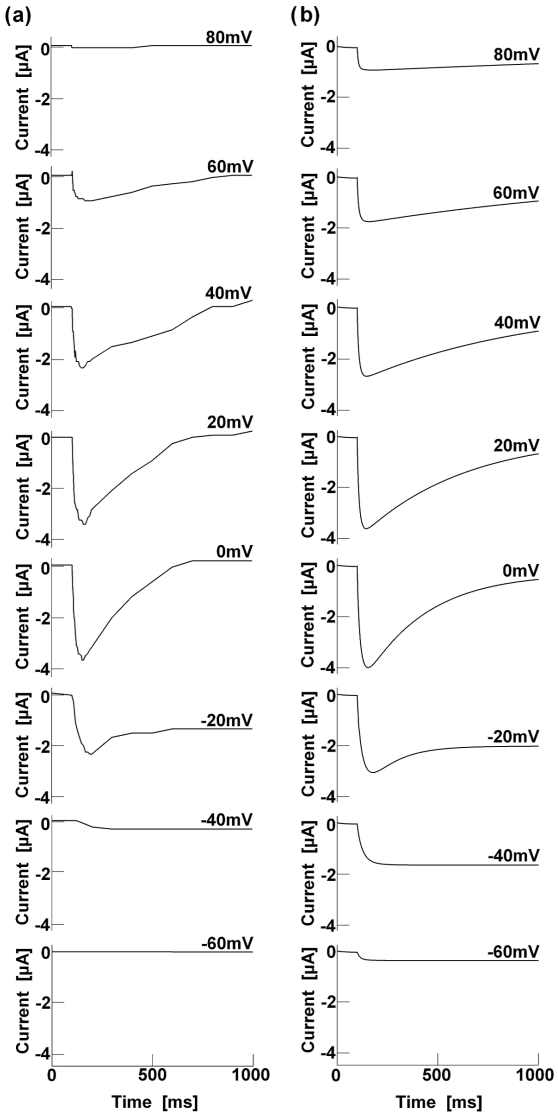

Figure 3.17: Comparison in the I_{si} as the function of time between the hybrid model and the Luo-Rudy phase I model in response to various intensity of the voltage step (from -60mV to 80mV) for an initial holding voltage of -100 mV.

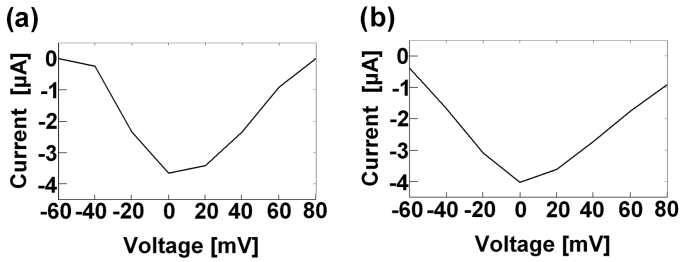

Figure 3.18: Comparison of the maximum values of the I_{si} against the intensity of the voltage step between the hybrid model and the Luo-Rudy phase I model.

3.5 Action Potential Waveform

The action potential (AP) generation is initiated by an external stimulus applied to the membrane cell, which can bring the cell to the threshold point where I_{Na} is activated and causes the rapid depolarization of the AP. Then, the upstroke is followed by an early repolarization phase, caused by an outward potassium current and the following plateau phase depends on a balance between inward and outward currents. The AP waveform for a single membrane cell produced by the hybrid cell model is shown in the Figure 3.19(a). The AP produced by the LR-I model is shown in Figure 3.19(c). The AP produced by the hybrid model in the panel (a) was converted to the scales of LR-I as shown in Figure 3.19(b). In this study, an impulsive stimulation with a duration of 1 ms and an intensity of 80 μA was applied to the hybrid cell model and to the LR-I model, showing that the action potential waveform produced by the hybrid cell model was quantitatively the same as that by LR-I model. In particular, both models showed almost the same action potential duration around 350 ms.

3.6 Response Characteristics to Trains of Stimulations

Simulated action potential patterns in response to periodic current impulse trains with different interval (period) T are shown in Figure 3.20, where the panels (a) and (b) represent, respectively, the AP patterns for the hybrid model and for the LR-I model. By comparing the response patterns in both models, it could be noted that the hybrid

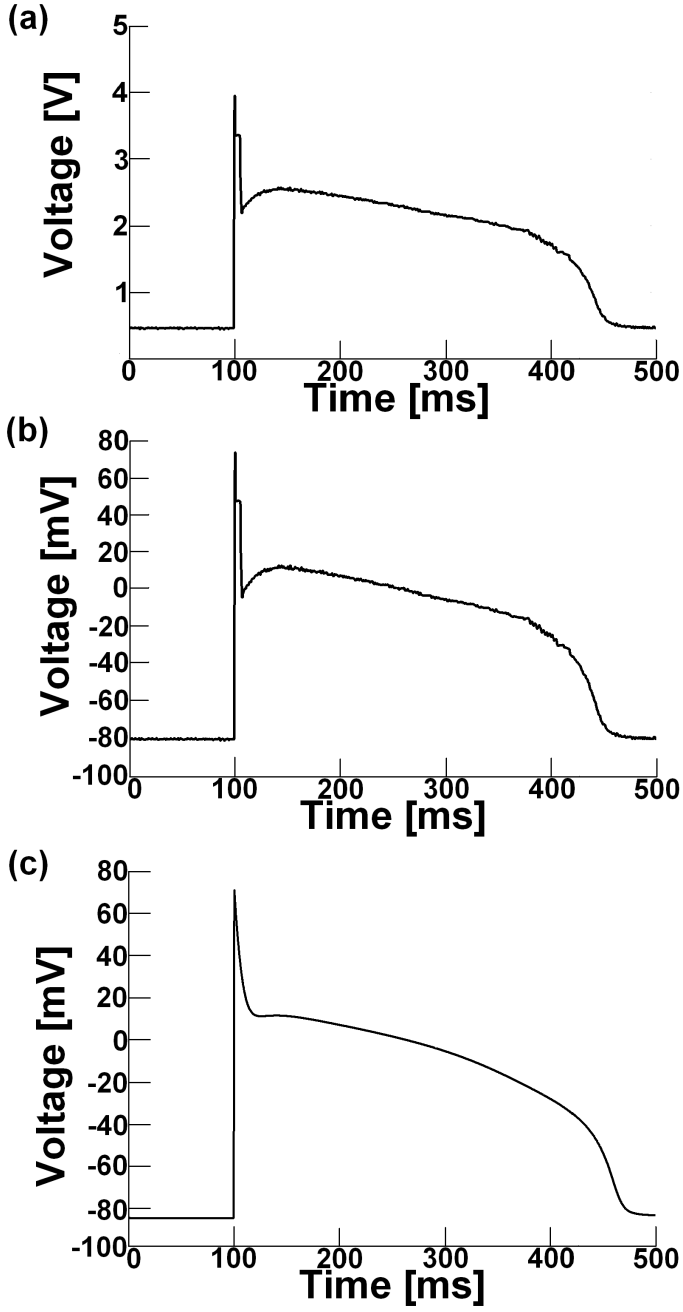

Figure 3.19: Action potential waveforms of LR-I and the hybrid cell model. Panels (a) and (c) represent the action potential waveforms generated by the analog-digital hybrid cell model and the LR-I model, respectively, in response to a single current pulse. Panel (b) shows the action potential waveform in the hybrid cell model after the scale conversion.

model could simulate almost similar AP wave patterns to those of the LR-I model. Moreover, irregular response patterns here showed the non-uniformity of the AP responses to particular repetitive impulse stimulations with relatively small time intervals. This may imply to refractoriness of a cell, the condition which the cell cannot fully induce the action potential wave before it had regained excitability.

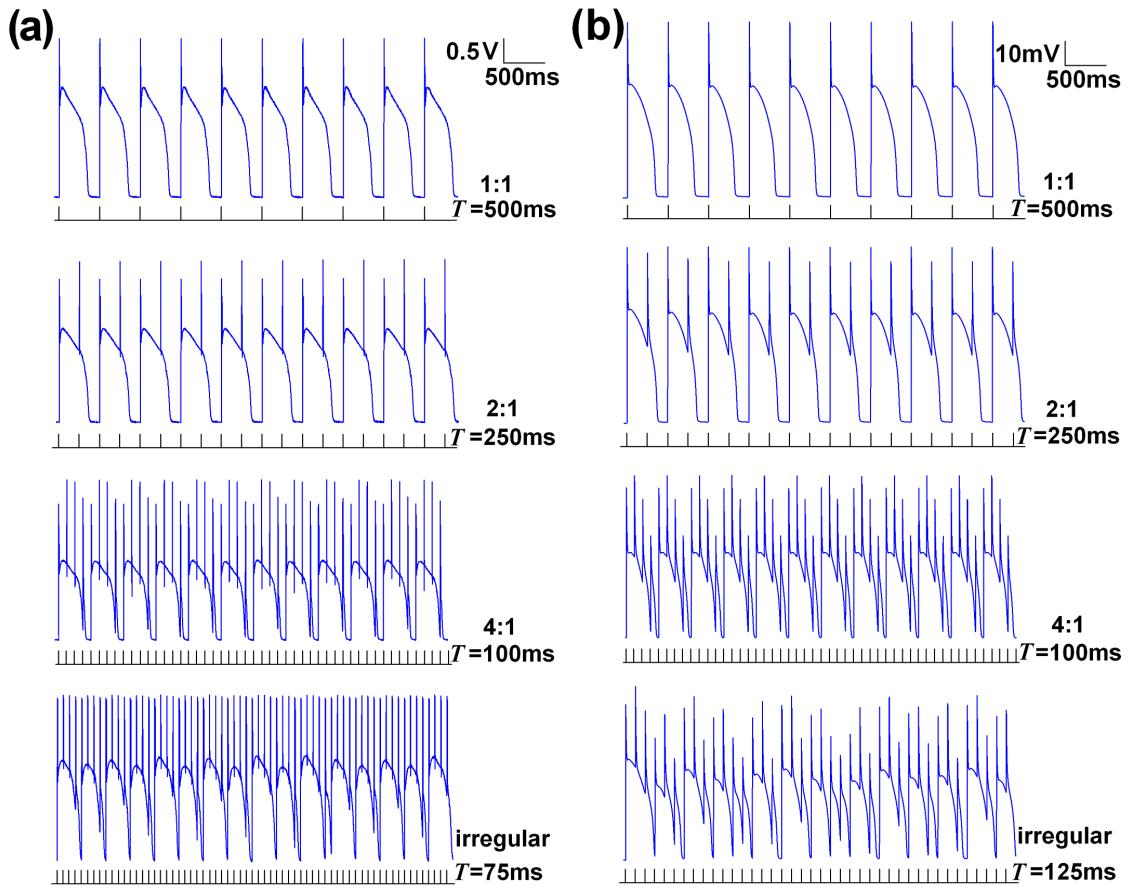

Figure 3.20: Simulated action potential waveform patterns for different interval (period) T of periodic current impulse trains. Panels (a) and (b) represent, respectively, the action potential waveform generated by the hybrid model and the Luo-Rudy phase I model. Ratio on the right-hand side of each waveform represents the number of the impulse stimulations to the number of succeeded excitations in response to the stimulations.

The response characteristics of the hybrid model and the LR-I model to the periodic current impulse trains by systematically varying two parameters of the stimulation, that are, the intensity A and the interval (period) T of the impulse train were also analyzed. The results were also compared between two models. Figure 3.21 shows the response

characteristics of the models to periodic stimulation with the hybrid model, shown in (a) and with the LR-I model, shown in (b), in which the response patterns of the model were classified on the parameter plane of the intensity A and interval T of the impulse trains. For the panel (a), the dynamics of the hybrid model were examined for 26 equally spaced T values on the interval [70, 500] and 22 equally spaced (-A) values on the interval [0.5, 80]. For the panel (b), the dynamics of the LR-I model were simulated for 26 equally spaced T values on the interval [70, 500] and 20 equally spaced (-A) values on the interval [21, 80]. Symbols in the both figures indicate various types of response patterns obtained from each of the stimulations. The combination of the intensity and the interval of the impulse determined if the AP was generated or not as well as the pattern of the responses. From both of the panels, it could be noted clearly that low intensity of the stimulation could generate no AP waves. Furthermore, for the low intensity stimulation, long interval T of the impulse did not guarantee the generation of the AP. Figure 3.21 also showed that the results in the hybrid model were generally comparable to those in the LR-I model.

However, the major difference between the two models was that the threshold of the stimulation intensity for the hybrid model necessary for generating AP was lower (at around 2.5 μA) than the one for the LR-I model (at around 28 μA). The possible explanation to this difference might be due to small differences in the I-V relationships between the LR1 model and the hybrid model, although the I-V relationships of ion channels in both models were noted to be generally comparable. In particular, the I-V relationship of I_{Na}, which plays a role for the onset of the depolarization, could lead to the variant of threshold of the stimulation intensity.

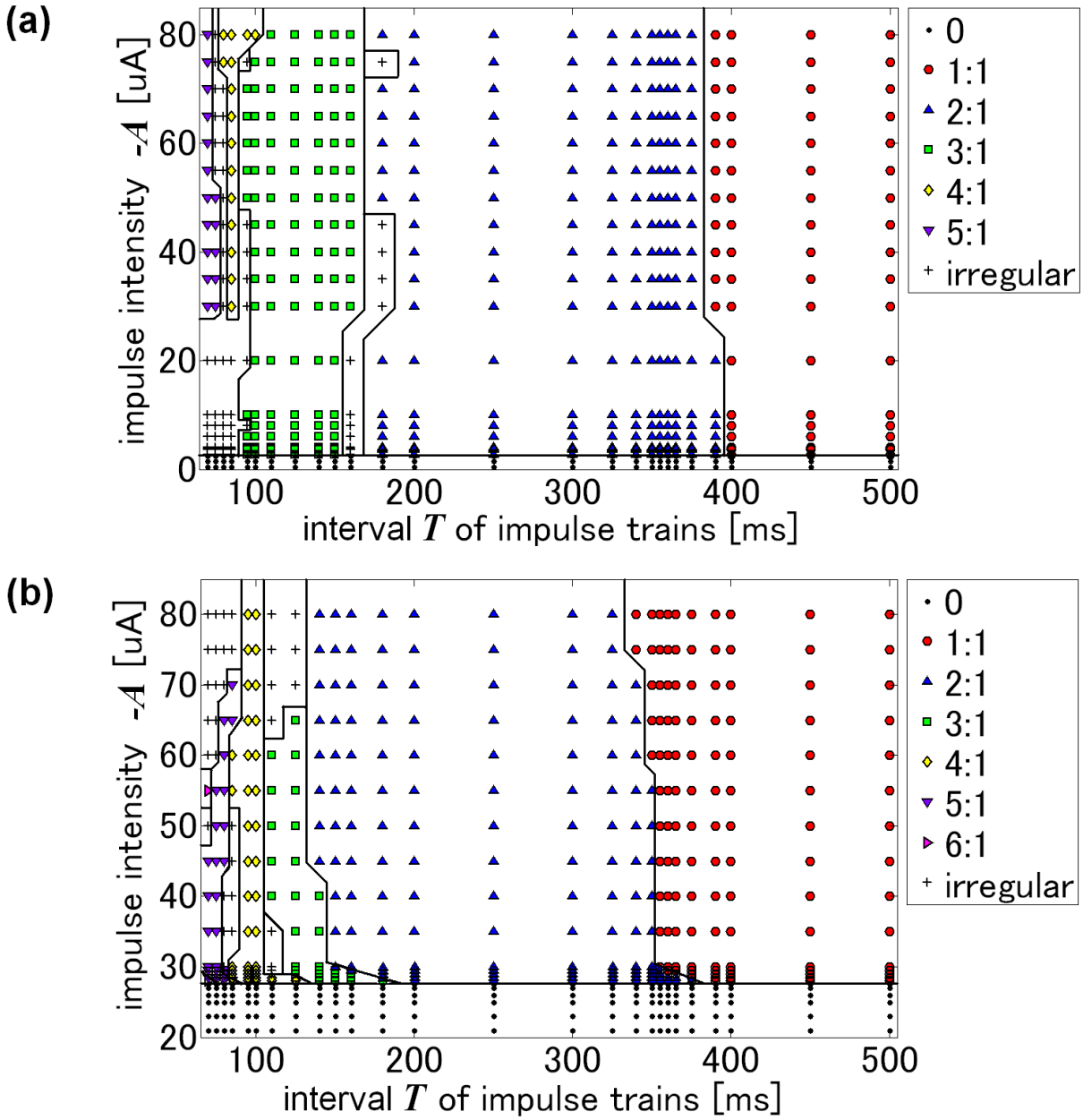

Figure 3.21: Classification of excitation response patterns on the parameter plane spanned by the period T and the intensity (-A) of the impulse trains. Panels (a) and (b) representing the results with the hybrid model and the Luo-Rudy phase I model, respectively. The ratios indicate represents the number of the impulse stimulations to the number of succeeded excitations in response to the stimulations.

3.7 Summary and Discussion

In this chapter, the subject on how the analog-digital hybrid circuit model of the action potential was developed based on the mathematically described Luo-Rudy phase I model of a cardiac ventricular cell has been elaborated. The LR-I model became the subject as for among various biophysically-detailed models of ventricular cells, the LR-I is a categorized as one of simpler mathematical models. Nevertheless it is well-described fundamental ionic mechanisms. The simulation the action potential by the hybrid model has been carried out and the characteristic responses of the action potential to periodic current impulse trains with various intervals were analyzed, they were conducted in real-time performance. The validity of the hybrid model also has been examined by comparing to the results of the LR-I model .

From the simulation results, they show that the action potential waveform produced by the hybrid cell model was quantitatively the same as that by LR-I model. Moreover, it was confirmed that the dynamics of the hybrid cell model were well reproduced the corresponding dynamics of LR-I model, in response to periodic current impulse trains with a variety of the period. Primarily, the objectives of this study were to perform a real-time simulation of cardiac excitation and reproduce the LR-I model quantitatively by replicating the I-V relationships of the six-type ion channel currents. Thus, as far as possible, it is desirable that only the analog circuit implementation should be used to fulfill the objective of this research as it can provide valuable tools for real-time operating system. However, without application of specialized design analog ICs with the features and the performance desired for the specific tasks, they are less suited in modeling biophysically-detailed, complicated mechanisms and fluctuating characteristics of the ion currents. Therefore, in this study, the time-dependent ion currents with large time constants, I_K and I_{si}, were reproduced by the digital implementations of dsPIC microcontroller. Apparently, for a use of analog circuits, capacitors with relatively large size are required to produce the slow dynamics of the ion currents.

Numerous challenges have been faced in developing the hybrid model. The transient dynamics of fast inward sodium current I_{Na} implemented as the analog circuit here, only qualitatively reproduced the I-V relationship of the I_{Na} in the LR-I model. One of the solutions to this problem is to use the specific hardware implementation of such a model using a MOSFET device by the CMOS technology to reproduce quantitatively the transiently-induced I_{Na}. Moreover, calculating mathematical functions (i.e., $\log(x)$ (logarithm to the base e) and $\exp(x)$ (e to the power x)) in equations which represent the ion currents of the I_K and I_{si} by using the embedded applications based dsPIC may present problems to rapid calculation in performing the real-time operation of the hybrid model. Thus, to increase the speed of calculation, the initiative of accessing certain data from constructed tables stored in the memory of the dsPIC has been taken rather than computing the functions in the equations.

In behalf of the challenges as eleborated above, small differences in the I-V relationships between the LR-I model and the hybrid model have occured, although the I-V relationships of ion channels in both models were noted to be generally comparable, in point of fact of getting the satisfied results as has been described before. Then, by considering the advantage of the hybrid model of allowing real-time simulation of the action potential dynamics that were quantitatively comparable to a single biophysical cellular membrane, the hybrid model is therefore thought to be useful for analyzing the dynamics in cardiac physiology. Thus, this becomes a platform for developing large scale modeling of action potential propagation in cardiac tissue structure for basic understanding underlying mechanisms of excitable systems in the heart, as will be discussed in the next chapter.

Chapter 4

Spatio-Temporal Dynamics and Control of Reentrant Action Potential Conduction in Active Cable Models

4.1 Introduction

An excitable cell rarely exists in isolation, instead, the cell operates as part of a network of similar cells and to function there must be communications between the cells. The communication of electrical information is achieved through the propagation of action potential along the cell membranes of tissue. Cardiac cells, also known as myocytes are strongly interconnected via low-resistance gap junctions. The presence of these intercellular couplings thus causes the cardiac tissue to behave electrophysiologically as a functional syncytium. Consequently, the underlying mechanisms of the heart cannot be described or analyzed as the excitation dynamics of isolated cells.

Action potential propagation modeling of cardiac tissue is applied to simulate the normal and abnormal conditions in coupled nonlinear systems of the heart dynamics. Using this approach, it may be possible to identify the underlying mechanisms that are primarily responsible for the abnormal activity in excitable systems such as cardiac arrhythmias. As for the heart dynamics, some cardiac arrhythmias are perpetuated by reentrant mechanisms. To model the action potential propagation, the cardiac tissue is often represented by a one-dimensional cable model, as a simple analog circuit for a single fiber under

the assumption that the effect of the extracellular potential is negligible and considered grounded(Figure 4.1). This is called the mono-domain model.

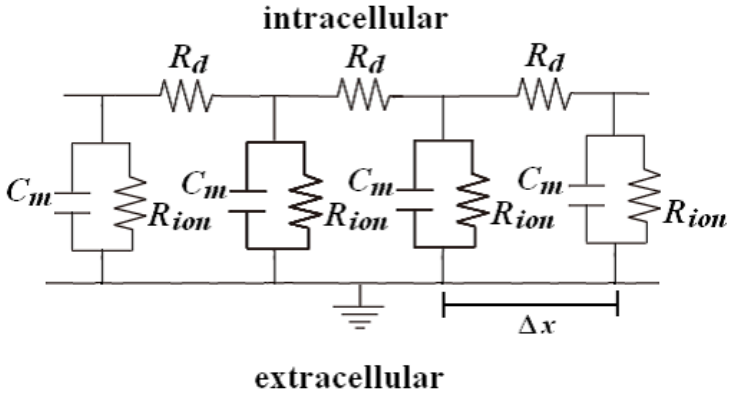

Figure 4.1: An equivalent circuit for a single fiber of cardiac tissues model. Parameters are as follows: R_d is the intracellular resistance which also known as the gap junction resistance, R_{ion} is the membrane resistance refering to specific ionic channels and C_m is the membrane capacitance. This continuous structure described as the limit of an infinite number of resistor and capacitor elements found by subdividing the continuum into segments of length Δx, and every Δx also can be referred as a spatial of one cardiac cell model. As $\Delta x \to 0$, the discrete representation approaches a continuous presentation.

In this chapter, the reentrant conduction of the action potential in a one dimensional ring-topology-network of the hybrid active circuit cable model are discussed. Resetting and annihilation of the reentrant wave under the influence of a single stimulus are investigated and the relationship between the phase reset of the reentry and the stimulation phase are presented by using a phase resetting curve (PRC). Then, sequential phase resettings by periodic stimulation that leads to annihilations of the reentry are predicted by the PRC, where one-dimensional discrete Poincare mappings illustrate the predictions. Comparisons between the results from the hybrid active cable model and from the LR-I cable model are also carried out.

4.2 Cable Model

The conductive strength of the intercellular connections enables the cardiac tissue to be well approximated macroscopically as a functionally continuous excitable medium.

Propagation of action potentials in an excitable tissue is often modeled by using significantly simplified quantitative method that can be represented by the one-dimensional cable model, described by a mono domain reaction-diffusion equation. In particular, the cable model is considered as a spatially one dimensional and homogeneous medium. Thus it can be described as

$$\frac{\partial V_m(x,t)}{\partial t} = D\nabla^2 V_m(x,t) - \frac{I_{ion}(x,t)}{C_m} + \frac{I_{ext}(x,t)}{C_m} \tag{4.1}$$

where $V_m(x,t)$ is the cardiac cellular membrane potential at position x and time t, ∇^2 is the second derivative with respect to the position x, $C_m = 1.0$ μF cm^{-2} is the membrane capacitance, $D = (C_m S_v \rho)^{-1}$ is the diffusion coefficient, where S_v and ρ are the surface-to-volume ratio of the cardiac cells and the longitudinal tissue resistivity of cardiac muscle, respectively. This single differential equation can be extended to two and three dimension. According to the literatures that use models of one and two dimensional cardiac tissues[42, 53], By considering the case with $S_v = 5000$ cm^{-1} and $\rho = 0.2$ kΩcm, leading to $D = 1$ cm^{2}s^{-1}. $I_{ion}(x,t)$ is the ion channel current at position x and time t. Here the I_{ion} was specified by LR-I model. I_{ext} may also be position dependent if the externally applied current are spatially distributed. More specifically, a one-dimensional ring of LR-I active cable has been considered to represent as a model for exhibiting a circus movement reentry, which is thought to be a typical mechanism of anatomical reentrant cardiac arrhythmia. Here the ring of length $L = 4.7$ cm was considered.

The forward Euler spatial discretization with Δx for Eq. 5 gives the ordinary differential equation of the compartment model at position x of LR-I cable as follows:

$$\begin{aligned} \frac{dV_m(x,t)}{dt} &= \frac{D}{(\Delta x)^2}\left(V_m(x+\Delta x,t) - V_m(x,t)\right) \\ &+ \frac{D}{(\Delta x)^2}\left(V_m(x-\Delta x,t) - V_m(x,t)\right) \\ &- \frac{I_{ion}(x,t)}{C_m} + \frac{I_{ext}(x,t)}{C_m}. \end{aligned} \tag{4.2}$$

For numerical simulation of LR-I cable, the ring were segmented into $N = 80$ compartments, i.e., $\Delta x \simeq 0.058$ cm. This is equivalent with considering the gap junction resistivity between every adjacent compartments as $R_d = 3.45$ kΩcm^2. For the one-dimensional ring

tissue, the compartment model with a set of ordinary differential equations can then be represented as

$$C_m \frac{dV_m^i}{dt} = \frac{1}{R_d}(V_m^{i+1} - V_m^i) + \frac{1}{R_d}(V_m^{i-1} - V_m^i) - I_{ion}^i + I_{ext}^i. \tag{4.3}$$

where $i = 1, \cdots, N = 80$. V_m^i and I_{ion}^i are the membrane potential and the ion channel current of i-th compartment, respectively. Note that $(i-1)$ refers to N for $i = 1$, and $(i+1)$ refers to 1 for $i = N$, because of the ring geometry of the model as illustrated in Figure 4.2. That is, the 1st and the N-th compartments are connected by the resistive gap junction of resistivity R_d. This set of ordinary differential equations together with channel gating dynamics of every compartment were integrated numerically using explicit Euler method with time step $\Delta t = 0.001$ ms.

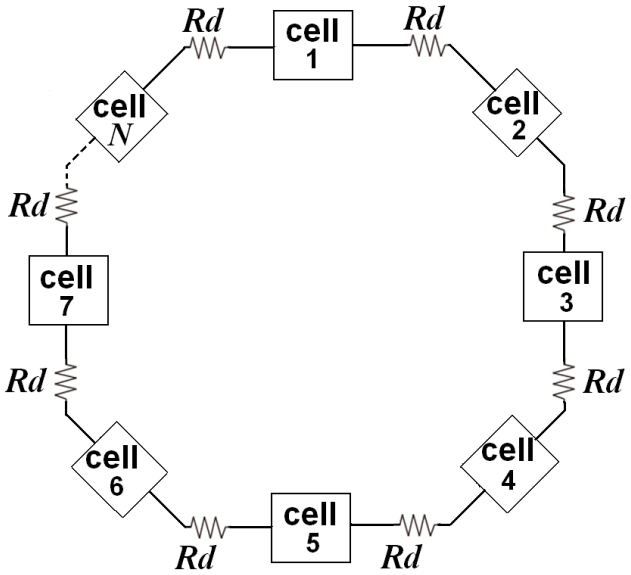

Figure 4.2: The ring-shaped active cable model. The ring model consists of N(=80) cell models connected by the gap junction resistance R_d.

Although it is desirable to have quantitative reproduction of this LR-I cable model as much as possible using a ring-topology-network of 80 hybrid cell models as in Figure 4.2, there was a need to modify the value of the gap junction resistance to $R_d = 2.35$ kΩcm^2, by which conduction velocity of the action potential along the hybrid cable model became

almost the same with that of LR-I cable model as shown below. The one-dimensional ring of the hybrid cable model was built as shown in Figure 4.3.

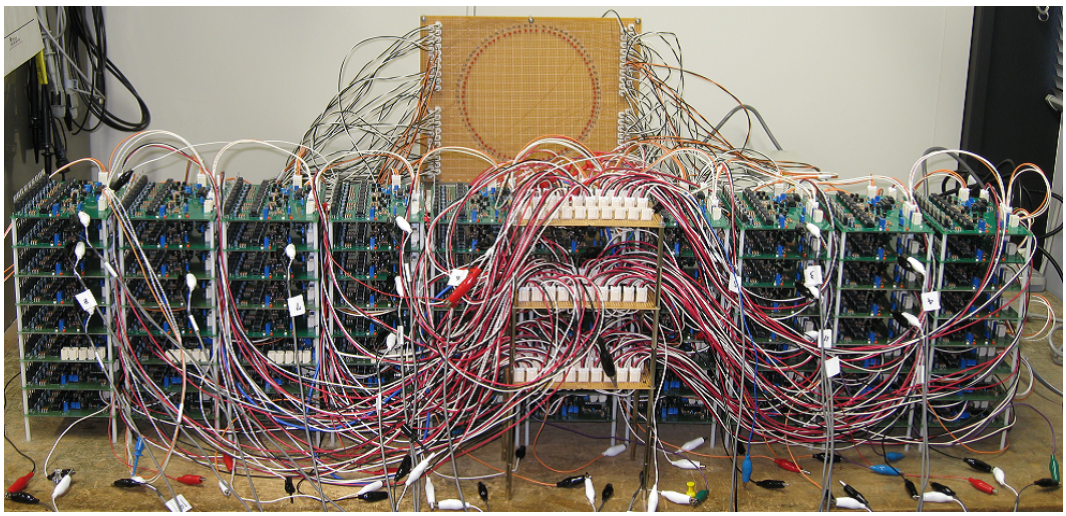

Figure 4.3: Photograph of the analog-digital hybrid cable model circuits.

4.3 Circus Movement Reentry in Active Cable Models

For the circus movement reentry to occur in the ring-shaped LR-I and the hybrid cable models, unidirectional conduction block of conducting action potentials and the presence of excitable gap, which is defined as a spatial interval of the medium with enough excitability, are essential. Unidirectional block occurs when an action potential wave-front fails to propagate in one particular direction, but can continue to propagate in other directions. Yet, the presence of the excitable gap is closely related to the conduction velocity of the action potential wave and the length of the path around the block. Here an unidirectional block was induced by using the so called $S1$-$S2$ protocol[9, 54], where single or several (usually equally-time spaced) impulsive stimulations referred to as $S1$ were applied at a given location of the ring, and then another impulsive stimulation referred to as $S2$ was applied at a different location from the $S1$ site in a particular time.

Panels (a) and (b) in Figure 4.4 show space-time diagrams showing changes in the membrane potential as a function of time and position around the ring during initiation of reentry in the hybrid and LR-I cable models, respectively, by which quantitative repro-

duction of LR-I cable dynamics by the hybrid cable model can be confirmed. Impulsive stimulations for $S1$ and $S2$ with a duration of 1 ms and an intensity of 150 μA were used. In each figure, two $S1$ stimulations were applied to the ring at the compartment of number $i = 1$, at time $t = 0$ ms and $t = 400$ ms (red arrows marked the area and the time where the stimulations were applied), pacing the excitation of the medium. Each stimulus evokes excitation at the stimulated site, generating two conducting action potentials. One propagates clockwise and the other counter-clockwise along the ring. As common in excitable media, each conducting action potential possesses its wave-front and tail. The wave-front progressively excites the compartments ahead of the wave-front, and the wave-tail is accompanied with refractoriness that decreases as being distant from the action potential. These two conducting action potentials were eventually collide with each other at the opposite side of the stimulated site, leading to annihilation of the action potentials due to the refractoriness located at each of the wave-tails. The $S2$, corresponding to an ectopic focus excitation in the real heart, was then applied at a position (the compartment number $i = 18$) slightly away from the $S1$ site at an appropriate time interval after the second application of $S1$.

According to Figure 4.4, the panel (a), $S2$ was applied at $t = 534$ ms, where the time interval of $S1$ and $S2$ was 134 ms. Meantime, in the panel (b), $S2$ was applied at $t = 511$ ms, with the time interval of 111 ms after the $S1$ stimulation. In order to initiate the reentrant wave, the $S2$ must be applied when the action potential generated by the $S1$ has passed through the $S2$ site and refractoriness of the wave-tail is still large in the one side of the $S2$ site (near side of the leaving action potential, referred to here as refractory side) but the excitability has regained on the other side referred to here as excitable gap. The $S2$ with this specific timing generates an action potential that can propagate only to the excitable side (unidirectional block). Since the action potentials generated by the $S1$ were annihilated eventually, the single action potential generated by the $S2$ alone was left, initiating the circus movement reentrant wave.

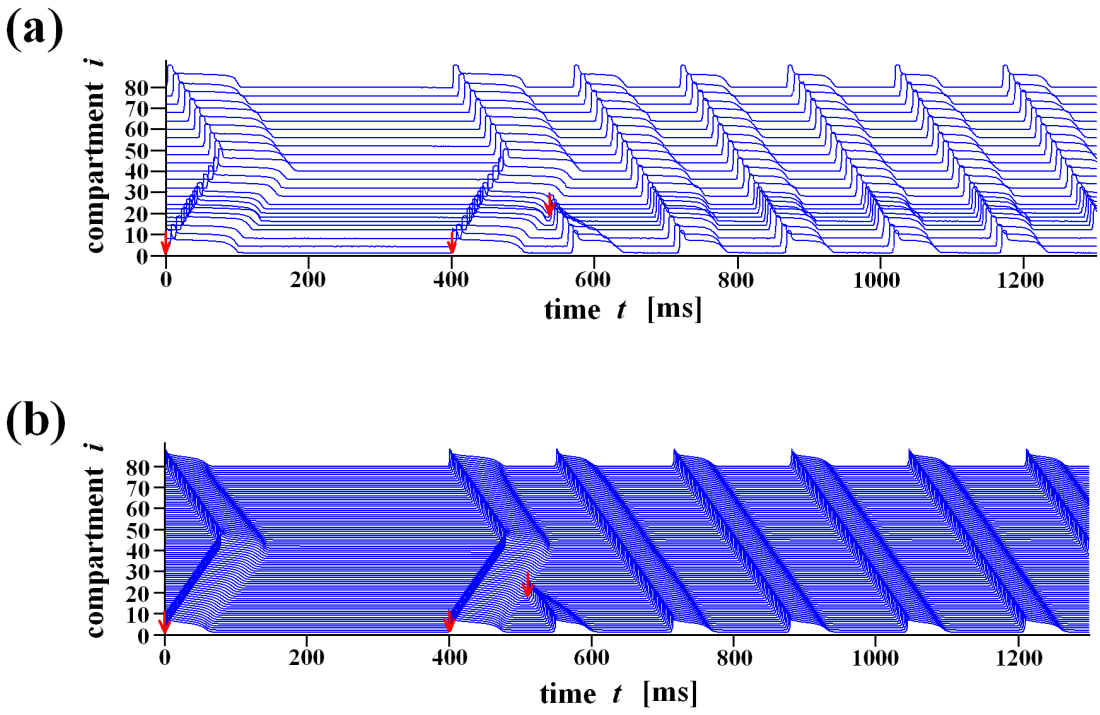

Figure 4.4: Space-time diagrams showing the membrane potential as a function of time and position around the ring tissue. (a) The analog-digital hybrid cable model. (b) LR-I cable model. For the hybrid cable model, the membrane potentials were recorded only for the compartments 1, 4, 8, 12, 14, 16, 18, 20, 22, 24, 28, 32, 36, 40, 44, 48, 52, 56, 60, 64, 68, 72, 76, and 80, using a 24 ch recording device with analog-to-digital converters.

The cycle length of the reentry in its steady state was $\bar{T}_{LR} = 165$ ms for LR-I cable, and that for the hybrid cable model was $\bar{T}_{hyb} = 148$ ms. Note that action potential duration after the initiation of reentry was about 80 ms which was shorter than those generated in response to $S1$ stimulations in both LR-I and hybrid cable models. This is because the wave-front of the reentrant wave is always chasing the wave-tail, and thus excitability of the ring cable cannot be fully recovered.

For delivering $S1$ and $S2$ stimulations to the hybrid cable model, an impulsive stimulator was constructed by using an H8/3694F microcontroller to control the timings of the stimulations systematically as shown in Figure 4.5. The programmable stimulator is also able to regulate the impulsive duration and intensity, other than controlling the stimulation timings. The circuit is powered by the same source that is used for the digital part. Details of the electronic components and the source program written into the H8 microcontroller are described in the Appendix B and C, respectively.

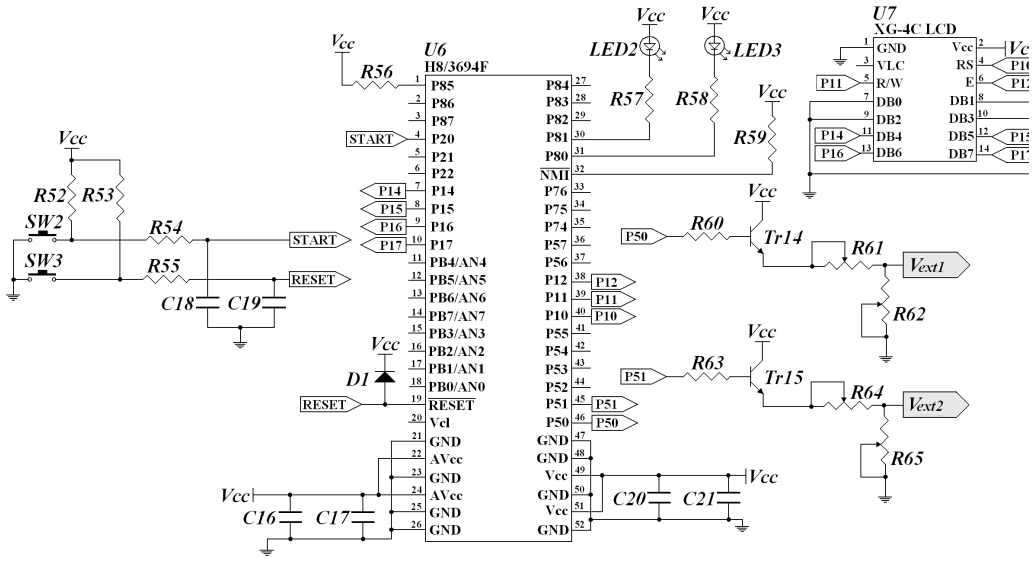

Figure 4.5: The circuit diagram of the impulsive stimulator used to control timing of current injections to the hybrid cable model.

4.4 Resetting and Annihilation of Reentry in Active Cable Models

Reentrant arrhythmia often raise risks of insufficient blood pumping from the heart, and it thus can be potentially fatal. Therefore termination of the reentry excitation is highly desirable. Clinically, this is usually accomplished by delivering electrical stimulations through a catheter penetrated into the heart, possibly somewhere closed to a reentry pathway, leading to annihilation of the reentry. Glass and his colleagues have been establishing a theory to handle this issue based on the phase resetting of nonlinear oscillators[55, 56, 57, 58]. Here their theory was utilized for LR-I and the hybrid cable models to show that the latter behaves satisfactory the same as the former.

In numerical and hardware experiments below, single and/or finite sequences of impulsive current stimulations were delivered to the cable models that support the reentry excitation as shown in the previous section. Those stimulations with the same stimulus intensity as in the unidirectional block experiment were applied again at the compartment of the number $i = 18$.

Panels (1a-1c) and (2a-2c) in Figure 4.6 show space-time diagrams exemplifying the responses of the reentrant excitation to single stimulations as a function of time and position in the hybrid cable and LR-I cable models, respectively. One could observe a fairly good coincidence between the dynamics of the hybrid cable and the LR-I cable models. Red arrows marked in the figure correspond to the applied stimulations. In each of Figure 4.6(1a) and Figure 4.6(2a), the stimulation was applied at t = 419 ms and t = 463 ms, respectively while still in the fully refractory side of the wave-tail. Thus, the stimulus failed to generate any propagating action potentials, affecting less the original reentry.

In each of Figure 4.6(1b) and Figure 4.6(2b), the stimulus was applied at a slightly later time instant than (1a) and (2a), generating a single action potential propagating only in a clockwise direction to collide with the originally counterclockwise propagating

action potential, leading to the annihilation of the reentry. Where, the stimulation was applied at time $t = 421$ ms coresponding to the hybrid cable model and time $t = 468$ ms corresponding to the LR-I model. This result suggests that a single stimulation delivered at an appropriate time interval referred to here as the annihilation interval, at which the wave-tail of the original reentry is located slightly away from the stimulation site, could annihilate the reentry.

In each of Figure 4.6(1c) and Figure 4.6(2c), the stimulus was applied at the excitable gap located far behind the wave-tail of the original reentry, at $t = 460$ ms and $t = 492$ ms, respectively. This causes the induction of two propagating action potentials in both clockwise and counterclockwise directions. The wave propagating in the clockwise direction collided with the original reentrant wave, and they were annihilated with each other. The wave traveling in the counterclockwise direction persisted, leading to the resetting of the reentrant circulation rhythm, where the successive occurrence times of excitation at every compartment were advanced about 50 ms in comparison with the expected times for the original reentry excitation. These three cases are typical responses of the reentry.

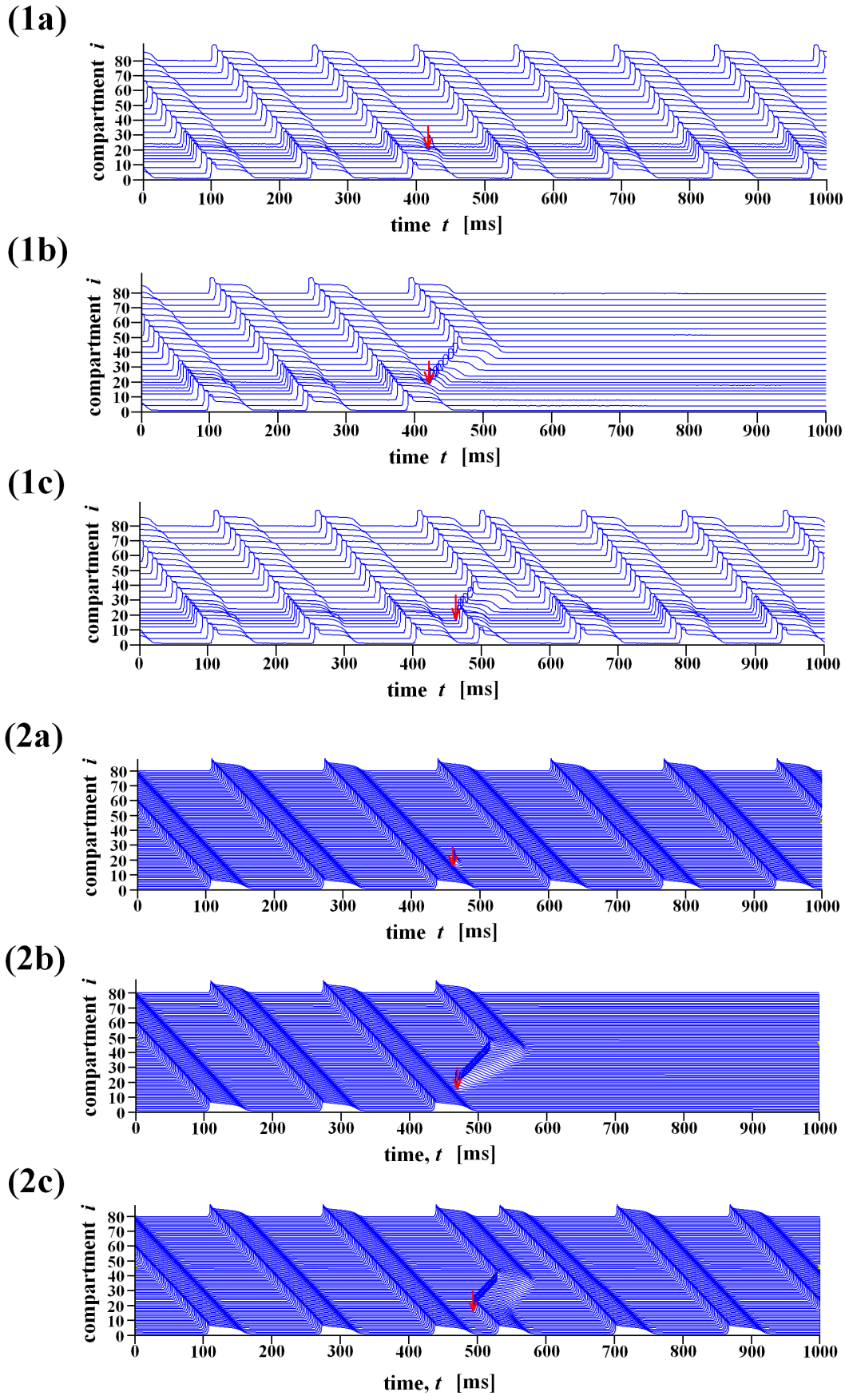

Figure 4.6: Responses of the reentry dynamics to single impulsive stimulations. (1a)-(1c): Responses of the hybrid cable model. (2a)-(2c): Responses of LR-I cable model.

4.4.1 Phase Resetting Curve

The resetting (delay and advance of the circulation rhythm of the reentrant wave) and the annihilation of the reentry can be analyzed using the phase resetting curve (PRC) as performed in the previous studies[55, 56] in both hybrid and LR-I cable models. To this end, the phase of the reentrant wave is defined based on the time instant when the reentrant action potential is detected at a given recording site. Here the recording site was located same as the stimulation site, i.e., the compartment number $i = 18$. First, the stimulation phase ϕ that takes a value between 0 and 1 is defined as

$$\phi = \frac{t_{stim}}{\bar{T}} \tag{4.4}$$

where $\bar{T}$ is the period of the steady state reentry with no stimulations, and t_{stim} is the time elapsed from the time instant when the last propagating reentrant action potential is detected at the recording site before the stimulation is applied. A small stimulation phase roughly between $0 < \phi < 0.45$, corresponding to roughly $0 < t_{stim} < 75$ ms, implies that the stimulation is applied when the stimulation site is in the middle of the reentrant action potential. A stimulation phase close to 1, corresponding to $t_{stim} \sim \bar{T}$, implies that the stimulation is applied close to an oncoming wave-front of the reentry excitation.

The amount of phase reset $\Delta\phi$ in response to a stimulation with its phase ϕ is defined as

$$\Delta\phi = \frac{\Delta T}{\bar{T}} \tag{4.5}$$

where ΔT is the difference between the expected time instant of detecting the original reentrant action potential (when no stimulation is applied) and the time instant of detecting the reentrant action potential that is affected or newly generated by the stimulation. Positive and negative ΔT corresponds to phase delay and advance, respectively.

Result of detailed examinations on the responses of the reentry to stimulations delivered at various phases can be summarized using PRC. Figure 4.7 shows the PRC of the hybrid cable model (a) and that of LR-I cable model. In both cases, the phase resetting

was largely negative (advance) when the stimulation phase was in the latter half of the reentry cycle. Only small amount of the phase resetting could be found for the stimulation phase between 0.1 and 0.45. When a stimulation was applied around the middle of the cycle length, roughly $0.47 < \phi < 0.56$ for the hybrid cable model and roughly $0.42 < \phi < 0.51$ for LR-I cable model as depicted by vertical gray bands in Figure 4.7(a) and Figure 4.7(b), the reentry was annihilated by the stimulation as shown in Figure 4.6(1b) and Figure 4.6(2b). The phase interval corresponding to this gray band was referred to as the annihilation phase interval. Similarity between Figure 4.7(a) and Figure 4.7(b) was satisfactory, though the PRC of the hybrid cable model was not as smooth as that of LR-I cable model, possibly due to internal noise contaminated in the hardware circuits and small differences in parameter values of every analog devices.

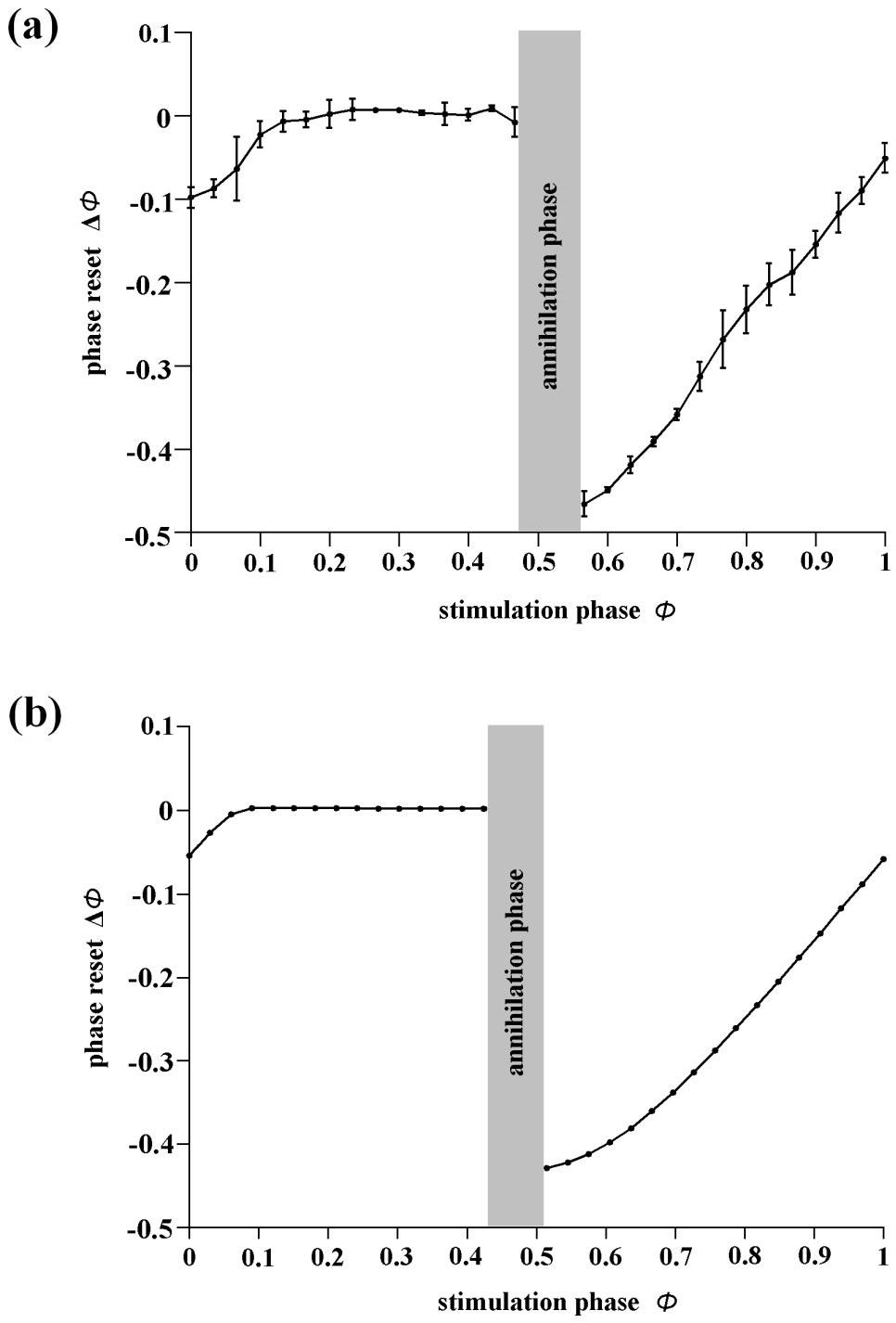

Figure 4.7: The phase resetting curves (PRCs) showing the amount of phase reset $\Delta\phi$ against the stimulation phase ϕ. (a) PRC of the hybrid cable model. (b) PRC of LR-I cable model. Negative $\Delta\phi$ implies phase advance. The vertical gray band represents the annihilation phase interval. That is, the reentry is annihilated, if a stimulation falls within this interval.

4.4.2 Sequential Phase Resettings and Innihilation of Reentry

Once the PRC representing the response of the reentrant wave to single stimulations at various stimulation phases is obtained, the dynamics of the reentry in response to a periodic sequence of the stimulations should be able to be predicted as examined in the previous study[56]. By considering the response of the reentry to a sequence of the stimulations with period T_{stim}. According to the theory of PRC, for a given phase of the first stimulation ϕ_1, the second stimulation is applied at the phase $\phi_2 = \phi_1 - \Delta\phi_1 + T_{stim}/\bar{T}$ (mod 1). In general, for a given n-th stimulation phase, $(n+1)$-th stimulation phase can be described as follows:

$$\phi_{n+1} = \phi_n - \Delta\phi_n + \frac{T_{stim}}{\bar{T}}, \text{ (mod 1)}. \tag{4.6}$$

Using this iterative mapping formulation, a sequence of stimulation phases $\{\phi_n\}$ for a given initial stimulation phase ϕ_1 can be obtained. If ϕ_n falls within the annihilation phase interval for the first time along the sequence, It can be predicted that the reentry is annihilated by the n-th stimulation of the periodic train of the stimulations with period T_{stim}.

To confirm whether this theory could predict the reentry dynamics or not, evaluations were held by applying the theory in the hybrid cable model and LR-I cable model. For each of these two cable models, the PRC obtained in Figure 4.7 was used to establish the iterative mapping as in equation (4.6). As an example, $T_{stim} = 185$ ms and $\phi_1 = 0.6875$ were set for the hybrid cable model. Equation (4.6) with the PRC shown in Figure 4.7(a) predicts that the first stimulation induces a relatively large advanced $\Delta\phi_1 \sim -0.38$, followed by $\phi_2 = \phi_1 - \Delta\phi_1 + 1.25$ (mod 1)$= 0.3193$, and $\phi_3 = \phi_2 - \Delta\phi_2 + 1.25$ (mod 1)$= 0.5693$ which was within the annihilation interval. For comparison, another example was performed by the LR-I cable. This time, the stimulations with $T_{stim} = 200$ ms and $\phi_1 = 0.8182$ were set. By referring to the PRC shown in Figure 4.7(b), $\Delta\phi_1 \sim -0.23$ was obtained. Thus, equation (4.6) predicts $\phi_2 = \phi_1 - \Delta\phi_1 + 1.12$ (mod 1)$= 0.2636$, and

$\phi_3 = \phi_2 - \Delta\phi_2 + 1.12 \pmod 1 = 0.4732$ falls within the annihilation phase interval.

These predictions can be shown with the one dimensional discrete Poincaré mappings hold as in equation (4.6)(Figure 4.8). According to the previous study of analyzing the dynamics of the reentry in response to a periodic sequence of the stimulations by using the Poincaré mappings[56], the Poincaré mappings imply the predictions by the following rules : (1) If there is a stable periodic point in the Poincaré mapping, there will be stable entrainment of the periodically stimulated reentrant wave. (2) If the iterates of the Poincaré mapping land in the annihilation phase after $n-1$ iterates, then the reentrant wave will be annihilated after n stimuli. The Poincaré mapping in Figure 4.8(a) and (b) illustrates the example performed by the hybrid cable model and the LR-I cable model, respectively, in which $T_{stim} = 185$ ms and $\phi_1 = 0.6875$ for the hybrid cable model and $T_{stim} = 200$ ms and $\phi_1 = 0.8182$ for the LR-I cable model lead to termination after two iterations. Thus, Figure 4.8(a) and (b) imply the second rule describe as above.

Furthermore, Figure 4.9(1a,1b) and (2a,2b), respectively show the dynamics of the hybrid and the LR-I cable models in response to this set of stimulations. The results confirm the prediction of the theory. As for two stimulations separated by $T_{stim} = 185$ ms in the hybrid cable model and $T_{stim} = 200$ ms in the LR-I cable model could not annihilate the reentry as in Figure 4.9(1a) and (2a), but three did as in Figure 4.9(1b) and (2b). From this remark, quantitative similarity between Figure 4.9(1a,1b) and Figure 4.9(2a,2b) was found to be satisfactory, confirming a capability of reproducing LR-I cable dynamics by the hybrid cable model.

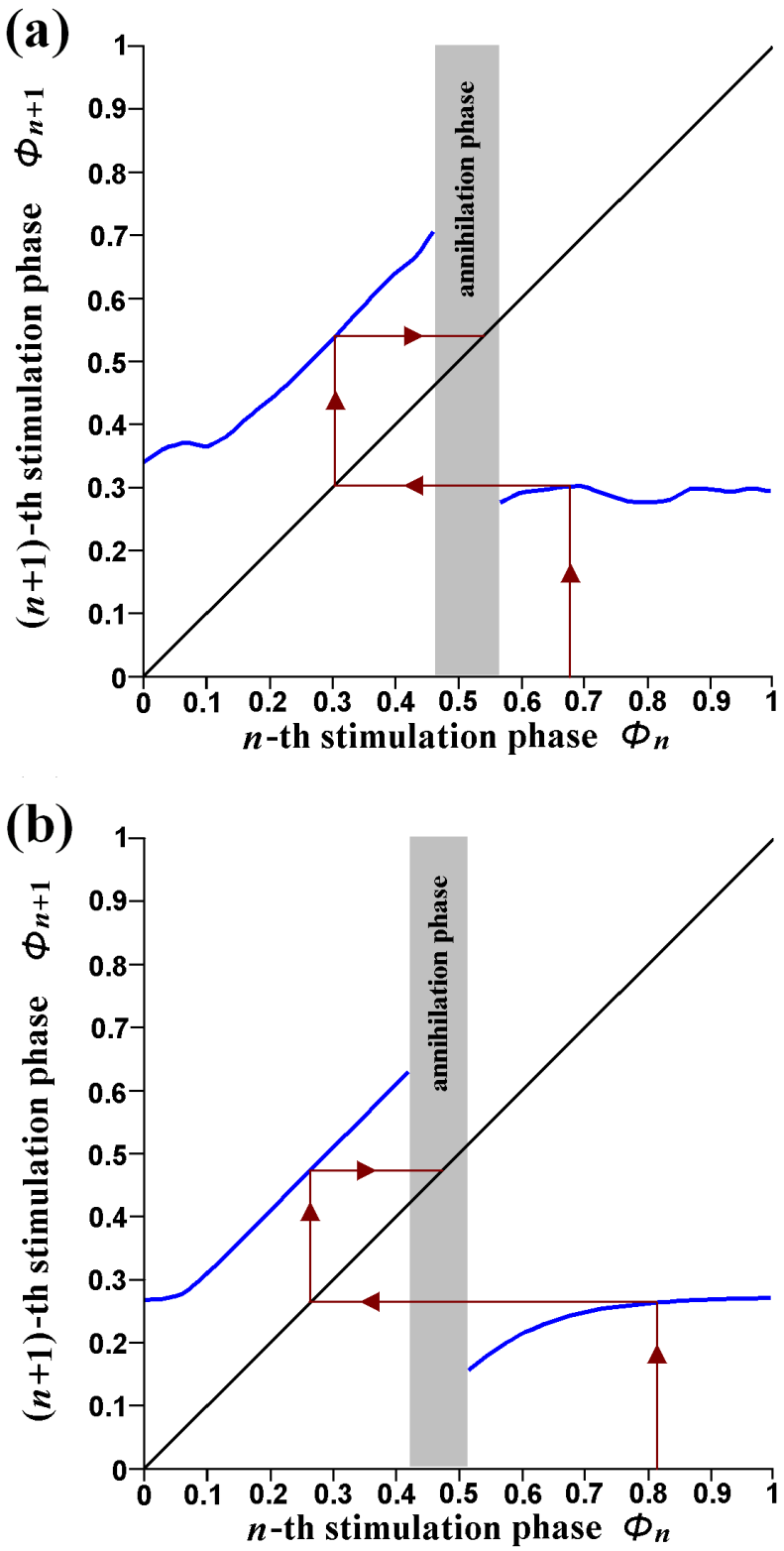

Figure 4.8: The one dimensional discrete Poincare mappings. (a) Poincare mapping of the hybrid cable model. (b)Poincare mapping of LR-I cable model. The horizontal axis and verticle axis corresponds the n-th stimulation phase and the next $n+1$-th stimulation phase, respectively. The vertical gray band represents the annihilation phase interval. That is, the reentry is annihilated, if the mapping falls within this interval.

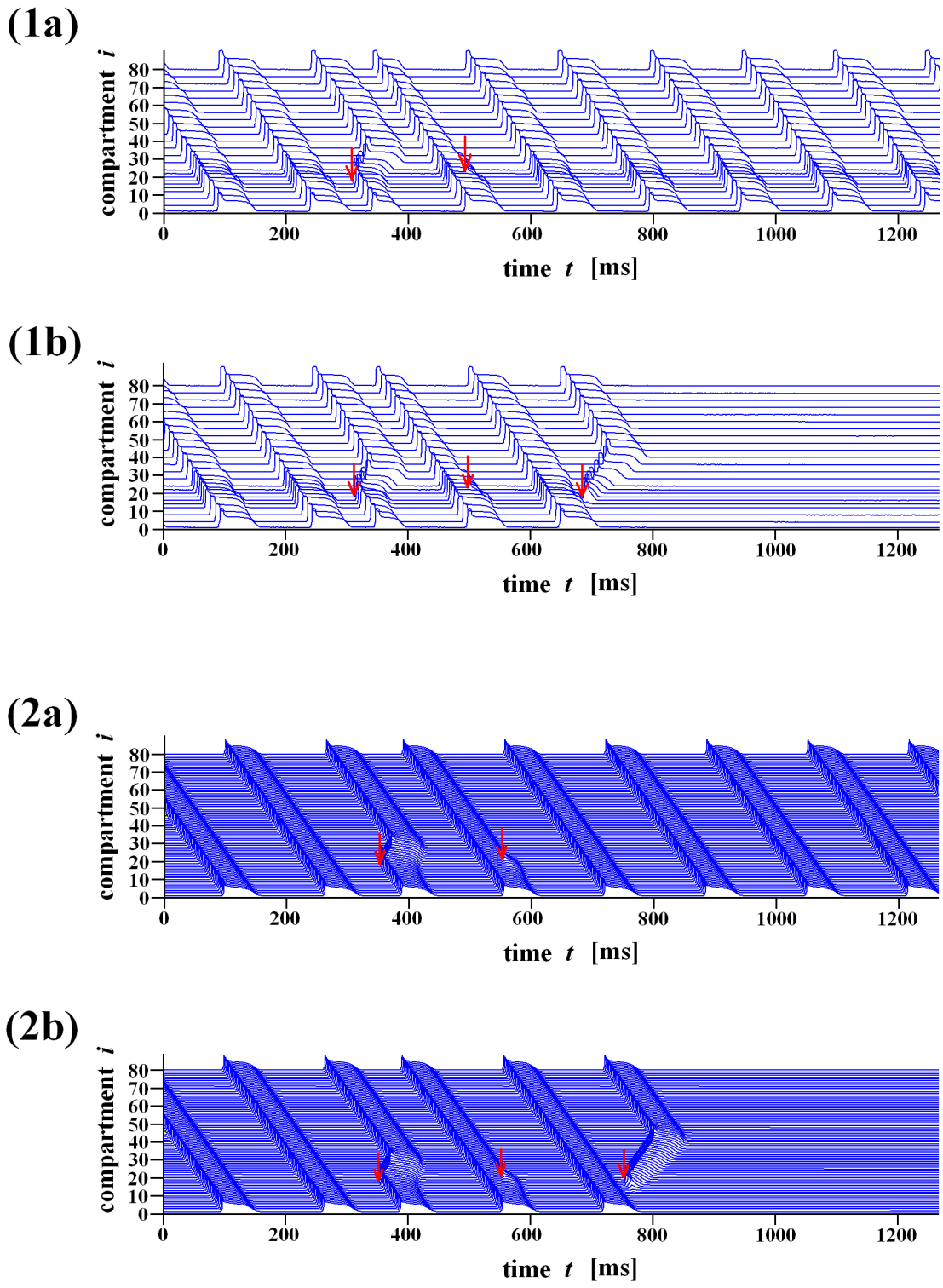

Figure 4.9: Sequential phase resettings that leads to annihilation of the reentry by a train of stimulations. In the hybrid cable model the reentry was annihilated by three stimulations equally separated by $T_{stim} = 185$ ms in (1b), but not by two stimulations in (1a). In LR-I cable model the reentry was annihilated by three stimulations equally separated by $T_{stim} = 200$ ms in (2b), but not by two stimulations in (2a).

4.5 Summary and Discussion

The one dimensional ring of the analog-digital hybrid active circuit cable model in performing the reentrant action potential conductions has been proposed. For comparison, the reentrant simulations by the LR-I cable model were also presented for comparison of the reentrant dynamics responses. In the study, the anatomical circus movement reentry was able to be performed as a result in the development of unidirectional conduction block by $S1$-$S2$ impulsive current induced. The simulation of phase resetting and reentrant wave annihilation in response to single impulsive stimulations were also carried out. The phase resetting curve (PRCs) of both models were presented to show the relationship between the phase reset of the reentry and the stimulation phase. From the theory introduced in previous studies by Glass and his colleagues, phase resettings by periodic stimulation that leads to annihilations of the reentry were predicted by using the PRCs and the results were illustrated with one-dimensional discrete Poincare mappings. From the result presented in the paper, there were quantitative correspondence in dynamic responses of the reentry between the hybrid cable model and LR-I cable model.

The hybrid cable model was able to perform real-time simulations of excitation propagation in cardiac tissues. In this study, a PC with Intel(R) Core(TM) 2 Quad CPU Q9550 2.83 GHz and 3.25 GB RAM was being used in purpose of the numerical simulations. For the numerical simulation of LR-I cable with 80 compartments, it took about 20 seconds for 200 ms simulation time span that was roughly equal to one cycle length of the reentry. This means that the hybrid cable model was able to realize simulations over 100 times faster than those required for the numerical simulations of the LR-I cable model. It is important to emphasize that increase in the number of the hybrid cell models consisting of a tissue model does not reduce the speed, as each of the nodal cell models always operates in real-time.

According to the relevant results and the advantage as above, these approve that the analog-digital hybrid circuit model could be one of alternative tools used in better

understanding the mechanisms of reentry.

In constructing a large quantity of hybrid cell models to develop the hybrid cable model, there were challenges in designing the circuits especially the analog part. In the study, the gap junction resistance value of $R_d = 2.35$ kΩcm^2 was used to keep the reentrant conduction velocity near to the velocity presented by the LR-I cable model with the value of $R_d = 3.45$ kΩcm^2. The different of the R_d value between both models might be due to small differences in the I-V characteristics between the LR-I model and the analog-digital hybrid circuit model, as discussed in the previous chapter.

Besides, analog design is characterized by the need to pay attention to multiple aspects such as noise, input and output voltage range, gain and etc. If these have not been taken seriously into consideration, a mismatch of components occurs, which cause variations of characteristics in every analog-digital hybrid active circuit and might give problems with reproducibility of the hybrid circuit model. Figure 4.10 shows an example of unique feature in the reentrant response by the hybrid cable model. According to the figure, in the three times of reentrant annihilation attempts by the stimulation given at exactly at the same time, it happened that the reentrant wave in the first trial (Figure 4.10(a)) is terminated but not in the second and the third trials (Figure 4.10(b) and (c)). This kind of feature showed up sometimes at a particular time in the beginning or in the end of the reentrant annihilation phase. However, a slight difference among the hybrid cell models can be thought to be "natural," since real cardiac cells are not identical and might not possess exactly the same physiological properties. Therefore, it is thought that, the slight differences in the characteristics among the hybrid cell models might also bring the simulations closer to the behavior of real cardiac tissues.

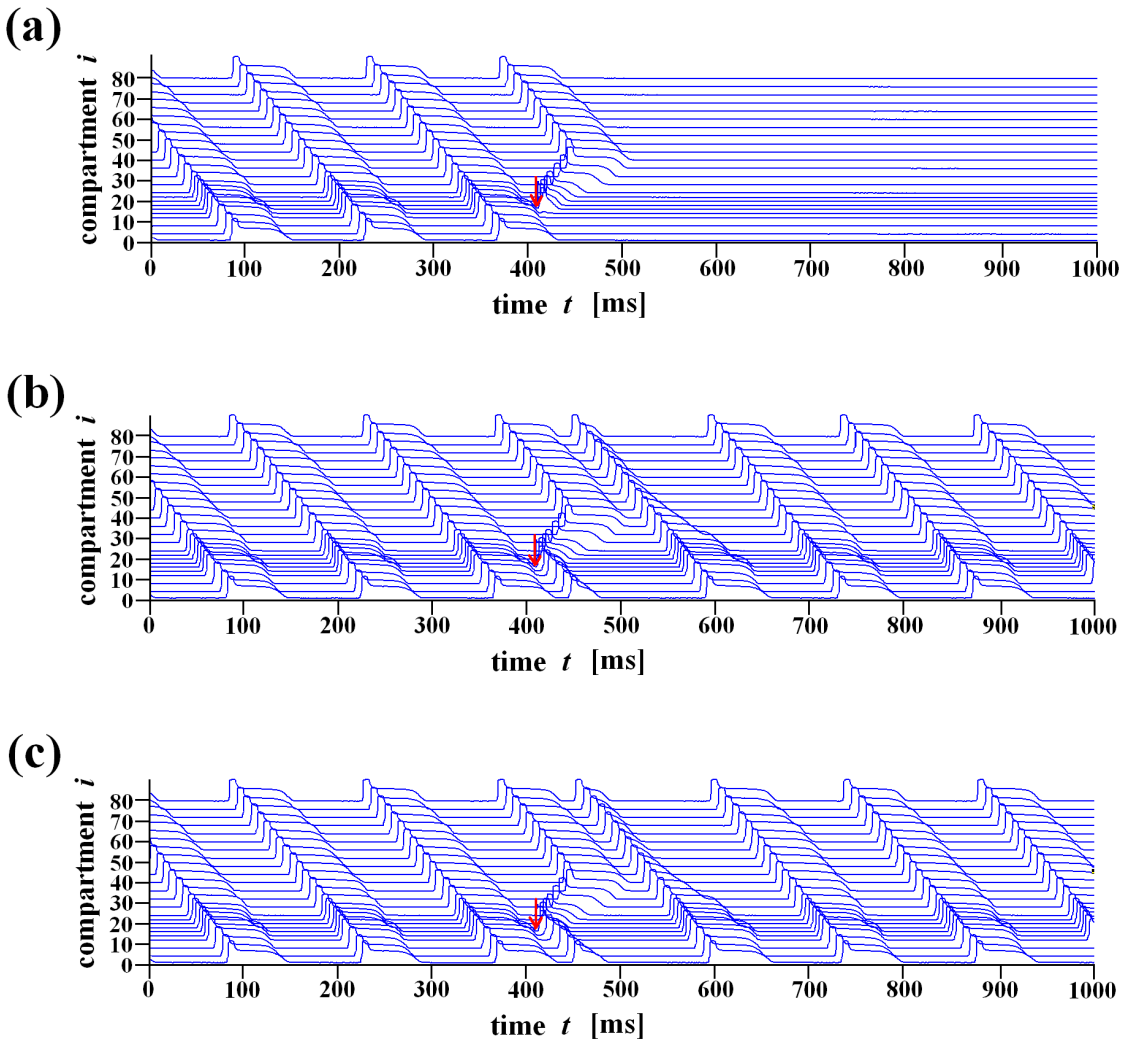

Figure 4.10: The three attempts of reentrant annihilation by the single impulsive stimulation, with a duration of 1 ms and an intensity of 150 μA given at $t = 409$ ms, at 18-th compartment of the hybrid cable model.

Chapter 5

Discussion and Conclusion

In this research, firstly, the single analog-digital hybrid circuit model, also described as the hybrid cell model, based on the standard mathematical model of Luo Rudy phase I model for generating the cardiac ventricular action potential has been developed. The Hybrid cell model was capable to operate in real-time. Then, a one-dimensional ring-topology-network of 80 compartments of the hybrid cell model, referred to here as the hybrid cable model, was constructed through interconnection of gap junction resistances for exhibiting the reentrant action potential conduction. The hybrid cable model was also able to perform real-time simulations of action potential conduction in cardiac tissues. It is interesting to note that, increase in the number of the cell models has absolutely no affect on the real-time performance of the cable model. The validity and reliability of the hybrid cell model and the hybrid cable model were examined with the comparison to the numerically simulated LR-I cell model and its cable model.

In the single cell simulations, the action potential characteristics of the hybrid cell model and the LR-I cell model were comparable as the hybrid cell model was generally reproduced the current-voltage (I-V) relationships of ion currents described in the LR-I cell model. Those involve (1) the action potential waveform, and (2) the excitation dynamics of the hybrid cell model in response to periodic current impulse trains with various intervals and intensity levels.

In the simulations of the reentrant action potential conduction, quantitative correspondences between the hybrid cable model and the LR-I cable model were demonstrated using a one dimensional active cable as a model of the anatomical reentry in a cardiac tissue with various conditions. Those include (1) unidirectional block to initiate reentry, (2) phase resetting by single impulsive stimulations, (3) annihilations of the reentry by appropriately timed single stimulations, (4) phase resetting curves (PRCs) that can characterize the reentry dynamics in response to single stimulations at various timings, and (5) sequential phase resetting that leads to annihilation of the reentry as predicted by the one dimensional discrete Poincare mappings.

To the best of my knowledge, this is the first attempt to design and implement a hardware circuit model of spatially distributed cardiac tissue with biophysically detailed ion channel currents responsible for the cellular excitations. From the satisfactory correspondences that were examined here between the hybrid and the LR-I cable models, and taking into account the real-time simulation capability of the hybrid model, these can be concluded that the hybrid model might be a useful tool for large scale simulations of cardiac tissue dynamics, as an alternative to numerical simulations, toward further understanding of the reentrant mechanisms.

In this study, each analog-digital hybrid cell model used in this study was powered with ± 9 V, and the peak total current measured at the DC power sources $V+$ and $V-$ of Figure 3.4 for the analog part of the model was 0.08 A and -0.06 A, respectively. For the digital part with 5 V DC power source (V_{CC}) of Figure 3.6, it was 0.14 A. Simple calculations give us a rough estimation of the energy consumption in a single hybrid cell model, and it is about 2 W at most. For the hybrid cable model with N cell models, this becomes $2N$ W. The energy consumption of the hybrid cable model with $N = 80$ is thus about 160 W, which is roughly comparable order with an energy consumption single

desktop PC. This estimation implies that a large quantity of energy might be consumed for large scale real-time dynamics simulations.

As the mission of the current study was to perform real-time simulations of excitation propagation, the issue of minimizing the power consumption in the circuits was not taken into concern. However, nowadays, the focus on developing minimum power consumption in devices and products has been uplifted most. Therefore, one way to achieve reduction in the energy consumption, as well as reduction in the physical size of the circuit, is to implement this analog-digital hybrid circuit using LSI technology. Indeed, development of technology begins to allow for such realizations as attempted in some recent studies[59, 60]. Therefore, if the proposed hybrid cell model can be implemented as a LSI circuit in the future, dynamics of a large scale aggregation of the hybrid cell models as a cardiac tissue model can be simulated in real-time with a smaller energy consumption, where it would be possible to model more complex dynamics of the heart tissue as a large scale excitable medium than the one exhibited by one dimensional tissue and control of them, such as spiral wave propagations, break-up of spiral waves, and defibrillation of them[21, 61].

Acknowledgements

First of all, I would like to express my deepest sense of gratitude to Prof. Taishin Nomura as my supervisor. This work would not have been possible without his patient guidance, encouragement and nourishment advice throughout this study. His excellent supports and feedbacks always motivate me to meet goals and objectives in this study.

I would like to express my gratitude to Prof. Osamu Oshiro and Prof. Toshimitsu Ushio as reviewers of this thesis. I also would like to thank Dr. Naruhiro Shiozawa for his valuable advice and providing me with useful information for the research. My special thanks to Dr. Rachid Ait Haddou for his kind support and great assistance. I also would like to give my fully gratitude to Miss Yukiko Ichihara for being very comfort and always lend a helping hand during my three years of study at Osaka University. Without their full cooperation, I may not possible to finish my research.

This thesis would not also have been possible without partly supports by the Global COE program " in silico medicine " from the Center for Advanced Medical Engineering and Informatics of Osaka University in providing excellent chances of earning knowledges and materials for this research. It is an honor for me to dedicate my special thanks to the former graduate students from Biodynamics Laboratory of Osaka University, Toshihiro Shimizu, Takashi Sakuhana and Takuji Nishimura for getting involved in developing this research.

I would also like to express my sincere thanks to the second-year PhD student, Mr.

Yasuyuki Suzuki for sharing experiences and knowledge during my three years of research and to the first-year PhD student, Mr. Fu Chunjiang for great discussions and ideas. I also would like to acknowledge my gratitude to all the second-year Master's students, Mr. Kesuke Tominaga, Mr. Kosuke Taru, Miss Nana Sugie, Mr. Yoshinori Kousoku, Mr. Yoshitaka Todate, Mr. Yosuke Yumikura for their great help and valuable assistance in the research and to all the first-year Master's students, Mr. Kazuya Okawa, Mr. Nobuhisa Yoshida, Mr. Ryota Hasegawa, Mr. Shota Tateyama, Mr. Yuichiro Nakamura for their great help and valuable assistance in the research. I would also like to thank all the fourth-year Bachelor students, Mr. Daichi Sakai, Mr. Hiroyuki Shakuda, Mr. Naoya Yoshikawa, Mr. Toshiya Teramura for their warmest support during the research time. Their diligence motivation and excellent actions during research and studies always encourage me to move forward.

A very special thanks to Prof. Kazuo Sasaki and Prof. Kazuki Nakajima, my former supervisors from University of Toyama who have been very supportive in guiding me to getting the chance of furthering my studies at Osaka University. And I would like to dedicate this thesis to my husband, Aizan Bin Masdar, my parents and my family in Malaysia for their moral support and encouragement during my study in Japan. Their endless courage and conviction will always inspire me. I could hardly end this without thanking my late sister, Elyahani Binti Mahmud for her memorable supports and loves.

Last but not least, the warmest regards to all the persons above, their kindness and professionalism are much appreciated and will never be forgotten.

References

[1] Hille B. Ion Channels of Excitable Membranes (3rd Edition). HilleBook, 2001.

[2] Yehia A.R., Shrier A. and Lo K.C.-L. and Guevara M.R. Transient outward current contributes to Wenckebach-like rhythms in isolated rabbit ventricular cells. American Journal of Physiology - Heart and Circulatory Physiology,Vol 273, No 1 42-1: H1-H11, 1997.

[3] Luo C.H. and Rudy Y. A Model of the Ventricular Cardiac Action Potential. Depolarization, Repolarization, and Their Interaction. Circulation Research Vol 68, No 6: 1501-1526, 1991.

[4] Kaplan D. and Glass L. Understanding Nonlinear Dynamics. Springer-Verlag, 1995.

[5] Winfree A.T. Spiral waves of chemical activity. Science Vol 175: 634-636, 1972.

[6] Winfree A.T. Varieties of spiral wave behavior: An experimentalist's approach to the theory of excitable media. Chaos Vol 1, No 3: 303-334, 1991.

[7] Markus M., Kloss G. and Kusch I. Disordered waves in a homogeneous, motionless excitable medium. Chaos Vol 371: 402-404, 1994.

[8] Francis X. W., L. Joshua Leon, Patricia A. P., Wayne R. G., Mark L.S., William L.D. and Arthur T.W. Satiotemporal evolution of ventricular fibrillation. Nature, Vol 392: 78-82, 1998.

[9] Josephson M.E. and Wellens H.J.J. Tachycardias: Mechanisms and Management. Futura, 1993.

[10] Hodgkin A.L. and Huxley A.F. A quantitative description of membrane current and its application to conduction and excitation in nerve. J. Physiol. Vol 117: 500-544, 1952.

[11] Fitzhugh R. Thresholds and Plateaus in the Hodgkin-Huxley Nerve Equations. J. Gen. Physiol. Vol 43, No 5: 867-896, 1960.

[12] Noble D. Cardiac action potential and pacemaker potentials based on the Hodgkin-Huxley equations. Nature Vol 188: 495-497, 1960.

[13] Beeler G.W. and Reuter H. Reconstruction of the action potential of ventricular myocardial fibres. J. Physiol. Vol 268: 177-210, 1977.

[14] Luo C.H and Rudy Y. A dynamic model of the cardiac ventricular action potential. I. Simulations of ionic currents and concentration changes. Circ. Res. Vol 74 : 1071-1096, 1994.

[15] Luo C.H and Rudy Y. A dynamic model of the cardiac ventricular action potential. II. Afterdepolarizations, triggered activity, and potentiation. Circ. Res. Vol 74 : 1097-1113, 1994.

[16] Alonso J.M., Ferrero J.M., Hernndez V., Molto G., Monserrat M. and Saiz J. Three-Dimensional Cardiac Electrical Activity Simulation on Cluster and Grid Platforms, in High Performance Computing for Computational Science - VECPAR 2004, Lecture Notes in Computer Science, Eds. Dayde M. et al. Journal of Cardiovascular Electrophysiology Vol 3402, No 3: 219-232, 2005.

[17] Harmon L.D. Studies with Artificial Neurons, I: Properties and Functions of an Artificial Neuron. Kybernetik Vol 1, No 3: 89-101, December 1961.

[18] Nagumo J., Arimoto S. and Yoshizawa S. An Active Pulse Transmission Line Simulating Nerve Axon. Proceedings of the IRE Vol 50, No 10: 2061 -2070, October 1962.

[19] Nagumo J., Yoshizawa S. and Arimoto S. Bistable Transmission Lines. IEEE Transactions on Circuit Theory Vol 12, No 3: 400-412, September 1965.

[20] Rachmuth G. and Poon C.-S. Transistor analogs of emergent iono-neuronal dynamics. HFSP Journal Vol 2, No 3: 156-166, June 2008.

[21] Fenton F.H., Evans S.J. and Hastings H.M. Memory in an Excitable Medium: A Mechanism for Spiral Wave Breakup in the Low-Excitability Limit. Physical Review Letters Vol 83, No 19: 3964-3967, November 1999.

[22] Henry H. and Rappel W.-J. The role of M cells and the long QT syndrome in cardiac arrhythmias: Simulation studies of reentrant excitations using a detailed electrophysiological model. Chaos Vol 14, No 1: 172-182, 2004.

[23] Schwartz P.J., Priori S.G., Spazzolini C., Moss, A.J., Michael Vincent G., Napolitano C., Denjoy I., Guicheney P., Breithardt G., Keating M.T., Towbin J.A., Beggs A.H., Brink P., Wilde A.A.M., Toivonen L., Zareba, W., Robinson J.L. and Timothy K.W., Corfield V., Wattanasirichaigoon D., Corbett C., Haverkamp W., Schulze-Bahr E., Lehmann M.H., Schwartz K., Coumel P. and Bloise R. Genotype-phenotype correlation in the long-QT syndrome: Gene-specific triggers for life-threatening arrhythmias. Circulation Vol 103, No 1: 89-95, 2001.

[24] Arthur C.G. Textbook of Medical Physiology, Asian Edition. Igaku Shoin LTD, 1976.

[25] Bowditch H.P. On the peculiarities of excitability which the fibres of cardiac muscle show. American Journal of Mathematics. Vol 23: 652-689, 1871.

[26] Hodgkin A.L. and Huxley A.F. Action potentials recorded from inside a nerve fiber. Nature (Lond). Vol 144: 710-711, 1939.

[27] Hodgkin A.L. and Huxley A.F. Resting and action potentials in nerve fibers. J Physiol (Lond). Vol 104: 176-195, 1945.

[28] Curtis H.J. and Cole K.S. Membrane action potentials from the squid axon. J Cell Comp Physiol. Vol 15: 147-157, 1940.

[29] Curtis H.J. and Cole K.S. Membrane resting potential and action potentials from the squid axon. J Cell Comp Physiol. Vol 15: 135-144, 1942.

[30] Ling G. and Gerard R.W. The normal membrane potentials of frog sartorius fibers. J Cell Comp Physiol. Vol 34: 383-396, 1949.

[31] Nastuk W.L and Hodgkin A.L. The electrical activity of single muscle fibers. J Cell Comp Physiol. Vol 35: 39, 1950.

[32] Coraboeuf E. and Weidmann S. C R Soc Biol (Paris). Vol 143: 1329, 1949.

[33] Draper M.H. and Weidmann S. Cardiac resting and action potentials recorded with an intracellular electrode. J Physiol. Vol 115: 74-94, 1951.

[34] Woodbury L.A., Woodbury J.W. and Hecht H.H. Membrane resting and action potential of single cardiac muscle fibers. Circulation. Vol 1: 264-266, 1950.

[35] Hermann H. Contributions to the physiology and physics of Nerves. Pflügers Archiv: European Journal of Physiology. Vol 109: 95-144, 1905.

[36] Curtis H.J. and Cole K.S. Transverse electrical impedance of the squid giant axon. J Gen Physiol. Vol 21: 757-165, 1938.

[37] Candido C. and David S. R. Quantitative Cardiac Electrophysiology. Marcel Dekker, Inc., 2002.

[38] Noble D. and Rudy Y. Models of cardiac ventricular action potentials: iterative interaction between experiment and simulation. Phil. Trans. R. Soc. Lond. A Vol 359, No. 1733 : 1127-1142, 2001.

[39] Winslow R.L., Rice J., Jafri S., Marban E and O'Rourke B. Mechanisms of altered excitation-contraction coupling in canine tachycardia-induced heart failure, II: Model studies. Circ Res Vol 84: 571-586, July 1999.

[40] Rudy Y. and Silva J.R. Computational biology in the study of cardiac ion channels and cell electrophysiology. Quarterly Reviews of Biophysics Vol 39, No 1: 57-116, March 2006.

[41] Faber G.M., Silva J., Livshitz L. and Rudy Y. Kinetic Properties of the Cardiac L-Type Ca21 Channel and Its Role in Myocyte Electrophysiology: A Theoretical Investigation. Biophysical Journal Vol 92: 1522-1543, March 2007.

[42] Xu A. and Guevara M.R. Two forms of spiral-wave reentry in an ionic model of ischemic ventricular myocardium. Chaos Vol 8, No 1: 157-174, 1998.

[43] Tran D.X., Yang M.-J., Weiss J.N., Garfinkel A. and Qu Z. Vulnerability to reentry in simulated two-dimensional cardiac tissue: Effects of electrical restitution and stimulation sequence. Chaos Vol 17, No 4: 043115, 2007.

[44] Ashihara T., Namba T., Ikeda T., Ito M., Kinoshita M. and Nakazawa K. Breakthrough waves during ventricular fibrillation depend on the degree of rotational anisotropy and the boundary conditions: A simulation study. Journal of Cardiovascular Electrophysiology Vol 12, No 3: 312-322, 2001.

[45] FitzHugh R. Impulses and Physiological States in Theoretical Models of Nerve Membrane. Biophysical Journal Vol 1, No 6: 445-466, 1961.

[46] deCastro M., Hofer E., Munuzuri A.P., Gomez-Gesteira M., Plank G., Schafferhofer I., Perez-Munuzuri V. and Perez-Villar V. Comparison between the role of discontinuities in cardiac conduction and in a one-dimensional hardware model. Physical Review E Vol 59, No 5: 5962-5969, May 1999.

[47] Hoshimiya N., Yoshida S., Shogen K. and Matsuo T. Two-Terminal Electronic Circuit Neuron Model with Excitable Membrane V–I–t Characteristics Improvement and Application. Biol. Cybernetics Vol 35: 125-130, 1979.

[48] Yagi H. Special Articles on Biomedical Electronics. 1. Biological Cybernetics and Electronics (in Japanese). Transactions of The Institute of Electronics, Information and Communication Engineers Vol 75, No 9: 916-920, 1992. BioSystems Vol 58: 93-100, 2000.

[49] Maeda Y. and Makino H. A pulse-type hardware neuron model with beating, bursting excitation and plateau potential. BioSystems Vol 58: 93-100, 2000.

[50] Maeda Y., Yagi E. and Makino H. Synchronization with low power consumption of hardware models of cardiac cells. BioSystems Vol 79: 125-131, 2005.

[51] Sekine Y., Torita K. and Matsuoka J. Yagi-Type Hardware Neuron Model with CMOS IC. Electronics and Communications in Japan, Part 2 Vol 85, No 3: 23-29, 2002.

[52] Saeki K., Sekine Y. and Aihara K. Pulse-Type Bursting Neuron Model Using Enhancement Mode MOSFETs. Electronics and Communications in Japan, Part 2 Vol 85, No 11: 1-7, 2002.

[53] Courtemanche M., Keener J.P. and Glass L. A delay equation representation of pulse circulation on a ring in excitable media. SIAM Journal on Applied Mathematics Vol 56: 119-142, November 1996.

[54] Quan W. and Rudy Y. Unidirectional block and reentry of cardiac excitation: A model study. Circulation Research Vol 66, No 2: 367-382, November 1990.

[55] Glass L. and Josephson M.E. Resetting and annihilation of reentrant abnormally rapid heartbeat. Physical Review Letters Vol 75, No 10: 2059-2062, 1995.

[56] Nomura T. and Glass L. Entrainment and termination of reentrant wave propagation in a periodically stimulated ring of excitable media. Physical Review E. Vol 53, No 6: 6353-6360, 1996.

[57] Hal K. and Glass L. How to tell a target from a spiral: The two probe problem. Physical Review Letters. Vol 82, No 25: 5164-5167, 1999.

[58] Nagai Y., González H., Shrier A. and Glass L. Paroxysmal Starting and Stopping of Circulating Waves in Excitable Media. Physical Review Letters. Vol 824, No 18: 4248-4251, 2000.

[59] Kanoh S., Imai M. and Hoshimiya N. Analog LSI Neuron Model Inspired by Biological Excitable Membrane. Systems and Computers in Japan. Vol 36, No 6: 84-91, 2005.

[60] Wijekoon Jayawan H.B. and Dudek P. Spiking and Bursting Firing Patterns of a Compact VLSI Cortical Neuron Circuit. Proceedings of International Joint Conference on Neural Networks, Orlando, Florida, USA. 1332-1337, 2007.

[61] Sinha S., Pande A. and Pandit R. Defibrillation via the Elimination of Spiral Turbulence in a Model for Ventricular Fibrillation. Physical Review Letters. Vol 86, No 16: 3678-3681, April 2001.

[62] Nishimura T. Development of a Fast Simulation of Electrical Excitation Modeling in Isolated Cardiac Cell (in Japanese). Master Thesis of Engineering Science Osaka University in 2005.

[63] Shimizu T. Development of an Analog-Digital Hybrid Model and Real-Time Simulations of Cardiac Excitation-Conduction (in Japanese). Master Thesis of Engineering Science Osaka University in 2008.

[64] Sakuhana T. Development of an Analog-Digital Hybrid Model and Real-Time Simulations of Cardiac Electrical Dynamics (in Japanese). Master Thesis of Engineering Science Osaka University in 2010.

[65] Gokan T. Full-Use Guide for PIC18 (in Japanese). Gijutsu-Hyohron Co., 2004.

[66] Gokan T. Guidebook for dsPIC Application in Electronic Control and Signal Processing (in Japanese). Gijutsu-Hyohron Co., 2006.

[67] Shimada Y. H8/Tiny Microcontroller Perfect Manual (in Japanese). CQ Publishing Co., 2005.

Appendix A

Glossary of Circuit Diagrams

Figure A.1 shows nine circuit diagrams of the voltage sources ($V1$-$V9$) for generating the Nernst potentials and others of ion channel currents in the analog part shown in Figure 3.5. Basically, general-purpose 6 V regulators (7806) are used to fix the voltage signal of $V+$ to 6 V and capacitors are applied for smoothing the electrical signal. In some of the circuits, the voltage signal of 6 V is divided by voltage-dividing circuits which consist of resistors as shown in the figure. Then, voltage followers which are constructed by using a general-purpose operational amplifier, LF356N are applied to reinforce the current signal with the value of $V1$, $V2$, $V3$, $V4$, $V5$, $V6$, $V7$, $V8$, and $V9$ as 1.3 V, 1.2 V, 6 V, 1.52 V, 2.3 V, 6 V, 1 V, 3 V, and 3.6 V, respectively.

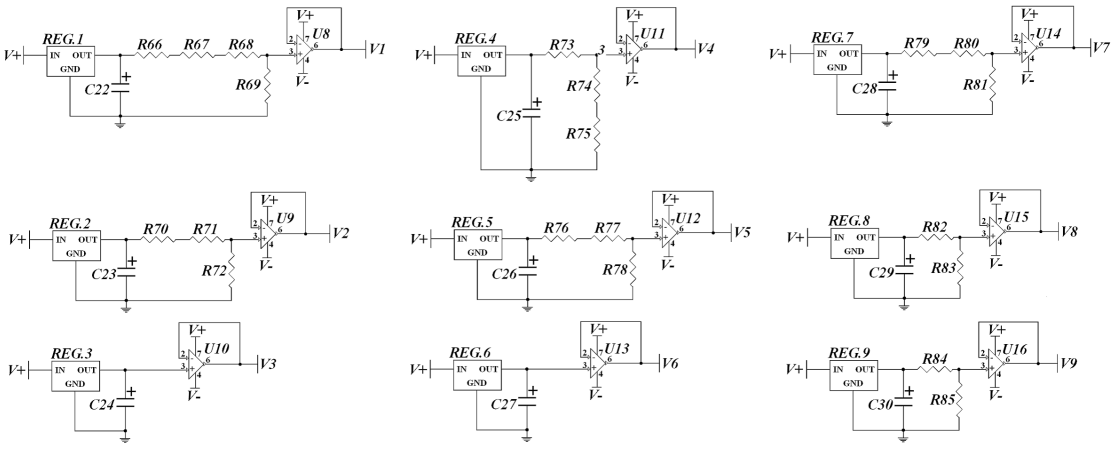

Figure A.1: Circuit diagrams of voltage sources in the analog part

Figure A.2 shows a regulated +5 V (V_{CC}) DC power supply with 1 A current limiter for the dsPIC in Figure 3.6 and the H8/3694F microcontroller in Figure 4.5. The base of this design is using a general-purpose 5 V regulator (7805, REG.10) to maintain a constant voltage level at 5V and the capacitors for over-voltage protection and smoothing the electrical signal. The $LED4$ will light up every time the power source is switched on. In this study, we used 9 V ($V+$) and -9 V ($V-$) that were supplied by a stabilized power source device.

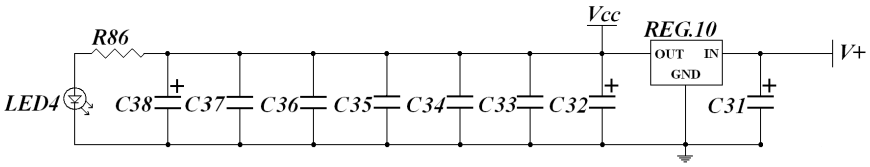

Figure A.2: A diagram of a power source circuit used in the digital part and the impulsive stimulator

Appendix B

Parameter of Components and PCB Layouts

Table B.1 presents the electronic components that are used in constructing the analog-digital hybrid active circuit and the impulsive stimulator circuit shown in Figure 3.4, Figure 3.5, Figure 3.6, Figure 4.5, Figure A.1 and Figure A.2.

PCB layout figures of the analog-digital hybrid circuit are also provided here. Those PCB layouts are prepared in actual size for available reproduction print of a double-sided circuit board, where Figure B.1, Figure B.2, and Figure B.3 correspond respectively to a top layer of signals traces, a bottom layer of signals traces and a symbol description of components for the analog part of the hybrid model.

The top layer of signals traces, the bottom layer of signals traces, and the symbol description of components in the digital part of the hybrid model are shown in Figure B.4, Figure B.5, and Figure B.6, respectively. Furthermore, black dotted symbols shown in Figure B.3 and Figure B.6, respectively, represent through holes which are used for connecting tracks between the top and the bottom layers of the analog part and the digital part.

Table B.1: The electronic components used in the analog-digital hybrid active circuit and the impulsive stimulator circuit

	Part	Model	Maker	Symbol
1	4-channel Op. Amplifier	TL084CN	Texas Instruments	U1
2	Dual-channel Op. Amplifier	TL082CN	ST Microelectronics	U2
3	dsPIC microcontroller	dsPIC30F4011-30I/P	Microchip	U3
4	D/A converter	AD5331BRUZ	Analog Devices	U4
5	SOP to DIP socket converter adapter	20P-SOD-065-300	Sunhayato	U4
6	2.5V precision voltage reference	MCP1525-I/TO	Microchip Technology	U5
7	Renesas Technology H8 microcontroller (HD64F3694FX) mounted board	MB-H8A	Sunhayato	U6
8	LCD character display module	SC1602BS-B	Sunlike Display Tech. Corp.	U7
9	Single-channel Op. Amplifier	LF356N/NOPB	National Semiconductor	U8-U16
10	Crystal oscillator	HC-49/U-S 7.3728MHz	Kyocera	X1
11	Diode	1S2076A-E	Renesas Electronics	D1
12	Red LED	L-7104SRD-G	Kingbright	LED1
13	Green LED	TLGU53C(F)	Toshiba	LED2
14	Red LED	TLSU163(F)	Toshiba	LED3
15	Yellow LED	TLPYE53T(F)	Toshiba	LED4
16	Tactile switch	SKRGAAD010	Alps Electric	SW1, SW2, SW3
17	NPN-type Bipolar transistor	2SC1815-O(F)	Toshiba	Tr1, Tr3, Tr4, Tr6, Tr8
18	PNP-type Bipolar transistor	2SA1015-O(F)	Toshiba	Tr2, Tr5, Tr7, Tr9
19	NPN-type Bipolar transistor	2SC1815-Y(F)	Toshiba	Tr10, Tr12, Tr14, Tr15
20	PNP-type Bipolar transistor	2SA1015-Y(F)	Toshiba	Tr11, Tr13
21	Ceramic condenser: 1 μF	RPER11H105K3M1C01A	MuRata	C1
22	Ceramic condenser: 0.22 μF	RPER11H224K2M1C01A	MuRata	C9
23	Ceramic condenser: 0.1 μF	RPER11H104K2M1A01A	MuRata	C2-C8, C13, C15, C17-C20, C33-C37
24	Ceramic condenser: 0.01 μF	RPER11H103K2M1C01A	MuRata	C16, C21

25	Ceramic condenser: 0.001 μF	RPER11H102K2K1A01B	MuRata	C12, C14
26	Ceramic condenser: 15 pF	RPE2C1H120J2M1Z01A	MuRata	C10
27	Ceramic condenser: 12 pF	RPE2C1H150J2M1Z01A	MuRata	C11
28	Capacitor: 16V/33 μF	ECEA1CKS330	Panasonic	C22-C32, C38
29	Linear regulator: 6V	MC7806CTG	ON Semiconductor	REG.1-REG.9
30	Linear regulator: 5V	MC7805ABTG	ON Semiconductor	REG.10
31	Potentiometer: 5kΩ	3296W-1-502LF	Bourns	R32, R61, R62, R64, R65, Rd
32	Resistor: 33MΩ	RCR25C336J	KOA	R43, R44
33	Resistor: 3MΩ	RMG25FX3M	Takman	R38
34	Resistor: 120kΩ	MF1/4CC1203F	KOA	R19, R30
35	Resistor: 30kΩ	CF1/4C303J	KOA	R22, R36, R66, R73, R76, R79, R85
36	Resistor: 20kΩ	CF1/4C203J	KOA	R10, R21, R33, R34, R35, R40, R41, R70, R71, R78, R80, R84
37	Resistor: 10kΩ	CF1/4C103J	KOA	R20, R27, R31, R49, R52, R53, R56, R59, R69, R72, R74, R81-R83
38	Resistor: 4.7kΩ	CF1/4C472J	KOA	R14
39	Resistor: 3.3kΩ	CF1/4C332J	KOA	R47, R51
40	Resistor: 3kΩ	CF1/4C302J	KOA	R8, R37, R67, R68
41	Resistor: 2kΩ	CF1/4C202J	KOA	R9, R42, R60, R63, R77
42	Resistor: 1.5kΩ	CF1/4C152J	KOA	R12, R23
43	Resistor: 1kΩ	CF1/4C102J	KOA	R1-R6, R28, R48, R54, R55
44	Resistor: 560Ω	CF1/4C561J	KOA	R50, R86
45	Resistor: 510Ω	CF1/4C511J	KOA	R24, R29
46	Resistor: 360Ω	CF1/4C361J	KOA	R15, R18, R25
47	Resistor: 330Ω	CF1/4C331J	KOA	R57, R58
48	Resistor: 200Ω	CF1/4C201J	KOA	R75
49	Resistor: 150Ω	CF1/4C151J	KOA	R39
50	Resistor: 100Ω	CF1/4C101J	KOA	R11, R13
51	Resistor: 68Ω	CF1/4C680J	KOA	R7
52	Resistor: 51Ω	CF1/4C510J	KOA	R45
53	Resistor: 33Ω	CF1/4C330J	KOA	R46
54	Resistor: 30Ω	CF1/4C300J	KOA	R16
55	Resistor: 15Ω	CF1/4C150J	KOA	R17, R26

56	3 pin connector	DF1EC-3P-2.5DSA(05)	Hirose Electric Co.	P1_POWER, P2_TO DIGITAL, P3_Vm, P4_Vm, P5_Vm, P1_ANALOG
57	2 pin connector	DF1EC-2P-2.5DSA(05)	Hirose Electric Co.	P2_POWER, P3_LED1
58	2.54mm pinch PCB pin header, jumper link	M20-9993645, M7571-05	RS	J1-J4
59	PCB signal check terminal	SLD-2-G	Sunhayato	TP1, TP2, TP3 Vm, TP4, TP5, TP6 V+, TP7 V-, TP8 V_IK+Isi, V_Iext IN

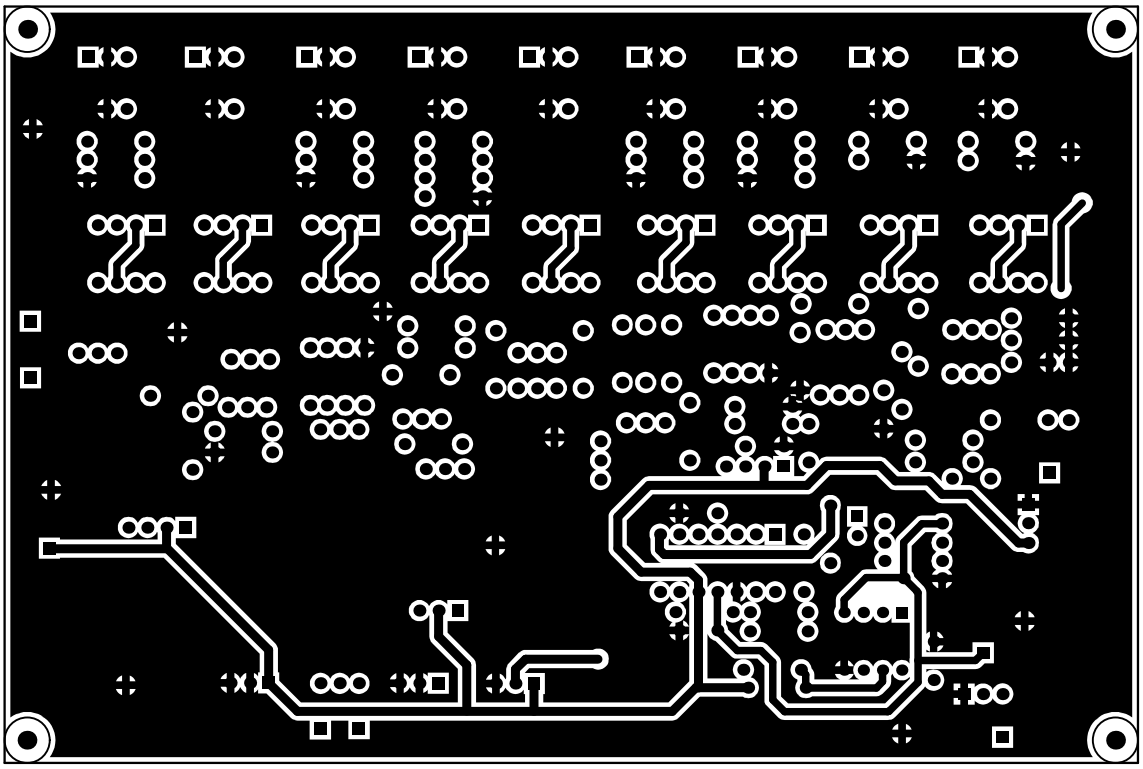

Figure B.1 Top layer of the analog part

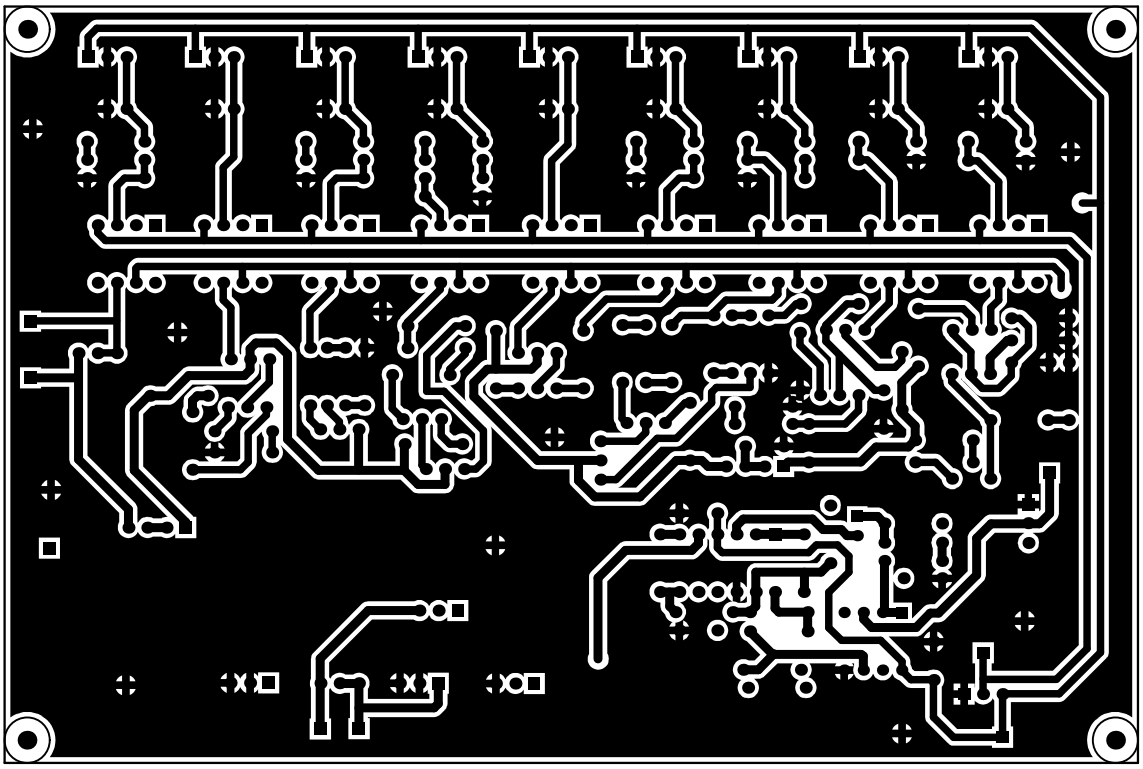

Figure B.2 Bottom layer of the analog part

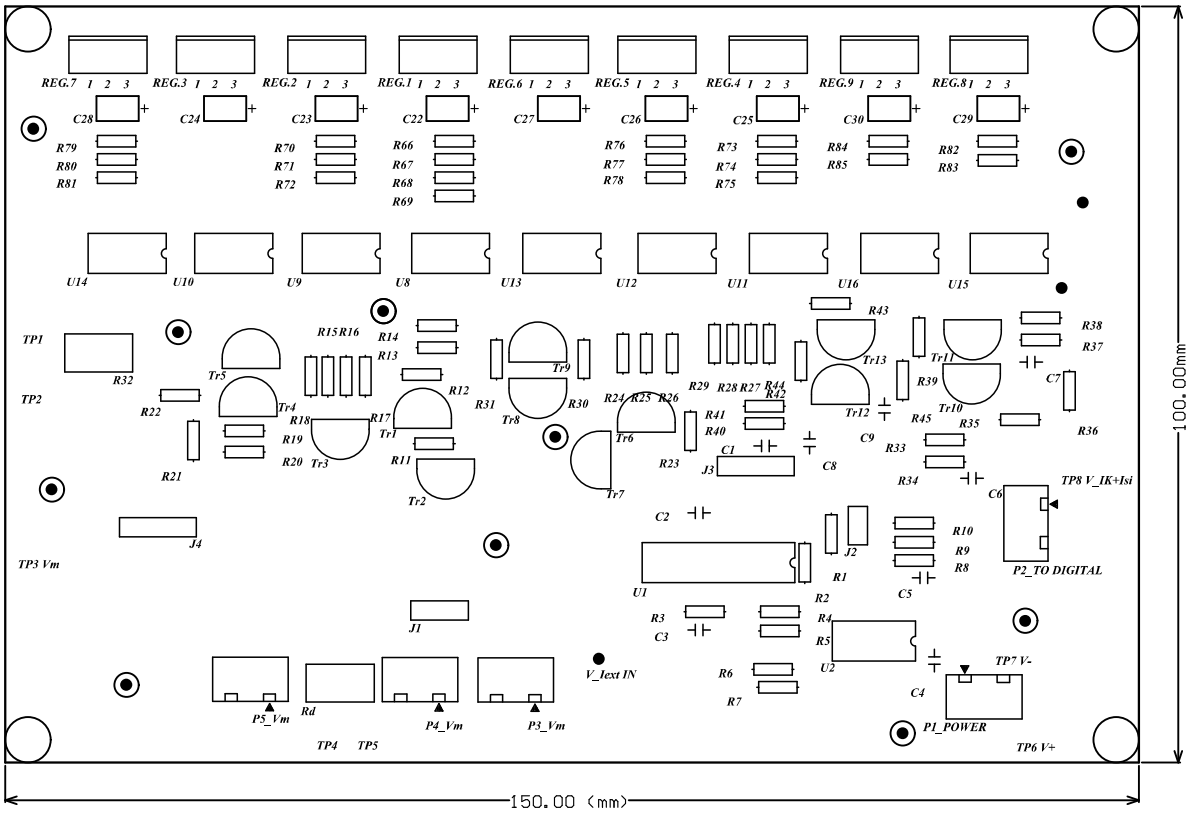

Figure B.3 Description of components in the analog part

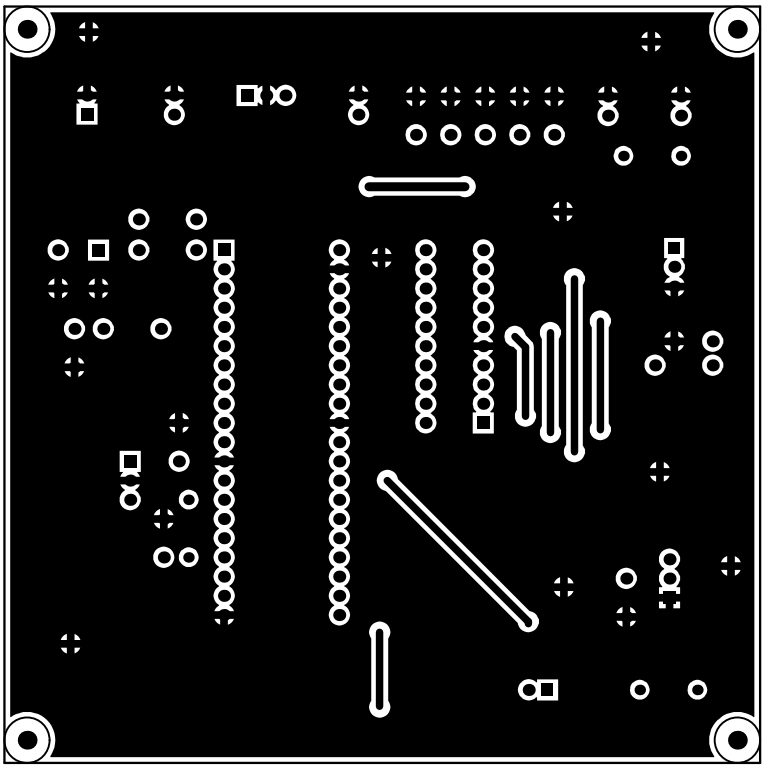

Figure B.4 Top layer of the digital part

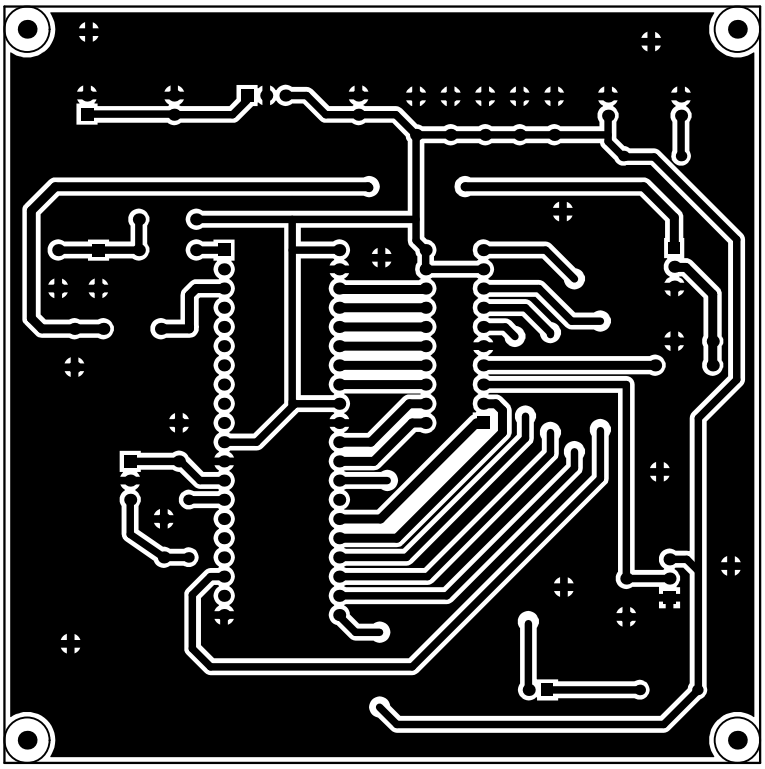

Figure B.5 Bottom layer of the digital part

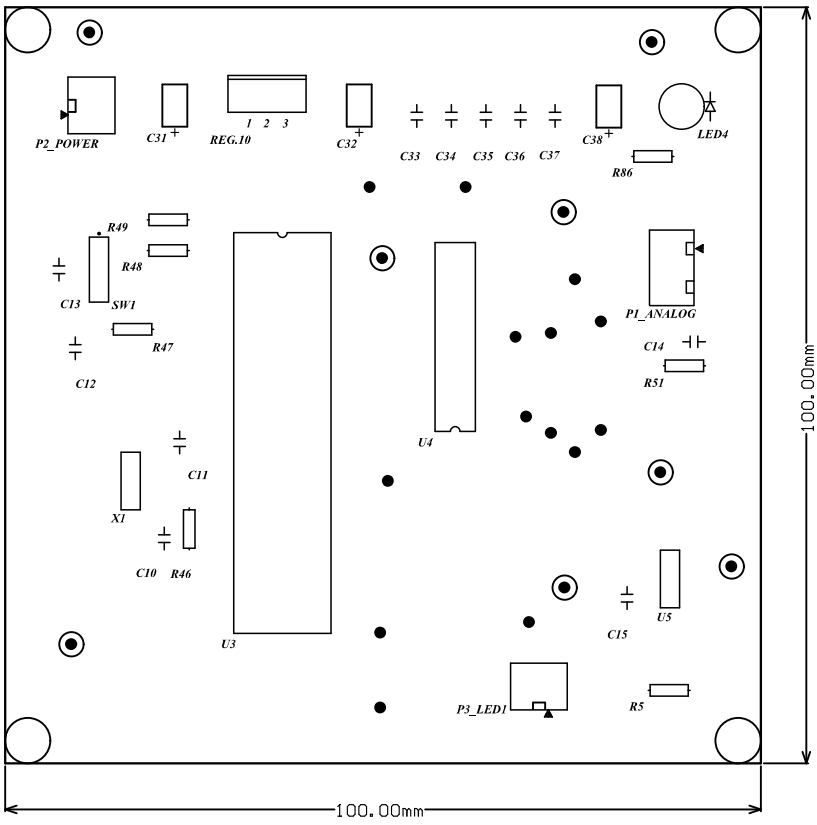

Figure B.6 Description of components in the digital part

Appendix C

Source Code Programs

List C.1 shows the C language source code program written for the dsPIC to implement the digital part of the hybrid model in reproducing the ion currents IK and Isi of the Luo-Rudy phase I model. In this work, MPLAB IDE (ver.7.50) was used as the dsPIC development environment software and a C compiler of MPLAB C30 was also used. Both can be downloaded for free from the Microchip (USA) official website. Moreover, Microchip MPLAB ICD2 was used as a tool to program the dsPIC microcontroller.

List C.1: The source code program for the dsPIC.

```
// INCLUDE DEVICE FILE
#include "p30f4011.h"
#include "timer.h"
#include "math.h"
#include "adc10.h"
// SETUP CONFIGURATION PARAMETER
_FOSC(CSW_FSCM_OFF & XT_PLL16); // 7.3728MHz x 16=117.9648MHz
_FWDT(WDT_OFF);
_FBORPOR(PBOR_ON & BORV_20 & PWRT_64 & MCLR_EN);
_FGS(CODE_PROT_OFF);
// DECLARATION OF TABLES
const double __attribute__ ((space(psv), address (0x1000)))
Ad_table[810] = {
0.00014133,0.00014578,0.00015037,0.0001551,0.00015998,0.00016501,0.0001702,0.00017556,0.00018108,0.00018678,
0.00019265,0.00019871,0.00020496,0.00021141,0.00021806,0.00022492,0.00023199,0.00023929,0.00024681,0.00025458,
0.00026258,0.00027084,0.00027935,0.00028814,0.0002972,0.00030654,0.00031618,0.00032612,0.00033637,0.00034694,
0.00035784,0.00036909,0.00038069,0.00039265,0.00040499,0.00041771,0.00043084,0.00044437,0.00045833,0.00047272,
0.00048757,0.00050288,0.00051867,0.00053496,0.00055175,0.00056907,0.00058693,0.00060535,0.00062435,0.00064393,
0.00066414,0.00068497,0.00070645,0.0007286,0.00075145,0.000775,0.00079929,0.00082434,0.00085017,0.00087681,
0.00090427,0.00093259,0.00096178,0.00099189,0.0010229,0.0010549,0.0010879,0.001122,0.001157,0.0011932,
0.0012305,0.0012689,0.0013086,0.0013494,0.0013916,0.001435,0.0014798,0.0015259,0.0015735,0.0016225,
0.001673,0.0017251,0.0017788,0.0018342,0.0018912,0.00195,0.0020106,0.002073,0.0021374,0.0022037,
0.002272,0.0023424,0.002415,0.0024897,0.0025667,0.0026461,0.0027278,0.002812,0.0028988,0.0029882,
0.0030802,0.003175,0.0032726,0.0033732,0.0034768,0.0035834,0.0036932,0.0038063,0.0039227,0.0040425,
0.0041658,0.0042928,0.0044235,0.004558,0.0046965,0.0048389,0.0049855,0.0051363,0.0052914,0.005451,
0.0056151,0.0057839,0.0059575,0.006136,0.0063195,0.0065081,0.0067021,0.0069014,0.0071061,0.0073166,
0.0075328,0.0077548,0.0079829,0.0082171,0.0084576,0.0087044,0.0089578,0.0092179,0.0094847,0.0097584,
0.010039,0.010327,0.010622,0.010925,0.011235,0.011553,0.011878,0.012211,0.012553,0.012902,
0.01326,0.013626,0.014,0.014382,0.014774,0.015173,0.015582,0.015999,0.016425,0.01686,
0.017303,0.017756,0.018217,0.018687,0.019167,0.019655,0.020151,0.020657,0.021171,0.021694,
0.022226,0.022766,0.023314,0.02387,0.024435,0.025007,0.025587,0.026175,0.02677,0.027372,
0.027981,0.028596,0.029217,0.029845,0.030478,0.031116,0.031759,0.032407,0.033059,0.033714,
0.034373,0.035035,0.035699,0.036366,0.037033,0.037702,0.038371,0.03904,0.039709,0.040377,
0.041043,0.041707,0.042368,0.043026,0.043681,0.044331,0.044976,0.045617,0.046251,0.046879,
0.0475,0.048114,0.04872,0.049317,0.049906,0.050485,0.051055,0.051615,0.052164,0.052703,
0.05323,0.053745,0.054249,0.05474,0.055219,0.055685,0.056138,0.056578,0.057005,0.057418,
0.057817,0.058202,0.058574,0.058931,0.059275,0.059604,0.059919,0.06022,0.060507,0.06078,
0.061039,0.061284,0.061515,0.061732,0.061936,0.062126,0.062303,0.062467,0.062618,0.062756,
0.062881,0.062994,0.063095,0.063184,0.063261,0.063327,0.063381,0.063425,0.063457,0.063479,
0.063491,0.063493,0.063485,0.063467,0.063441,0.063405,0.063361,0.063308,0.063247,0.063177,
0.063101,0.063016,0.062925,0.062826,0.062721,0.062609,0.062491,0.062367,0.062237,0.062101,
0.06196,0.061814,0.061663,0.061507,0.061346,0.061181,0.061012,0.060838,0.060661,0.06048,
0.060296,0.060108,0.059917,0.059723,0.059526,0.059326,0.059124,0.058919,0.058712,0.058503,
0.058292,0.058078,0.057863,0.057646,0.057428,0.057208,0.056986,0.056763,0.056539,0.056314,
0.056088,0.055861,0.055633,0.055404,0.055174,0.054944,0.054713,0.054482,0.05425,0.054017,
0.053785,0.053552,0.053319,0.053086,0.052853,0.052619,0.052386,0.052152,0.051919,0.051686,
0.051453,0.05122,0.050987,0.050755,0.050523,0.050291,0.05006,0.049829,0.049598,0.049368,
0.049138,0.048909,0.048681,0.048452,0.048225,0.047998,0.047771,0.047546,0.047321,0.047096,
0.046872,0.046649,0.046427,0.046205,0.045984,0.045763,0.045544,0.045325,0.045107,0.04489,
0.044673,0.044457,0.044242,0.044028,0.043815,0.043602,0.043391,0.04318,0.04297,0.042761,
0.042552,0.042345,0.042138,0.041932,0.041727,0.041523,0.04132,0.041117,0.040916,0.040715,
0.040515,0.040316,0.040118,0.039921,0.039725,0.039529,0.039335,0.039141,0.038948,0.038756,
0.038565,0.038375,0.038185,0.037997,0.037809,0.037622,0.037436,0.037251,0.037067,0.036884,
0.036701,0.036519,0.036339,0.036159,0.03598,0.035801,0.035624,0.035447,0.035271,0.035097,
0.034922,0.034749,0.034577,0.034405,0.034234,0.034064,0.033895,0.033727,0.033559,0.033393,
0.033227,0.033062,0.032897,0.032734,0.032571,0.032409,0.032248,0.032088,0.031928,0.031769,
```

```
0.031611,0.031454,0.031298,0.031142,0.030987,0.030833,0.030679,0.030526,0.030375,0.030223,
0.030073};

const double __attribute__ ((space(psv), address (0x2000)))
Bd_table[810] = {
0.17097,0.16927,0.16759,0.16592,0.16426,0.16261,0.16097,0.15934,0.15772,0.15612,
0.15452,0.15293,0.15135,0.14978,0.14822,0.14667,0.14513,0.1436,0.14208,0.14057,
0.13907,0.13757,0.13609,0.13461,0.13314,0.13168,0.13023,0.12879,0.12735,0.12593,
0.12451,0.1231,0.1217,0.12031,0.11892,0.11755,0.11618,0.11481,0.11346,0.11212,
0.11078,0.10945,0.10812,0.10681,0.1055,0.1042,0.10291,0.10162,0.10034,0.099072,
0.097809,0.096553,0.095305,0.094064,0.09283,0.091604,0.090385,0.089173,0.087969,0.086772,
0.085583,0.084401,0.083227,0.082059,0.0809,0.079748,0.078603,0.077466,0.076337,0.075216,
0.074102,0.072995,0.071897,0.070806,0.069724,0.068649,0.067582,0.066523,0.065472,0.06443,
0.063396,0.06237,0.061352,0.060342,0.059342,0.058349,0.057365,0.05639,0.055424,0.054466,
0.053517,0.052577,0.051646,0.050724,0.049812,0.048908,0.048013,0.047128,0.046252,0.045386,
0.044529,0.043681,0.042844,0.042015,0.041197,0.040388,0.039588,0.038799,0.038019,0.03725,
0.03649,0.03574,0.035,0.03427,0.03355,0.03284,0.03214,0.03145,0.03077,0.0301,
0.02944,0.02879,0.02815,0.02752,0.0269,0.02629,0.02569,0.0251,0.02452,0.023949,
0.023389,0.022838,0.022296,0.021765,0.021242,0.02073,0.020227,0.019733,0.019249,0.018773,
0.018307,0.017851,0.017403,0.016964,0.016534,0.016112,0.0157,0.015295,0.0149,0.014512,
0.014133,0.013763,0.0134,0.013045,0.012698,0.012359,0.012027,0.011703,0.011386,0.011077,
0.010775,0.01048,0.010192,0.0099104,0.0096358,0.0093679,0.0091065,0.0088515,0.0086027,0.0083601,
0.0081236,0.007893,0.0076682,0.0074491,0.0072356,0.0070276,0.006825,0.0066277,0.0064354,0.0062483,
0.0060661,0.0058887,0.005716,0.005548,0.0053845,0.0052254,0.0050706,0.0049201,0.0047736,0.0046312,
0.0044928,0.0043582,0.0042273,0.0041001,0.0039765,0.0038563,0.0037396,0.0036262,0.003516,0.0034089,
0.0033049,0.0032039,0.0031059,0.0030106,0.0029181,0.0028284,0.0027412,0.0026566,0.0025745,0.0024948,
0.0024175,0.0023424,0.0022696,0.002199,0.0021304,0.0020639,0.0019994,0.0019368,0.0018762,0.0018173,
0.0017602,0.0017049,0.0016512,0.0015992,0.0015488,0.0014999,0.0014525,0.0014065,0.001362,0.0013188,
0.001277,0.0012364,0.0011971,0.001159,0.0011221,0.0010864,0.0010517,0.0010182,0.00098564,0.00095414,
0.00092362,0.00089405,0.00086541,0.00083768,0.00081081,0.00078479,0.00075958,0.00073517,0.00071153,0.00068864,
0.00066647,0.00064501,0.00062422,0.00060409,0.0005846,0.00056573,0.00054746,0.00052977,0.00051265,0.00049607,
0.00048002,0.00046448,0.00044944,0.00043488,0.00042079,0.00040714,0.00039394,0.00038116,0.00036878,0.00035681,
0.00034522,0.000334,0.00032314,0.00031264,0.00030247,0.00029263,0.0002831,0.00027389,0.00026497,0.00025634,
0.00024798,0.0002399,0.00023208,0.00022451,0.00021719,0.0002101,0.00020325,0.00019661,0.00019019,0.00018398,
0.00017797,0.00017216,0.00016653,0.00016109,0.00015583,0.00015073,0.0001458,0.00014103,0.00013642,0.00013196,
0.00012764,0.00012346,0.00011942,0.00011551,0.00011173,0.00010807,0.00010453,0.0001011,9.7791e-005,9.4586e-005,
9.1487e-005,8.8488e-005,8.5587e-005,8.2781e-005,8.0067e-005,7.7441e-005,7.4901e-005,7.2445e-005,7.0068e-005,6.7769e-005,
6.5546e-005,6.3395e-005,6.1315e-005,5.9302e-005,5.7356e-005,5.5473e-005,5.3652e-005,5.189e-005,5.0186e-005,4.8538e-005,
4.6944e-005,4.5403e-005,4.3911e-005,4.2469e-005,4.1074e-005,3.9724e-005,3.8419e-005,3.7157e-005,3.5936e-005,3.4755e-005,
3.3613e-005,3.2508e-005,3.144e-005,3.0406e-005,2.9407e-005,2.844e-005,2.7505e-005,2.6601e-005,2.5726e-005,2.488e-005,
2.4062e-005,2.3271e-005,2.2506e-005,2.1766e-005,2.105e-005,2.0358e-005,1.9688e-005,1.904e-005,1.8414e-005,1.7808e-005,
1.7223e-005,1.6656e-005,1.6108e-005,1.5578e-005,1.5066e-005,1.457e-005,1.4091e-005,1.3627e-005,1.3179e-005,1.2745e-005,
1.2326e-005,1.192e-005,1.1528e-005,1.1148e-005,1.0781e-005,1.0427e-005,1.0083e-005,9.7515e-006,9.4306e-006,9.1202e-006,
8.82e-006,8.5297e-006,8.2489e-006,7.9774e-006,7.7148e-006,7.4608e-006,7.2152e-006,6.9777e-006,6.748e-006,6.5258e-006,
6.311e-006,6.1032e-006,5.9023e-006,5.708e-006,5.52e-006,5.3383e-006,5.1625e-006,4.9925e-006,4.8282e-006,4.6692e-006,
4.5154e-006,4.3668e-006,4.223e-006,4.0839e-006,3.9494e-006,3.8194e-006,3.6936e-006,3.572e-006,3.4544e-006,3.3406e-006,
3.2306e-006,3.1242e-006,3.0213e-006,2.9218e-006,2.8256e-006,2.7326e-006,2.6426e-006,2.5555e-006,2.4714e-006,2.39e-006,
2.3113e-006,2.2352e-006,2.1615e-006,2.0903e-006,2.0215e-006,1.9549e-006,1.8905e-006,1.8283e-006,1.7681e-006,1.7098e-006,
1.6535e-006,1.599e-006,1.5464e-006,1.4954e-006,1.4462e-006,1.3986e-006,1.3525e-006,1.3079e-006,1.2649e-006,1.2232e-006,
1.1829e-006};

const double __attribute__ ((space(psv), address (0x3000)))
Af_table[810] = {
0.021346,0.021261,0.021176,0.021092,0.021007,0.020924,0.02084,0.020757,0.020674,0.020591,
0.020509,0.020427,0.020345,0.020264,0.020183,0.020102,0.020022,0.019942,0.019862,0.019783,
0.019704,0.019625,0.019547,0.019468,0.01939,0.019313,0.019236,0.019159,0.019082,0.019005,
0.018929,0.018853,0.018778,0.018703,0.018628,0.018553,0.018478,0.018404,0.01833,0.018257,
0.018183,0.01811,0.018037,0.017964,0.017892,0.01782,0.017748,0.017676,0.017605,0.017533,
0.017462,0.017391,0.017321,0.01725,0.01718,0.01711,0.01704,0.01697,0.0169,0.016831,
0.016761,0.016692,0.016623,0.016554,0.016485,0.016416,0.016347,0.016278,0.016209,0.01614,
0.016071,0.016002,0.015933,0.015864,0.015795,0.015725,0.015656,0.015586,0.015516,0.015445,
0.015375,0.015303,0.015232,0.01516,0.015087,0.015014,0.014941,0.014866,0.014791,0.014715,
0.014638,0.01456,0.014481,0.014401,0.01432,0.014237,0.014153,0.014068,0.01398,0.013891,
0.0138,0.013707,0.013612,0.013514,0.013414,0.013312,0.013206,0.013098,0.012986,0.012871,
0.012752,0.01263,0.012504,0.012374,0.01224,0.012101,0.011958,0.01181,0.011657,0.011499,
0.011335,0.011167,0.010993,0.010813,0.010628,0.010437,0.010241,0.010039,0.0098318,0.0096192,
0.0094013,0.0091785,0.0089509,0.0087189,0.0084828,0.0082429,0.0079998,0.0077539,0.0075057,0.0072557,
0.0070045,0.0067527,0.006501,0.0062498,0.006,0.0057521,0.0055066,0.0052643,0.0050256,0.0047912,
0.0045615,0.0043371,0.0041182,0.0039054,0.0036989,0.003499,0.003306,0.0031201,0.0029413,0.0027697,
0.0026055,0.0024485,0.0022988,0.0021563,0.0020208,0.0018922,0.0017704,0.0016552,0.0015464,0.0014437,
0.001347,0.001256,0.0011704,0.0010901,0.0010148,0.00094423,0.00087816,0.00081636,0.0007586,0.00070467,
0.00065433,0.00060739,0.00056365,0.0005229,0.00048496,0.00044967,0.00041684,0.00038632,0.00035797,0.00033163,
0.00030717,0.00028447,0.00026341,0.00024387,0.00022575,0.00020895,0.00019337,0.00017894,0.00016557,0.00015318,
0.00014171,0.00013108,0.00012125,0.00011214,0.00010371,9.591e-005,8.869e-005,8.2009e-005,7.5828e-005,7.0109e-005,
6.4819e-005,5.9926e-005,5.54e-005,5.1214e-005,4.7343e-005,4.3764e-005,4.0454e-005,3.7393e-005,3.4563e-005,3.1946e-005,
2.9527e-005,2.7291e-005,2.5224e-005,2.3313e-005,2.1546e-005,1.9913e-005,1.8403e-005,1.7008e-005,1.5718e-005,1.4526e-005,
1.3425e-005,1.2406e-005,1.1465e-005,1.0595e-005,9.7913e-006,9.0483e-006,8.3616e-006,7.7271e-006,7.1406e-006,6.5986e-006,
6.0977e-006,5.6348e-006,5.2071e-006,4.8118e-006,4.4465e-006,4.1089e-006,3.7969e-006,3.5086e-006,3.2422e-006,2.996e-006,
2.7685e-006,2.5583e-006,2.364e-006,2.1845e-006,2.0186e-006,1.8653e-006,1.7236e-006,1.5927e-006,1.4718e-006,1.36e-006,
1.2567e-006,1.1613e-006,1.0731e-006,9.9156e-007,9.1625e-007,8.4666e-007,7.8236e-007,7.2293e-007,6.6803e-007,6.1729e-007,
5.704e-007,5.2708e-007,4.8704e-007,4.5005e-007,4.1586e-007,3.8428e-007,3.5509e-007,3.2812e-007,3.0319e-007,2.8016e-007,
2.5888e-007,2.3922e-007,2.2105e-007,2.0426e-007,1.8874e-007,1.7441e-007,1.6116e-007,1.4892e-007,1.3761e-007,1.2715e-007,
1.175e-007,1.0857e-007,1.0032e-007,9.2703e-008,8.5662e-008,7.9155e-008,7.3142e-008,6.7586e-008,6.2453e-008,5.7709e-008,
5.3325e-008,4.9275e-008,4.5532e-008,4.2073e-008,3.8877e-008,3.5924e-008,3.3195e-008,3.0674e-008,2.8344e-008,2.6191e-008,
2.4201e-008,2.2363e-008,2.0664e-008,1.9095e-008,1.7644e-008,1.6304e-008,1.5066e-008,1.3921e-008,1.2864e-008,1.1887e-008,
1.0984e-008,1.0149e-008,9.3785e-009,8.6661e-009,8.0078e-009,7.3995e-009,6.8375e-009,6.3181e-009,5.8382e-009,5.3947e-009,
4.9849e-009,4.6063e-009,4.2564e-009,3.9331e-009,3.6343e-009,3.3582e-009,3.1031e-009,2.8674e-009,2.6496e-009,2.4484e-009,
2.2624e-009,2.0905e-009,1.9317e-009,1.785e-009,1.6494e-009,1.5241e-009,1.4083e-009,1.3014e-009,1.2025e-009,1.1112e-009,
1.0268e-009,9.4878e-010,8.7671e-010,8.1011e-010,7.4858e-010,6.9171e-010,6.3917e-010,5.9062e-010,5.4576e-010,5.043e-010,
4.6599e-010,4.306e-010,3.9789e-010,3.6767e-010,3.3974e-010,3.1393e-010,2.9008e-010,2.6805e-010,2.4769e-010,2.2887e-010,
2.1149e-010,1.9542e-010,1.8058e-010,1.6686e-010,1.5419e-010,1.4248e-010,1.3165e-010,1.2165e-010,1.1241e-010,1.0387e-010,
9.5983e-011,8.8692e-011,8.1955e-011,7.573e-011,6.9977e-011,6.4662e-011,5.975e-011,5.5212e-011,5.1018e-011,4.7142e-011,
4.3561e-011,4.0253e-011,3.7195e-011,3.437e-011,3.1759e-011,2.9346e-011,2.7117e-011,2.5057e-011,2.3154e-011,2.1395e-011,
1.977e-011,1.8268e-011,1.6881e-011,1.5598e-011,1.4414e-011,1.3319e-011,1.2307e-011,1.1372e-011,1.0508e-011,9.7102e-012,
8.9726e-012,8.291e-012,7.6612e-012,7.0793e-012,6.5415e-012,6.0446e-012,5.5855e-012,5.1612e-012,4.7692e-012,4.4069e-012,
4.0722e-012,3.7628e-012,3.477e-012,3.2129e-012,2.9688e-012,2.7433e-012,2.5349e-012,2.3424e-012,2.1645e-012,2.0001e-012,
1.8481e-012,1.7077e-012,1.578e-012,1.4582e-012,1.3474e-012,1.245e-012,1.1505e-012,1.0631e-012,9.8233e-013,9.0771e-013,
8.3876e-013};
```

```
const double __attribute__ ((space(psv), address (0x4000)))
Bf_table[810] = {
2.1918e-008,2.3982e-008,2.6241e-008,2.8712e-008,3.1416e-008,3.4374e-008,3.7612e-008,4.1154e-008,4.5029e-008,4.927e-008,
5.391e-008,5.8987e-008,6.4542e-008,7.062e-008,7.727e-008,8.4547e-008,9.2509e-008,1.0122e-007,1.1075e-007,1.2118e-007,
1.326e-007,1.4508e-007,1.5875e-007,1.737e-007,1.9005e-007,2.0795e-007,2.2753e-007,2.4896e-007,2.7241e-007,2.9806e-007,
3.2613e-007,3.5684e-007,3.9045e-007,4.2722e-007,4.6745e-007,5.1147e-007,5.5963e-007,6.1233e-007,6.7e-007,7.3309e-007,
8.0213e-007,8.7766e-007,9.6031e-007,1.0507e-006,1.1497e-006,1.2579e-006,1.3764e-006,1.506e-006,1.6478e-006,1.803e-006,
1.9728e-006,2.1585e-006,2.3618e-006,2.5841e-006,2.8274e-006,3.0937e-006,3.3849e-006,3.7036e-006,4.0523e-006,4.4338e-006,
4.8512e-006,5.3078e-006,5.8075e-006,6.3541e-006,6.9522e-006,7.6065e-006,8.3224e-006,9.1055e-006,9.9623e-006,1.09e-005,
1.1925e-005,1.3047e-005,1.4274e-005,1.5616e-005,1.7085e-005,1.8691e-005,2.0448e-005,2.237e-005,2.4472e-005,2.6771e-005,
2.9285e-005,3.2035e-005,3.5042e-005,3.8329e-005,4.1924e-005,4.5855e-005,5.0152e-005,5.4849e-005,5.9983e-005,6.5594e-005,
7.1725e-005,7.8425e-005,8.5744e-005,9.3738e-005,0.00010247,0.000112,0.00012241,0.00013376,0.00014616,0.00015967,
0.00017441,0.00019047,0.00020798,0.00022704,0.00024779,0.00027037,0.00029493,0.00032161,0.00035059,0.00038203,
0.00041612,0.00045305,0.00049301,0.0005362,0.00058284,0.00063312,0.00068727,0.00074547,0.00080793,0.00087484,
0.00094637,0.0010227,0.0011039,0.0011901,0.0012813,0.0013777,0.001479,0.0015853,0.0016964,0.0018121,
0.001932,0.0020558,0.002183,0.0023132,0.0024457,0.0025798,0.002715,0.0028504,0.0029852,0.0031187,
0.00325,0.0033784,0.0035032,0.0036235,0.0037389,0.0038487,0.0039524,0.0040496,0.00414,0.0042234,
0.0042997,0.0043687,0.0044305,0.0044852,0.004533,0.004574,0.0046085,0.0046368,0.0046591,0.0046759,
0.0046874,0.004694,0.004696,0.0046939,0.0046878,0.0046782,0.0046653,0.0046495,0.004631,0.0046101,
0.0045869,0.0045619,0.0045351,0.0045068,0.0044771,0.0044462,0.0044143,0.0043814,0.0043478,0.0043136,
0.0042787,0.0042434,0.0042077,0.0041717,0.0041355,0.004099,0.0040625,0.0040259,0.0039893,0.0039526,
0.0039161,0.0038796,0.0038432,0.0038069,0.0037708,0.0037349,0.0036992,0.0036637,0.0036284,0.0035933,
0.0035585,0.0035239,0.0034896,0.0034555,0.0034217,0.0033882,0.003355,0.003322,0.0032893,0.003257,
0.0032249,0.0031931,0.0031615,0.0031303,0.0030993,0.0030687,0.0030383,0.0030082,0.0029784,0.0029489,
0.0029197,0.0028907,0.002862,0.0028336,0.0028055,0.0027776,0.00275,0.0027227,0.0026957,0.0026689,
0.0026424,0.0026161,0.0025901,0.0025644,0.0025389,0.0025136,0.0024886,0.0024639,0.0024394,0.0024151,
0.0023911,0.0023673,0.0023438,0.0023205,0.0022974,0.0022745,0.0022519,0.0022295,0.0022073,0.0021854,
0.0021636,0.0021421,0.0021208,0.0020997,0.0020788,0.0020581,0.0020376,0.0020174,0.0019973,0.0019774,
0.0019578,0.0019383,0.001919,0.0018999,0.001881,0.0018623,0.0018437,0.0018254,0.0018072,0.0017893,
0.0017715,0.0017538,0.0017364,0.0017191,0.001702,0.0016851,0.0016683,0.0016517,0.0016353,0.001619,
0.0016029,0.0015869,0.0015711,0.0015555,0.00154,0.0015247,0.0015095,0.0014945,0.0014796,0.0014649,
0.0014503,0.0014359,0.0014216,0.0014075,0.0013935,0.0013796,0.0013659,0.0013523,0.0013388,0.0013255,
0.0013123,0.0012993,0.0012863,0.0012735,0.0012609,0.0012483,0.0012359,0.0012236,0.0012114,0.0011994,
0.0011874,0.0011756,0.0011639,0.0011523,0.0011409,0.0011295,0.0011183,0.0011072,0.0010961,0.0010852,
0.0010744,0.0010638,0.0010532,0.0010427,0.0010323,0.001022,0.0010119,0.0010018,0.00099184,0.00098197,
0.0009722,0.00096252,0.00095295,0.00094346,0.00093408,0.00092478,0.00091558,0.00090647,0.00089745,0.00088852,
0.00087968,0.00087093,0.00086226,0.00085368,0.00084519,0.00083678,0.00082845,0.00082021,0.00081205,0.00080397,
0.00079597,0.00078805,0.00078021,0.00077244,0.00076476,0.00075715,0.00074961,0.00074215,0.00073477,0.00072746,
0.00072022,0.00071305,0.00070596,0.00069893,0.00069198,0.00068509,0.00067828,0.00067153,0.00066485,0.00065823,
0.00065168,0.0006452,0.00063878,0.00063242,0.00062613,0.0006199,0.00061373,0.00060762,0.00060158,0.00059559,
0.00058967,0.0005838,0.00057799,0.00057224,0.00056655,0.00056091,0.00055533,0.0005498,0.00054433,0.00053891,
0.00053355,0.00052824,0.00052299,0.00051778,0.00051263,0.00050753,0.00050248,0.00049748,0.00049253,0.00048763,
0.00048278,0.00047797,0.00047322,0.00046851,0.00046385,0.00045923,0.00045466,0.00045014,0.00044566,0.00044123,
0.00043684,0.00043249,0.00042819,0.00042393,0.00041971,0.00041553,0.0004114,0.0004073,0.00040325,0.00039924,
0.00039527,0.00039133,0.00038744,0.00038358,0.00037977,0.00037599,0.00037225,0.00036854,0.00036488,0.00036125,
0.00035765,0.00035409,0.00035057,0.00034708,0.00034363,0.00034021,0.00033682,0.00033347,0.00033015,0.00032687,
0.00032362};

const double __attribute__ ((space(psv), address (0x5000)))
Ax_table[810] = {
7.4512e-006,7.7547e-006,8.0702e-006,8.3981e-006,8.739e-006,9.0933e-006,9.4615e-006,9.8441e-006,1.0242e-005,1.0655e-005,
1.1084e-005,1.153e-005,1.1993e-005,1.2474e-005,1.2974e-005,1.3492e-005,1.4031e-005,1.459e-005,1.5171e-005,1.5774e-005,
1.6399e-005,1.7048e-005,1.7722e-005,1.8421e-005,1.9146e-005,1.9898e-005,2.0678e-005,2.1487e-005,2.2326e-005,2.3195e-005,
2.4097e-005,2.5031e-005,2.6e-005,2.7003e-005,2.8043e-005,2.912e-005,3.0235e-005,3.139e-005,3.2586e-005,3.3824e-005,
3.5106e-005,3.6432e-005,3.7804e-005,3.9224e-005,4.0692e-005,4.2211e-005,4.3781e-005,4.5404e-005,4.7082e-005,4.8816e-005,
5.0607e-005,5.2457e-005,5.4368e-005,5.6341e-005,5.8378e-005,6.0481e-005,6.265e-005,6.4889e-005,6.7197e-005,6.9578e-005,
7.2032e-005,7.4562e-005,7.7169e-005,7.9855e-005,8.2622e-005,8.5471e-005,8.8404e-005,9.1423e-005,9.4529e-005,9.7725e-005,
0.00010101,0.00010439,0.00010787,0.00011144,0.0001151,0.00011887,0.00012274,0.00012671,0.00013079,0.00013497,
0.00013927,0.00014367,0.00014818,0.0001528,0.00015754,0.0001624,0.00016737,0.00017246,0.00017767,0.000183,
0.00018845,0.00019403,0.00019973,0.00020556,0.00021152,0.0002176,0.00022382,0.00023017,0.00023664,0.00024325,
0.00025,0.00025688,0.0002639,0.00027105,0.00027834,0.00028577,0.00029333,0.00030104,0.00030889,0.00031688,
0.00032501,0.00033328,0.00034169,0.00035025,0.00035895,0.0003678,0.00037679,0.00038593,0.00039521,0.00040464,
0.00041422,0.00042394,0.00043381,0.00044383,0.00045399,0.00046431,0.00047477,0.00048539,0.00049615,0.00050707,
0.00051814,0.00052935,0.00054072,0.00055225,0.00056392,0.00057575,0.00058773,0.00059987,0.00061216,0.00062461,
0.00063722,0.00064998,0.0006629,0.00067598,0.00068923,0.00070263,0.00071619,0.00072992,0.0007438,0.00075786,
0.00077208,0.00078647,0.00080102,0.00081575,0.00083064,0.00084571,0.00086095,0.00087636,0.00089196,0.00090773,
0.00092367,0.00093981,0.00095612,0.00097262,0.0009893,0.0010062,0.0010232,0.0010405,0.0010579,0.0010756,
0.0010934,0.0011115,0.0011297,0.0011482,0.0011669,0.0011857,0.0012048,0.0012241,0.0012436,0.0012634,
0.0012833,0.0013035,0.001324,0.0013446,0.0013655,0.0013866,0.001408,0.0014296,0.0014515,0.0014736,
0.0014959,0.0015186,0.0015414,0.0015646,0.001588,0.0016117,0.0016356,0.0016599,0.0016844,0.0017092,
0.0017343,0.0017597,0.0017854,0.0018114,0.0018377,0.0018643,0.0018913,0.0019185,0.0019461,0.001974,
0.0020023,0.0020308,0.0020598,0.002089,0.0021186,0.0021486,0.002179,0.0022097,0.0022407,0.0022722,
0.002304,0.0023363,0.0023689,0.0024019,0.0024353,0.0024692,0.0025034,0.0025381,0.0025732,0.0026087,
0.0026447,0.0026811,0.002718,0.0027553,0.0027931,0.0028313,0.0028701,0.0029093,0.002949,0.0029892,
0.0030299,0.0030711,0.0031128,0.0031551,0.0031979,0.0032412,0.003285,0.0033295,0.0033744,0.00342,
0.0034661,0.0035128,0.0035601,0.003608,0.0036565,0.0037057,0.0037554,0.0038058,0.0038568,0.0039085,
0.0039608,0.0040138,0.0040675,0.0041218,0.0041769,0.0042326,0.0042891,0.0043463,0.0044042,0.0044629,
0.0045223,0.0045825,0.0046434,0.0047051,0.0047677,0.004831,0.0048951,0.0049601,0.0050259,0.0050926,
0.0051601,0.0052285,0.0052977,0.0053679,0.005439,0.0055109,0.0055839,0.0056577,0.0057325,0.0058083,
0.005885,0.0059628,0.0060415,0.0061213,0.0062021,0.006284,0.0063669,0.0064509,0.0065359,0.0066221,
0.0067094,0.0067978,0.0068874,0.0069782,0.0070701,0.0071632,0.0072575,0.0073531,0.0074498,0.0075479,
0.0076472,0.0077478,0.0078497,0.007953,0.0080576,0.0081635,0.0082708,0.0083795,0.0084897,0.0086013,
0.0087143,0.0088288,0.0089448,0.0090622,0.0091813,0.0093018,0.009424,0.0095477,0.0096731,0.0098001,
0.0099287,0.010059,0.010191,0.010325,0.01046,0.010598,0.010737,0.010877,0.01102,0.011165,
0.011311,0.011459,0.01161,0.011762,0.011916,0.012072,0.012231,0.012391,0.012554,0.012718,
0.012885,0.013054,0.013225,0.013398,0.013574,0.013752,0.013932,0.014114,0.014299,0.014487,
0.014677,0.014869,0.015064,0.015261,0.015461,0.015663,0.015869,0.016076,0.016287,0.0165,
0.016717,0.016935,0.017157,0.017382,0.01761,0.01784,0.018074,0.018311,0.01855,0.018793,
0.019039,0.019289,0.019541,0.019797,0.020056,0.020319,0.020585,0.020855,0.021128,0.021404,
0.021684,0.021968,0.022256,0.022547,0.022843,0.023142,0.023445,0.023751,0.024062,0.024377,
0.024696,0.02502,0.025347,0.025679,0.026015,0.026356,0.026701,0.02705,0.027404,0.027763,
0.028126,0.028495,0.028867,0.029245,0.029628,0.030016,0.030409,0.030807,0.03121,0.031618,
0.032032,0.032451,0.032876,0.033306,0.033742,0.034184,0.034631,0.035085,0.035544,0.036009,
0.03648,0.036958,0.037441,0.037931,0.038428,0.038931,0.03944,0.039956,0.040479,0.041009,
0.041546};

const double __attribute__ ((space(psv), address (0x6000)))
Bx_table[810] = {
0.0061868,0.0061204,0.0060546,0.0059894,0.0059248,0.0058609,0.0057975,0.0057347,0.0056725,0.0056109,
```

```
0.0055499,0.0054894,0.0054295,0.0053701,0.0053113,0.005253,0.0051953,0.0051381,0.0050814,0.0050252,
0.0049696,0.0049144,0.0048598,0.0048057,0.004752,0.0046989,0.0046462,0.004594,0.0045423,0.0044911,
0.0044403,0.00439,0.0043401,0.0042907,0.0042418,0.0041932,0.0041452,0.0040975,0.0040503,0.0040035,
0.0039572,0.0039112,0.0038657,0.0038206,0.0037758,0.0037315,0.0036876,0.0036441,0.003601,0.0035582,
0.0035158,0.0034739,0.0034323,0.003391,0.0033502,0.0033097,0.0032695,0.0032297,0.0031903,0.0031513,
0.0031125,0.0030742,0.0030361,0.0029984,0.0029611,0.0029241,0.0028874,0.002851,0.002815,0.0027793,
0.0027439,0.0027089,0.0026741,0.0026397,0.0026055,0.0025717,0.0025382,0.002505,0.0024721,0.0024395,
0.0024072,0.0023752,0.0023435,0.002312,0.0022809,0.00225,0.0022195,0.0021892,0.0021592,0.0021295,
0.0021,0.0020708,0.002042,0.0020133,0.001985,0.0019569,0.0019291,0.0019015,0.0018742,0.0018472,
0.0018204,0.0017939,0.0017677,0.0017417,0.001716,0.0016905,0.0016653,0.0016403,0.0016156,0.0015911,
0.0015669,0.0015429,0.0015192,0.0014957,0.0014725,0.0014495,0.0014267,0.0014042,0.0013819,0.0013599,
0.0013381,0.0013166,0.0012952,0.0012741,0.0012533,0.0012327,0.0012123,0.0011921,0.0011722,0.0011525,
0.001133,0.0011138,0.0010947,0.0010759,0.0010574,0.001039,0.0010209,0.001003,0.00098532,0.00096786,
0.00095061,0.00093358,0.00091677,0.00090018,0.0008838,0.00086763,0.00085167,0.00083593,0.0008204,0.00080507,
0.00078996,0.00077505,0.00076035,0.00074585,0.00073156,0.00071746,0.00070357,0.00068988,0.00067639,0.0006631,
0.00065,0.0006371,0.00062439,0.00061187,0.00059955,0.00058741,0.00057546,0.0005637,0.00055213,0.00054073,
0.00052953,0.0005185,0.00050765,0.00049698,0.00048648,0.00047616,0.00046602,0.00045604,0.00044624,0.00043661,
0.00042714,0.00041783,0.00040869,0.00039972,0.0003909,0.00038224,0.00037373,0.00036539,0.00035719,0.00034915,
0.00034126,0.00033351,0.00032591,0.00031846,0.00031114,0.00030397,0.00029694,0.00029004,0.00028328,0.00027666,
0.00027016,0.0002638,0.00025756,0.00025145,0.00024546,0.0002396,0.00023386,0.00022823,0.00022273,0.00021733,
0.00021206,0.00020689,0.00020184,0.00019689,0.00019205,0.00018731,0.00018268,0.00017815,0.00017372,0.00016938,
0.00016515,0.000161,0.00015695,0.000153,0.00014913,0.00014535,0.00014165,0.00013804,0.00013451,0.00013107,
0.0001277,0.00012442,0.00012121,0.00011807,0.00011501,0.00011202,0.00010911,0.00010626,0.00010348,0.00010077,
9.8123e-005,9.5541e-005,9.3021e-005,9.0563e-005,8.8166e-005,8.5827e-005,8.3546e-005,8.1321e-005,7.9152e-005,7.7037e-005,
7.4974e-005,7.2963e-005,7.1003e-005,6.9092e-005,6.7229e-005,6.5414e-005,6.3644e-005,6.192e-005,6.024e-005,5.8603e-005,
5.7008e-005,5.5454e-005,5.394e-005,5.2466e-005,5.1029e-005,4.963e-005,4.8268e-005,4.6941e-005,4.5649e-005,4.439e-005,
4.3165e-005,4.1972e-005,4.0811e-005,3.9681e-005,3.858e-005,3.7509e-005,3.6466e-005,3.5451e-005,3.4463e-005,3.3502e-005,
3.2566e-005,3.1656e-005,3.077e-005,2.9908e-005,2.907e-005,2.8254e-005,2.746e-005,2.6688e-005,2.5937e-005,2.5206e-005,
2.4495e-005,2.3804e-005,2.3131e-005,2.2477e-005,2.1841e-005,2.1223e-005,2.0621e-005,2.0036e-005,1.9468e-005,1.8915e-005,
1.8377e-005,1.7854e-005,1.7346e-005,1.6851e-005,1.6371e-005,1.5904e-005,1.545e-005,1.5008e-005,1.4579e-005,1.4162e-005,
1.3757e-005,1.3363e-005,1.298e-005,1.2608e-005,1.2246e-005,1.1894e-005,1.1553e-005,1.1221e-005,1.0898e-005,1.0584e-005,
1.028e-005,9.9836e-006,9.6959e-006,9.4164e-006,9.1448e-006,8.8809e-006,8.6245e-006,8.3754e-006,8.1334e-006,7.8982e-006,
7.6698e-006,7.4479e-006,7.2323e-006,7.0229e-006,6.8194e-006,6.6218e-006,6.4298e-006,6.2434e-006,6.0622e-006,5.8863e-006,
5.7154e-006,5.5494e-006,5.3882e-006,5.2316e-006,5.0795e-006,4.9318e-006,4.7883e-006,4.649e-006,4.5136e-006,4.3822e-006,
4.2546e-006,4.1306e-006,4.0103e-006,3.8934e-006,3.7798e-006,3.6696e-006,3.5625e-006,3.4586e-006,3.3576e-006,3.2596e-006,
3.1644e-006,3.072e-006,2.9822e-006,2.8951e-006,2.8105e-006,2.7283e-006,2.6485e-006,2.5711e-006,2.4959e-006,2.4228e-006,
2.3519e-006,2.2831e-006,2.2162e-006,2.1514e-006,2.0883e-006,2.0272e-006,1.9678e-006,1.9101e-006,1.8541e-006,1.7998e-006,
1.747e-006,1.6958e-006,1.6461e-006,1.5978e-006,1.5509e-006,1.5054e-006,1.4612e-006,1.4184e-006,1.3767e-006,1.3363e-006,
1.2971e-006,1.259e-006,1.222e-006,1.1861e-006,1.1513e-006,1.1175e-006,1.0846e-006,1.0528e-006,1.0218e-006,9.9179e-007,
9.6264e-007,9.3434e-007,9.0687e-007,8.802e-007,8.5432e-007,8.292e-007,8.0481e-007,7.8113e-007,7.5815e-007,7.3585e-007,
7.142e-007,6.9318e-007,6.7278e-007,6.5298e-007,6.3376e-007,6.1511e-007,5.97e-007,5.7942e-007,5.6236e-007,5.4581e-007,
5.2973e-007,5.1413e-007,4.9899e-007,4.8429e-007,4.7003e-007,4.5618e-007,4.4275e-007,4.297e-007,4.1704e-007,4.0475e-007,
3.9283e-007,3.8125e-007,3.7002e-007,3.5911e-007,3.4853e-007,3.3825e-007,3.2828e-007,3.1861e-007,3.0921e-007,3.001e-007,
2.9125e-007};

const double __attribute__ ((space(psv), address (0x7000)))
xi_table[810] = {
1.00,0.98748,0.97622,0.96512,0.95418,0.9434,0.93276,0.92228,0.91194,0.90175,
0.8917,0.8818,0.87203,0.86239,0.85289,0.84353,0.83429,0.82518,0.8162,0.80734,
0.79861,0.78999,0.78149,0.77311,0.76485,0.7567,0.74866,0.74073,0.73291,0.72519,
0.71758,0.71008,0.70267,0.69537,0.68816,0.68105,0.67404,0.66712,0.6603,0.65357,
0.64692,0.64037,0.6339,0.62752,0.62122,0.61501,0.60888,0.60283,0.59687,0.59098,
0.58516,0.57943,0.57377,0.56818,0.56267,0.55723,0.55186,0.54656,0.54133,0.53616,
0.53107,0.52604,0.52107,0.51617,0.51133,0.50656,0.50184,0.49719,0.49259,0.48805,
0.48358,0.47915,0.47479,0.47048,0.46622,0.46202,0.45787,0.45377,0.44972,0.44573,
0.44178,0.43789,0.43404,0.43024,0.42649,0.42278,0.41912,0.4155,0.41193,0.4084,
0.40492,0.40148,0.39808,0.39472,0.3914,0.38813,0.38489,0.38169,0.37853,0.37541,
0.37232,0.36928,0.36627,0.36329,0.36035,0.35745,0.35458,0.35174,0.34894,0.34617,
0.34343,0.34073,0.33805,0.33541,0.3328,0.33022,0.32767,0.32515,0.32265,0.32019,
0.31776,0.31535,0.31297,0.31062,0.30829,0.30599,0.30372,0.30147,0.29925,0.29705,
0.29488,0.29274,0.29061,0.28851,0.28644,0.28438,0.28235,0.28035,0.27836,0.2764,
0.27445,0.27253,0.27063,0.26875,0.2669,0.26506,0.26324,0.26144,0.25966,0.2579,
0.25616,0.25444,0.25273,0.25105,0.24938,0.24773,0.2461,0.24448,0.24289,0.2413,
0.23974,0.23819,0.23666,0.23514,0.23364,0.23216,0.23069,0.22923,0.22779,0.22637,
0.22496,0.22356,0.22218,0.22081,0.21946,0.21812,0.21679,0.21548,0.21418,0.21289,
0.21162,0.21036,0.20911,0.20787,0.20665,0.20543,0.20423,0.20305,0.20187,0.2007,
0.19955,0.19841,0.19728,0.19615,0.19504,0.19395,0.19286,0.19178,0.19071,0.18965,
0.1886,0.18757,0.18654,0.18552,0.18451,0.18351,0.18252,0.18154,0.18057,0.1796,
0.17865,0.1777,0.17677,0.17584,0.17492,0.17401,0.17311,0.17221,0.17133,0.17045,
0.16958,0.16871,0.16786,0.16701,0.16617,0.16534,0.16451,0.16369,0.16288,0.16208,
0.16128,0.16049,0.15971,0.15894,0.15817,0.1574,0.15665,0.1559,0.15516,0.15442,
0.15369,0.15296,0.15225,0.15153,0.15083,0.15013,0.14943,0.14874,0.14806,0.14738,
0.14671,0.14605,0.14539,0.14473,0.14408,0.14344,0.1428,0.14216,0.14154,0.14091,
0.14029,0.13968,0.13907,0.13847,0.13787,0.13727,0.13668,0.1361,0.13552,0.13494,
0.13437,0.1338,0.13324,0.13268,0.13213,0.13158,0.13104,0.13049,0.12996,0.12942,
0.1289,0.12837,0.12785,0.12733,0.12682,0.12631,0.12581,0.12531,0.12481,0.12431,
0.12382,0.12334,0.12285,0.12237,0.1219,0.12143,0.12096,0.12049,0.12003,0.11957,
0.11911,0.11866,0.11821,0.11777,0.11732,0.11688,0.11645,0.11601,0.11558,0.11516,
0.11473,0.11431,0.11389,0.11348,0.11306,0.11265,0.11225,0.11184,0.11144,0.11104,
0.11065,0.11025,0.10986,0.10948,0.10909,0.10871,0.10833,0.10795,0.10757,0.1072,
0.10683,0.10646,0.1061,0.10574,0.10538,0.10502,0.10466,0.10431,0.10396,0.10361,
0.10326,0.10292,0.10258,0.10224,0.1019,0.10156,0.10123,0.1009,0.10057,0.10024,
0.099916,0.099593,0.099272,0.098953,0.098636,0.098321,0.098008,0.097696,0.097387,0.09708,
0.096774,0.096471,0.096169,0.095869,0.095571,0.095274,0.09498,0.094687,0.094396,0.094107,
0.093819,0.093534,0.093249,0.092967,0.092686,0.092407,0.09213,0.091854,0.091579,0.091307,
0.091036,0.090766,0.090498,0.090232,0.089967,0.089704,0.089442,0.089182,0.088923,0.088665,
0.088409,0.088155,0.087902,0.08765,0.0874,0.087151,0.086904,0.086658,0.086413,0.08617,
0.085928,0.085687,0.085448,0.08521,0.084973,0.084738,0.084504,0.084271,0.08404,0.083809,
0.08358,0.083352,0.083126,0.0829,0.082676,0.082453,0.082231,0.082011,0.081791,0.081573,
0.081356,0.08114,0.080925,0.080711,0.080498,0.080287,0.080076,0.079867,0.079658,0.079451,
0.079245,0.07904,0.078836,0.078633,0.078431,0.07823,0.07803,0.077831,0.077633,0.077436,
0.07724};
// DEFINE D/A CONTROL SIGNAL PIN
#define DA_CS LATFbits.LATF6 // Select
#define DA_WR LATDbits.LATD0 // Write
#define DA_LDAC LATDbits.LATD2 // Load
#define DA_GAIN LATDbits.LATD1 // gain
// DEFINE INITIAL VALUE
#define Gsi 0.09
```

```
#define Gk 0.282
#define Ek -77.567
// DECLARATION VARIABLES USED IN TIMER1
unsigned long Fsample; // declare sampling frequency
unsigned int SetTime; // declare timer1
// DECLARATION VARIABLES USED IN INTERRUPT FUNCTION
double I_si_old;
double Cai_old;
double d_old;
double f_old;
double x_old;
unsigned int adbuf;
unsigned int psv_shadow;
double h;
double Ad,Bd,Af,Bf,Ax,Bx;
double Cai_eq_value,Cai_new,Esi_new ;
double D_eq_value ,F_eq_value,X_eq_value,d_new,f_new,x_new,xi;
double I_si_original,IK_original,I_flow_original,I_flow,V_flow,V_output;
int n;
unsigned int OUTPUTBIT;
// MAIN FUNCTION
int main(void)
{
// SETUP INITIAL CONDITIONS
I_si_old = 0.0;
Cai_old=0.0002;//0.1;//0.1??
d_old=0.001;//0.01;
f_old=0.001;//1.0;
x_old=0.001;//1.0;
// CORCON bit on
CORCONbits.PSV = 1;
// SETUP INPUT/OUTPUT PORT
TRISD = 0x08; // RD3 is input 0000 0000 0000 1000
TRISE = 0x100; // RE8 is input 0000 0001 0000 0000
TRISF = 0; // all output 0000 0000 0000 0000
TRISC = 0x9FFF; // 1001 1111 1111 1111
// INITIALIZE A/D
ADPCFG = 0xFFF0; //1111 1111 1111 0000
ADCON1 = 0x80EC; //1000 0000 1110 1100
ADCON2 = 0x020C; //0000 0010 0000 1100
ADCON3 = 0x0880; //0000 1000 1000 0000
ADCHS = 0x0003; //0000 0000 0000 0011
ADCSSL = 0;
// SETUP INITIAL VALUE FOR SIGNAL CONTROL IN D/A
DA_GAIN = 0; //GAIN
DA_CS = 1; // CS
DA_WR = 1; // WR
DA_LDAC = 1; // LDAC
// SETUP SAMPLING FREQUENCY
Fsample = 2500.0;
// SETUP TIMER 1 AND SAMPLING PERIOD
SetTime = (int)(29491200.0 / Fsample - 1.0);
OpenTimer1(T1_ON & T1_GATE_OFF & T1_PS_1_1 & T1_SOURCE_INT,SetTime);
ConfigIntTimer1(T1_INT_PRIOR_5 & T1_INT_ON); // enabling interrupt
// SETUP INITAIL LED CONDITION
LATFbits.LATF4 = 1; // LED OFF
// INFINITE LOOP WHILE WAITING COUNTING CLOCK IN TIMER 1
while(1);
{}
}
// INTERRUPT FUNCTION
void __attribute__((interrupt,auto_psv)) _T1Interrupt(void)
{
IFS0bits.T1IF = 0; // Clear interrupt flag
// READ DATA FROM A/D CONVERTER
adbuf = ReadADC10(2);

// SETUP FOR LED SIGNAL (if value of data is 3.3V and over, LED start to ON and if small that 0.6V、LED OFF)
if( adbuf >= 0x2A3 )
{
LATFbits.LATF4 = 0; // LED ON
}
if( adbuf < 0x7A )
{
LATFbits.LATF4 = 1; // LED OFF
}
// CONVERT DATABIT TO VOLTAGE
v_trans = (double)(((adbuf*220.0)/1023.0)-100.0);
n=(int)(2*(v_trans+100.0));
h=1000.0*1.0/Fsample;      // DELTA T
// SETUP FOR READ OUT DATA FROM TABLES
/* save the PSVPAG */
psv_shadow = PSVPAG;
/* set the PSVPAG for accessing table[] */
PSVPAG = __builtin_psvpage (Ad_table);
// IMPORT VALUE FROM Ad_table
Ad=Ad_table[n];
/* restore the PSVPAG for the compiler-managed PSVPAG */
PSVPAG = psv_shadow;
// Bd_table ROUTIN
/* save the PSVPAG */
psv_shadow = PSVPAG;
/* set the PSVPAG for accessing table[] */
PSVPAG = __builtin_psvpage (Bd_table);
// IMPORT VALUE FROM Bd_table
Bd=Bd_table[n];
/* restore the PSVPAG for the compiler-managed PSVPAG */
PSVPAG = psv_shadow;
// Af_table ROUTIN
```

```
/* save the PSVPAG */
psv_shadow = PSVPAG;
/* set the PSVPAG for accessing table[] */
PSVPAG = __builtin_psvpage (Af_table);
// IMPORT VALUE FROM Af_table
Af=Af_table[n];
/* restore the PSVPAG for the compiler-managed PSVPAG */
PSVPAG = psv_shadow;
// Bf_table ROUTIN
/* save the PSVPAG */
psv_shadow = PSVPAG;
/* set the PSVPAG for accessing table[] */
PSVPAG = __builtin_psvpage (Bf_table);
// IMPORT VALUE FROM Bf_table
Bf=Bf_table[n];
/* restore the PSVPAG for the compiler-managed PSVPAG */
PSVPAG = psv_shadow;
// Ax_table ROUTIN
/* save the PSVPAG */
psv_shadow = PSVPAG;
/* set the PSVPAG for accessing table[] */
PSVPAG = __builtin_psvpage (Ax_table);
// IMPORT VALUE FROM Ax_table
Ax=Ax_table[n];
/* restore the PSVPAG for the compiler-managed PSVPAG */
PSVPAG = psv_shadow;
// Bx_table ROUTIN
/* save the PSVPAG */
psv_shadow = PSVPAG;
/* set the PSVPAG for accessing table[] */
PSVPAG = __builtin_psvpage (Bx_table);
// IMPORT VALUE FROM Bx_table
Bx=Bx_table[n];
/* restore the PSVPAG for the compiler-managed PSVPAG */
PSVPAG = psv_shadow;
// xi_table ROUTIN
/* save the PSVPAG */
psv_shadow = PSVPAG;
/* set the PSVPAG for accessing table[] */
PSVPAG = __builtin_psvpage (xi_table);
// IMPORT VALUE FROM xi_table
xi=xi_table[n];
/* restore the PSVPAG for the compiler-managed PSVPAG */
PSVPAG = psv_shadow;
// CALCULATE Isi
Cai_eq_value = -(1.0e-4)*I_si_old+0.07*((1.0e-4)-Cai_old);
D_eq_value = Ad-(Ad+Bd)*d_old;
F_eq_value = Af-(Af+Bf)*f_old;
d_new = d_old + h*D_eq_value;
f_new = f_old + h*F_eq_value;
Cai_new = Cai_old + h*Cai_eq_value;
Esi_new = 7.7-13.0287*log(Cai_new);
I_si_original = Gsi*d_new*f_new*(v_trans - Esi_new);
// CALCULATE IK
X_eq_value=Ax*(1.0-x_old)-Bx*x_old;
x_new=x_old+h*X_eq_value;
IK_original=Gk*x_new*xi*(v_trans-Ek);
// CALCULATE TOTAL IONIC CURRENTS IK+Isi
I_flow_original = I_si_original+IK_original;
I_flow = -0.375*I_flow_original;
// CONVERT CURRENT TO VOLTAGE SIGNAL_Vdigital=(IK+Isi)*R7
V_flow= I_flow*0.068;
// CONVERT OUTPUT VOLTAGE TO THE RANGE OF 0-5V
V_output=1.25*(V_flow+1.8);
OUTPUTBIT = (unsigned int)((V_output*1023.0)/5.0);
// RENEW INITIAL VALUE
d_old=d_new;
f_old=f_new;
Cai_old=Cai_new;
x_old = x_new;
I_si_old = I_si_original;
// OUTPUT TO D/A CONVERTER
LATE = OUTPUTBIT; // outputdata of lower 6 bits
LATF = (OUTPUTBIT>>6) & 0x0F; // outputdata of upper 4 bits
DA_GAIN = 1;
DA_CS = 0;
DA_WR = 0;
DA_WR = 1;
DA_CS = 1;
DA_LDAC = 0;
DA_LDAC = 1;
}
```

List C.2 shows the C source code program of H8/3694F microcontroller to produce two channels of impulsive stimulation at specific timing and duration of the stimulations. H8/3694F development software, HEW (High-performance Embedded Workshop) (Ver. 4.06) and programming software, FDT (Flash Development Toolkit) (Ver. 4.05) provided free by Renesas Electronic Corporation was used in this work. Both can be obtained from the Renesas official website. The program is written into the H8/3694F microcontroller through a serial communication interface.

List C.2: The source program for the H8/3694F

```
#include <string.h>
#include "iodefine.h"
#include <machine.h>

/* Declaration of functions */
void main(void);

void timerW_init( void );
void wait_1ms( unsigned int time );
void wait_50us( unsigned int time );
void wait_10us( void );
char sw_delay( int wait );
void start_sw( void );

void lcd_init( void ); // LCD initialization,4bit transmission mode
void lcd_busy( void );            // Buzy check (RS=Low,R/W=High)
void lcd_cmnd_8( unsigned char uc_data ); // Write 8bit control signal (RS=Low,R/W=Low) without buzy check
void lcd_cmnd_4( unsigned char uc_data ); // Write 4bit control signal (RS=Low,R/W=Low) with buzy check
void lcd_clear( void ); // Clear LCD
void lcd_putc( char c_data ); // Display one character (RS=Hi,R/W=Low) with buzy check
void lcd_puts( char *pc_string ); // Display character string
void lcd_locate_puts( char c_x, char c_y, char c_leng, char *pc_str ); // Display character string at the specified
                                                                       // position with limited character length
void lcd_locate( char c_x, char c_y ); // Specify cursor position
void lcd_cursor( unsigned char uc_mode, unsigned char uc_su ); // Control cursor

/* Macro definition */
#define SW_DELAY 20
#define LCD // Comment out if no LCD use

// Port definition for Switch use
#define SW_CHECK() IO.PDR2.BIT.B0

// Port definition for Pulse Output use
#define PULSE1_ON() IO.PDR5.BIT.B0 = 1
#define PULSE1_OFF() IO.PDR5.BIT.B0 = 0
#define PULSE2_ON() IO.PDR5.BIT.B1 = 1
#define PULSE2_OFF() IO.PDR5.BIT.B1 = 0

// Port definition for Led use
#define LED_G_ON() IO.PDR8.BIT.B1 = 0
#define LED_G_OFF() IO.PDR8.BIT.B1 = 1
#define LED_R_ON() IO.PDR8.BIT.B0 = 0
#define LED_R_OFF() IO.PDR8.BIT.B0 = 1

// Command definition for LCD control
#define RIGHT 0x14 // Right shifting
#define LEFT 0x10 // Left shifting
#define HOME 0x80 // Origin
#define CLEAR 0x20 // Clear
#define TAB_1 0x02 // Shifting to 1st row
#define TAB_2 0xc0 // Shifting to 2nd row

// Port definition for LCD use
#define LCD_RS_LO() IO.PDR1.BIT.B0 = 0
#define LCD_RS_HI() IO.PDR1.BIT.B0 = 1
#define LCD_RW_LO() IO.PDR1.BIT.B1 = 0
#define LCD_RW_HI() IO.PDR1.BIT.B1 = 1
#define LCD_E_LO() IO.PDR1.BIT.B2 = 0
#define LCD_E_HI() IO.PDR1.BIT.B2 = 1
#define LCD_W_DATA(x) IO.PDR1.BYTE = ( IO.PDR1.BYTE & 0x0f ) | ( (x) & 0xf0 )
#define LCD_R_DATA() ( IO.PDR1.BYTE & 0xf0 )
#define Lcd_blink() lcd_cmnd_4( 0x0d ) // Blinking cursor
#define Lcd_fix() lcd_cmnd_4( 0x0c ) // Fix cursor

/* Global variables */
int Dur_initiate = 134;
int Dur_terminate = 1090;



/* Function for LCD */
////////////////////////////////////////
//  LCD initialization
//  4bit transfer mode
////////////////////////////////////////
void lcd_init( void )
{
#ifdef LCD
```

```
wait_1ms( 15 ); // Over 15msec wait after power on
lcd_cmnd_8( 0x30 );
wait_1ms( 4 ); // 4msec
lcd_cmnd_8( 0x30 );
wait_50us( 2 ); // 100usec
lcd_cmnd_8( 0x30 );
wait_50us( 1 ); // 50usec
lcd_cmnd_8( 0x20 );
wait_50us( 1 ); // 50usec

lcd_cmnd_4( 0x2e ); // Function set
lcd_cmnd_4( 0x08 ); // LCD off, no cursor display and blinking

lcd_cmnd_4( 0x01 ); // Lcd home clear
lcd_cmnd_4( 0x06 ); // Entry mode setting
lcd_cmnd_4( 0x0c ); // LCD on, no cursor display and blinking

lcd_cursor( HOME, 1 );
#endif
}

//////////////////////////////////////////
// LCD busy check(RS=Low,R/W=High)
//////////////////////////////////////////
void lcd_busy( void )
{
#ifdef LCD

unsigned char uc_busy = 1;
int i_timeup = 0;
char c_buf[21];

    IO.PCR1 = 0x07; // Set data port for LCD to input
LCD_RS_LO(); // Start getting busy signal (RW=1, RS=0)
LCD_RW_HI();

while( 1 )
{
LCD_E_HI(); // Input upper 4bit
uc_busy = LCD_R_DATA() & 0x80;
LCD_E_LO();

LCD_E_HI(); // Input lower 4bit
nop(); // Delay 220nsec is needed
nop();
nop();
LCD_E_LO();

if( uc_busy == 0 )
{
break;
}

}

IO.PCR1 = 0xf7; // Set data port for LCD back to output

#endif
}

//////////////////////////////////////////////////
// Writing 8bit control signal (RS=Low,R/W=Low)
// Without buzy check
//////////////////////////////////////////////////
void lcd_cmnd_8( unsigned char uc_data )
{
#ifdef LCD
LCD_RW_LO();
LCD_RS_LO();
LCD_W_DATA( uc_data );
LCD_E_HI(); // Writing
wait_10us();
LCD_E_LO();

#endif
}

//////////////////////////////////////////////////
// Writing 4 bit control signal (RS=Low,R/W=Low)
// With buzy check
//////////////////////////////////////////////////
void lcd_cmnd_4( unsigned char uc_data )
{
#ifdef LCD
LCD_RW_LO();
LCD_RS_LO();
LCD_E_HI(); // Writing
LCD_W_DATA( uc_data );
LCD_E_LO();

LCD_E_HI(); // Writing
LCD_W_DATA( uc_data << 4 );
LCD_E_LO();

lcd_busy();

#endif
}
```

```
//////////////////////////////////////
// Clearing LCD
//////////////////////////////////////
void lcd_clear( void )
{
#ifdef LCD
lcd_cmnd_4( 0x01 ); // LCD home clear
#endif
}

//////////////////////////////////////
// Displaying one character
// With buzy check
//////////////////////////////////////
void lcd_putc( char c_data )
{
#ifdef LCD
LCD_RW_LO();
LCD_RS_HI();
LCD_E_HI(); // Writing
LCD_W_DATA( c_data );
LCD_E_LO();

LCD_E_HI(); // Writing
LCD_W_DATA( c_data << 4);
LCD_E_LO();

lcd_busy();
#endif
}

//////////////////////////////////////
// Displaying character string
//////////////////////////////////////
void lcd_puts( char *pc_string )
{
#ifdef LCD
while( *pc_string )
{
lcd_putc( *(pc_string++) );
}
#endif
}

//////////////////////////////////////////////////////////////////
// Displaying at the specified position with limited character length
//////////////////////////////////////////////////////////////////////////////
void lcd_locate_puts( char c_x, char c_y, char c_leng, char *pc_str )
{
#ifdef LCD
char c_i, c_j;

c_j = 0;
lcd_locate( c_x, c_y );
while ( ( *pc_str != '\0') && ( c_j < c_leng ) )
{
lcd_putc( *pc_str++ );
c_j++;
}
for ( c_i = 0; c_i < c_leng - c_j; c_i++ )
{
lcd_putc( ' ' ); // Insert 'blank space' if the character string length less than the length limit
}
#endif
}

//////////////////////////////////////////
// LCD cursor positioning
//////////////////////////////////////////
void lcd_locate( char c_x, char c_y )
{
#ifdef LCD
char c_i;
switch ( c_y )
{
case 1 :
lcd_cmnd_4( HOME ); // Go to 1st line
break;
case 2 :
lcd_cmnd_4( TAB_2 ); // Go to 2nd line
break;
}

for( c_i = 0; c_i < c_x - 1; c_i++ )
{
lcd_cmnd_4( RIGHT ); // Specify the row location
}
#endif
}

//////////////////////////////////////
// Controlling cursor position
//////////////////////////////////////
void lcd_cursor( unsigned char uc_mode, unsigned char uc_su )
{
#ifdef LCD
unsigned char uc_i, uc_j;
switch( uc_mode )
{
```

```
case RIGHT:
uc_j = RIGHT;
break;
case LEFT:
uc_j = LEFT;
break;
case HOME:
case TAB_1:
case TAB_2:
lcd_cmnd_4( uc_mode );
uc_j = RIGHT;
uc_su--;
break;
case CLEAR:
for( uc_i = 0; uc_i < uc_su; uc_i++ )
{
lcd_putc(' ');
}
uc_j = LEFT;
break;
default:
lcd_puts( "ERR" );
uc_su = 3;
uc_j = LEFT;
break;
}

for( uc_i = 0; uc_i < uc_su; uc_i++ )
{
lcd_cmnd_4( uc_j );
}
#endif
}


/* Function for Delay and Timer */
//////////////////////////////
// initialize Timer W
//////////////////////////////
void timerW_init( void )
{
TW.TMRW.BIT.CTS = 0; // Stop Timer W counter
TW.TIERW.BYTE = 0x70; // Prohibit all interruptions
TW.TCNT = 0; // Clear counter to 0
TW.TCRW.BIT.CCLR = 1; // Counter clear according to GRA
TW.TCRW.BIT.CKS = 0; // CKSO:0,CKS1:0,CKS2:0 ⇒ Counting by internal clock(20MHz)
TW.GRA = 20000; // Number of counts for 1ms delay
}

//////////////////////////////
// 1ms delay
//////////////////////////////
void wait_1ms( unsigned int time )
{
unsigned int cnt;

for( cnt = 0; cnt < time; cnt++ )
{
TW.TMRW.BIT.CTS = 1; // Start timer W counter
while( ! TW.TSRW.BIT.IMFA ); // Wait until Compare Match Flag (IMFA = 1) when ( TCNT == GRA )
TW.TSRW.BIT.IMFA = 0; // Clear Compare Match Flag (IMFA = 0)
TW.TMRW.BIT.CTS = 0; // Stop timer W counter
}
}

//////////////////////////////
// 50us delay
//////////////////////////////
void wait_50us( unsigned int time )
{
unsigned int cnt;

while( time-- != 0 )
{
for( cnt = 0; cnt < 165; cnt++ );
}

}

//////////////////////////////
// 10us delay
//////////////////////////////
void wait_10us( void )
{
unsigned int cnt;

for( cnt = 0; cnt < 30; cnt++ );

}

////////////////////////////////////////////
// Getting switch state with delay function
////////////////////////////////////////////
char sw_delay( int wait )
{
char dat;

while(1)
{
```

```
dat = SW_CHECK();  // 1st time of getting switch state
wait_1ms( wait );  // Prevention of chattering phenomenon done by getting switch state twice at different time
if( dat == SW_CHECK() )// 2nd time of getting switch state
{
return( dat );
}
}
}

/* Function for switch */
////////////////////////////////
// Starting switch
////////////////////////////////
void start_sw( void )
{
while( ! SW_CHECK() ); // Confirmation of Start switch is in off state
wait_1ms( 50 );

while( sw_delay( 10 ) ); // Wait until Start switch has been pushed
}

/* Main Function */
void main(void)
{
timerW_init(); // Initialize TimerW
while(1)
{
start_sw(); // Start switch

LED_R_OFF(); // LED RED OFF
LED_G_OFF(); // LED GREEN OFF

lcd_locate_puts( 1, 1, 16, "S1 IN" ); // Display "S1 IN"
LED_G_ON(); // LED GREEN ON →  1st Stimulus

PULSE1_ON(); // Stimulation1 ON
wait_1ms(1); // 1ms of pulse duration
PULSE1_OFF(); // Stimulation1 OFF

LED_G_OFF(); // LED GREEN OFF

wait_1ms( 400 );           // Time interval between stimulation1 and stimulation2

lcd_locate_puts( 1, 1, 16, "S1 IN *400ms" ); // Display "S1 IN *400ms"
LED_G_ON(); // LED GREEN ON →  2nd Stimulus

PULSE1_ON(); // Stimulation2 ON
wait_1ms(1); // 1ms of pulse duration
PULSE1_OFF(); // Stimulation2 OFF

LED_G_OFF(); // LED GREEN OFF

wait_1ms( 400 ); // Time interval between stimulation2 and stimulation3

lcd_locate_puts( 1, 1, 16, "S1 IN *400ms" ); // Display "S1 IN *400ms"
LED_G_ON(); // LED GREEN ON →  3th Stimulus

PULSE1_ON(); // Stimulation3 ON
wait_1ms(1); // 1ms of pulse duration
PULSE1_OFF(); // Stimulation3 OFF

LED_G_OFF(); // LED GREEN OFF

wait_1ms( 400 ); // Time interval between stimulation3 and stimulation4

lcd_locate_puts( 1, 1, 16, "S1 IN *400ms" ); // Display "S1 IN *400ms"
LED_G_ON(); // LED GREEN ON →  4th Stimulus

PULSE1_ON(); // Stimulation4 ON
wait_1ms(1); // 1ms of pulse duration
PULSE1_OFF(); // Stimulation4 OFF

LED_G_OFF(); // LED GREEN OFF

wait_1ms( 400 ); // Time interval between stimulation4 and stimulation5

lcd_locate_puts( 1, 1, 16, "S1 IN *400ms" ); // Display "S1 IN *400ms"
LED_G_ON(); // LED GREEN ON →  5th Stimulus

PULSE1_ON(); // Stimulation5 ON
wait_1ms(1); // 1ms of pulse duration
PULSE1_OFF(); // Stimulation5 OFF

LED_G_OFF(); // LED GREEN OFF

wait_1ms( 400 ); // Time interval between stimulation5 and stimulation6

lcd_locate_puts( 1, 1, 16, "S1 IN *400ms" ); // Display "S1 IN *400ms"
LED_G_ON(); // LED GREEN ON →  6th Stimulus

PULSE1_ON(); // Stimulation6 ON
wait_1ms(1); // 1ms of pulse duration
PULSE1_OFF(); // Stimulation6 OFF

LED_G_OFF(); // LED GREEN OFF

wait_1ms( 400 ); // Time interval between stimulation6 and stimulation7

lcd_locate_puts( 1, 1, 16, "S1 IN *400ms" ); // Display "S1 IN *400ms"
```

```
LED_G_ON(); // LED GREEN ON →  7th Stimulus

PULSE1_ON(); // Stimulation7 ON
wait_1ms(1); // 1ms of pulse duration
PULSE1_OFF(); // Stimulation7 OFF

LED_G_OFF(); // LED GREEN OFF

wait_1ms( 400 ); // Time interval between stimulation7 and stimulation8

lcd_locate_puts( 1, 1, 16, "S1 IN *400ms" ); // Display "S1 IN *400ms"
LED_G_ON(); // LED GREEN ON →  8th Stimulus

PULSE1_ON(); // Stimulation8 ON
wait_1ms(1); // 1ms of pulse duration
PULSE1_OFF(); // Stimulation8 OFF

LED_G_OFF(); // LED GREEN OFF

wait_1ms( Dur_initiate );          // Time interval between stimulation8 and stimulation9

lcd_locate_puts( 1, 1, 16, "S2 IN *134ms" ); // Display "S2 IN 134ms"
LED_R_ON(); // LED RED ON →  9th Stimulus

PULSE2_ON(); // Stimulation9 ON
wait_1ms(1); // 1ms of pulse duration
PULSE2_OFF(); // Stimulation9 OFF

LED_R_OFF(); // LED RED OFF

wait_1ms( Dur_terminate ); // Time interval between stimulation9 and stimulation10

LED_R_ON(); // LED RED ON →  10th Stimulus
lcd_locate_puts( 1, 2, 16, "S3 IN 1090ms" ); // Display "S3 IN 1090ms"

PULSE2_ON(); // Stimulation10 ON
wait_1ms(1); // 1ms of pulse duration
PULSE2_OFF(); // Stimulation10 OFF

LED_G_ON(); // LED GREEN + RED ON →  End Stimulus

}
}
```

Publications

Original Papers

1. Farhanahani Mahmud, Takashi Sakuhana, Naruhiro Shiozawa and Taishin Nomura. An Analog-Digital Hybrid Model of Electrical Excitation in a Cardiac Ventricular Cell. Trans. Jpn. Soc. Med. Biol. Eng. Vol 47, No 5: 428-435, 2009.

2. Farhanahani Mahmud, Naruhiro Shiozawa, Masaaki Makikawa and Taishin Nomura. Reentrant Excitation in an Analog-Digital Hybrid Circuit Model of Cardiac Tissue. Submitted to Chaos.

International Conference Proceeding

1. Farhanahani Mahmud, Takashi Sakuhana, Naruhiro Shiozawa and Taishin Nomura. An Analog-Digital Hybrid model of cardiac excitation-conduction. Transactions of the International Congress of Physiological Sciences, Kyoto, Julai 2009.

Domestic Conference Proceedings

1. Farhanahani Mahmud, Takashi Sakuhana, Naruhiro Shiozawa and Taishin Nomura. An Analog-Digital Hybrid model of Cardiac Excitation and Propagation (in Japanese). Transactions of the Japanese Society for Medical and Biological Engineering, Tokyo, April 2009.

2. Farhanahani Mahmud, Takashi Sakuhana, Naruhiro Shiozawa and Taishin Nomura. A Real-time simulation of an Analog-Digital Hybrid model of cardiac excitation.

Transactions of the Institute of Electronics, Information and Communication Engineers, Toyama, May 2009.

3. Farhanahani Mahmud, Takashi Sakuhana, Naruhiro Shiozawa and Taishin Nomura. An Analog-Digital Hybrid Model of Electrical Excitation in Ventricular Cardiac Cell. Transactions of the Japanese Society for Medical Biological Engineering, Chiba, September 2009.

4. Farhanahani Mahmud, Naruhiro Shiozawa and Taishin Nomura. Simulation of reentrant propagation in a ring of cardiac tissue: comparison between Luo Rudy numerical model and an analog-digital hybrid model. Transactions of the Japanese Society for Medical Biological Engineering, Hokkaido, September 2010.